Electrochemical Reduction of CO_2 on Copper, Copper Oxide and Mixed Metal Oxides of Lanthanum, Calcium, and Copper

Thesis submitted in partial fulfillment of the requirements

of the degree of

Master of Technology and Doctor of Philosophy

by

Giri Sachin Daulatgir

(Roll Number: 113020027)

Supervisor: Prof. Arindam Sarkar

Department of Chemical Engineering

INDIAN INSTITUTE OF TECHNOLOGY BOMBAY

2018

Dedicated to

my family, my friends and all supporter

Approval sheet

Department of Chemical Engineering

Indian Institute of Technology, Bombay

The Thesis report entitled, "Electrochemical Reduction of CO_2 on Copper, Copper oxides and Mixed Metal Oxides of Lanthanum, Calcium, and Copper " submitted by Giri Sachin Daulatgir (Roll No. 113020027) is accepted for evaluation.

Date: _____ Signature

(Prof. Arindam Sarkar)

Declaration

I declare that this written submission represents my ideas in my own words and where other ideas or words have been included; I have adequately cited and referred the original sources. I also declare that I have adhered to all principles of academic honesty and integrity and have not misrepresented or fabricated or falsified any idea/data/fact/source in my submission. I understand that any violation of the above will cause for disciplinary action by the Institute and can also evoke penal action from the sources which have thus not been properly cited or from whom proper permission has not been taken when needed.

Name: Giri Sachin Daulatgir

Roll No. 113020027

Date: _____

Place: _____

Acknowledgment

I express my deepest gratitude to my supervisor Prof. Arindam Sarkar for his constant encouragement, motivation, co-operation, and guidance during my research. His passion and dedication towards the research has always energized me to overcome barriers in research, which helped me to develop skills required for the research over time. Our discussions during the work improved my understanding of basic concepts of not only reaction engineering particularly but also electrochemical reaction, catalysis and the inorganic chemistry. Further, these discussions help me in thinking critically about the problem and which made me capable of carrying out research independently.

I would like to thank Prof. A. K. Suresh and Prof. Sanjay Mahajani (RPC committee members) for their valuable suggestion and generously sharing their ideas with me. Their critical inputs helped me in enriching the quality of my research work. Further, the lab facilities extended by RPC member's research group have helped me in my research work.

I acknowledge the support of Industrial Relation and Consultancy Centre (IRCC) Sophisticated Analytical Instrumentation Facility (SAIF), Metallurgical Engineering & Materials Science (MEMS) of IIT Bombay for extending their analytical facilities (TEM, SEM, XRD, GCMS, XPS) to me for the analysis of my catalyst and reaction products.

I acknowledge the financial support for my research from Department of Science and Technology, Government of India through the project DST/IS-STAC/CO2-SR-14212(G)) and Ramanujan fellowship. I am greatly thankful to Ministry of Human Resource and Development (MHRD) and Council for Scientific and Industrial Research (CSIR), New Delhi for providing the financial assistance to me. I would like to thank Industrial Relation and Consultancy Centre (IRCC) and Department of Chemical Engineering IIT Bombay for assisting me a scholarship for the remaining period. I acknowledge IIT Bombay for providing financial assistance for attending and presenting my research work in an international conference at PRiME 2016 Hawaii, USA.

I thank all chemical engineering teaching and non-teaching staff for their help in my Ph.D. I would like to especially thank Dr. Rohidas Bhoi and Detkeji for the valuable help. I would like to thank my seniors and my batch mates for the help in my research work. Particularly, I like to thank Bharghav Krishna for helping in getting the optical microscopy

images. I would like to thank all my labmates Nilam, Mahesh, Adhidesh, Ravi, Madhurima, Praveen, Suraj, Shariq for the valuable help and discussion during my research work. Thanks all.

I thank my mother, father, brother, and sister for their unbelievable support, help, and motivation which helped me to pursue higher education. Last, but not least, I thank my wife Shruti for her sacrifices, encouragement and valuable moral support. I thank my little bundle of joy Anay.

Abstract

The reduction of CO_2 (to commercially valuable products) has attracted much attention of the researchers due to the dual advantages. First, considering the environmental aspects, increasing concentration of CO_2 in the atmosphere has resulted in the global warming and hence it is necessary to reduce the emission of CO_2. Second, the use of CO_2 as feedstock for the synthesis of the commercially important chemicals such as alcohols, hydrocarbons, carboxylic acids, CO, etc. The electrochemical reduction of CO_2 is one of the promising methods for the reduction of the CO_2 to commercially important chemicals as it can be coupled with electricity generated by non-conventional sources of the energy such as solar and wind. Thus, electrochemical reduction of the CO_2 can be used as energy storage for energy generated from the non-conventional sources in the form of high-density fuels (alcohols and hydrocarbons).

The electrochemical reduction of CO_2 has been studied extensively by using copper as electrocatalyst due to the range of the products (alcohols/hydrocarbons/carboxylic acid) upon reduction. However, the use of copper as an electrocatalyst for the electrochemical reduction of the CO_2 suffers from the two major drawbacks, first overpotential and second selectivity of the products during reduction. It has been observed that the overpotential not only for the electrochemical reduction of CO_2 but also for other electrochemical reaction such as hydrogen evolution, chlorine evolution, etc., can be significantly reduced if the electrocatalyst is subjected to the deliberate oxidation. The deliberate oxidation of the copper can be achieved electrochemically or thermochemically. The electrochemical oxidation of copper in alkaline solution results in the formation of the different oxides and hydroxides of copper (Cu_2O, $Cu(OH)_2$ and CuO). On the other hand, the thermochemical oxidation of the copper results in the formation of different oxides mainly (CuO, Cu_2O and Cu_3O_4). However, it has been observed that the oxides produced by both these methods get reduced to the copper within few minutes during electrochemical reduction of CO_2. It essentially suggests that the reduction of CO_2 takes place on copper and not copper oxides. Apparently, the reduced copper was found to be more active than the un-oxidized copper.

The deliberate oxidation of copper by the electrochemical methods was accomplished by three methods viz. chronoamperometry (CA), linear sweep voltammetry (LSV) and cyclic voltammetry (CV). It was observed that both the reduction current and the amount of the formate ions produced were highest for the copper foil oxidized by the CV compared to the

CA and LSV. However, the amount produced on both CA and LSV oxidized copper foils is significantly higher than un-oxidized copper. The available literature proposes that the increase in the activity and the selectivity after oxidation may be due to the increase in the surface roughness or real surface area or electrochemically active surface area (EASA). The relative increase in EASA of the copper foil estimated using under potential deposition (UPD) of the lead (Pb). The relative increase in EASA was observed highest for the CV (17.5 times) followed by LSV (4.91 times) and then by CA (2.85 times) compared to un-oxidized copper. Moreover, the selectivity for the formation of the formate ion increases after the electrochemical oxidation and subsequent reduction of the copper oxides on copper foil.

This trend of increase in EASA due to oxidation and increased activity and selectivity continues even for the copper oxidized by the thermochemical method. The thermochemical oxidation results in the formation of a thick film of oxides compared to the electrochemical oxidation. The thick film of oxides gives more EASA upon reduction compared to electrochemical methods, and hence large reduction was current observed in the case of copper foil oxidized by the thermochemical method. The EASA estimated by UPD of Pb also showed that the relative increase in the EASA of thermochemically oxidized copper foil is almost double than the electrochemically oxidized (by CV) copper.

Further, the effect of the presence of the other metal oxides on the activity and selectivity of copper oxides for electrochemical reduction of CO_2 was studied by changing the atomic fraction of the lanthanum (La) and calcium (Ca) in copper. Initially started with an equal atomic fraction of copper and calcium, calcium fraction was systematically reduced and substituted with lanthanum. It was observed that when calcium was absent or very small in amount the major product of the electrochemical reduction of CO_2 was acetic acid, formic acid, and propanol. At a higher atomic fraction of the calcium, the major product was formic acid.

Table of Contents

Table of Figures

Table of Tables

Abbreviations and Nomenclatures

AFM	Atomic Force Microscopy
BET	Brunauer Emmett Teller
CA	Chronoamperometry
CCS	Carbon Capture and Sequestration
CV	Cyclic Voltammetry
DEA	Diethanolamine
DMF	Dimethylformamide
DMSO	Dimethyl Suifoxide
EASA	Electrochemically Active Surface Area
GC	Gas Chromatography
GDL/GDE	Gas Diffusion Layer/Electrode
GHG	Green House Gas
HER	Hydrogen Evolution Reaction
HPLC	High Performance Liquid Chromatography
LSV	Linear Sweep Voltammetry
MDEA	Methyl Diethanolamine
MEA	Monoethanolamine
SEM	Scanning Electron Microscopy
SHE	Standard Hydrogen Electrode
TEAP	Tetraethylammonium Perchlorate
TEM	Transmission Electron Microscopy
UPD	Under Potential Deposition
XPS	X-ray Photoelectron Spectroscopy
XRD	X-ray Diffraction

Chapter 1
Introduction

1.1 Introduction

Air surrounding us mainly consists of nitrogen (N_2) and oxygen (O_2), along with some water vapours, carbon dioxide (CO_2) and some other rare gases in small volumes. Out of these constituents of air, oxygen, carbon dioxide, and water vapours support life on earth directly or indirectly by taking part in the life cycle. Carbon dioxide takes part in life cycle through photosynthesis, where plants convert atmospheric CO_2 into chemical energy in the form of carbohydrate such as sugar, in the presence of light through photosynthesis. Before the start of industrialization in the late 18^{th} century, the concentration of CO_2 in the troposphere was around 280 ppm. The current concentration of CO_2 in the troposphere is 408.35 ppm (February 2018). Figure 1.1 shows the increase in the concentration of CO_2 over last 50 years (Keeling et al. 2009). The increase in the concentration of CO_2 in the atmosphere is primarily due to human activities (anthropogenic emissions) which can lead to an increase in the ambient temperature and subsequent global warming (Pachauri et al. 2014). Figure 1.2 shows that relation between the change in earth's temperature with the change in the concentration of the CO_2 over last 800,000 years (Jouzel et al. 2007; Lüthi et al. 2008). The figure shows that the current climate change and global warming is the result of the increasing concentration of the CO_2 in the atmosphere. Apart from CO_2, there are few other greenhouse gases (GHG) such as, CO_2, CH_4, and N_2O, etc. that are also contributing to the global warming. The rise in the temperature of earth's surface and surrounding due to global warming has resulted in an irreversible change in the climate. Climate change is detrimental not only for the economics of the world but also the very existence of life as we know it. As global warming touches every aspect of life in one form or other, these changes can result in severe damage to the normal ecological behaviour. Other than that, these changes will impact hydrology and water resources, food and fiber production, coastal system and human health too. Consequently, it is right time to act and prevent further damage to the earth's environment.

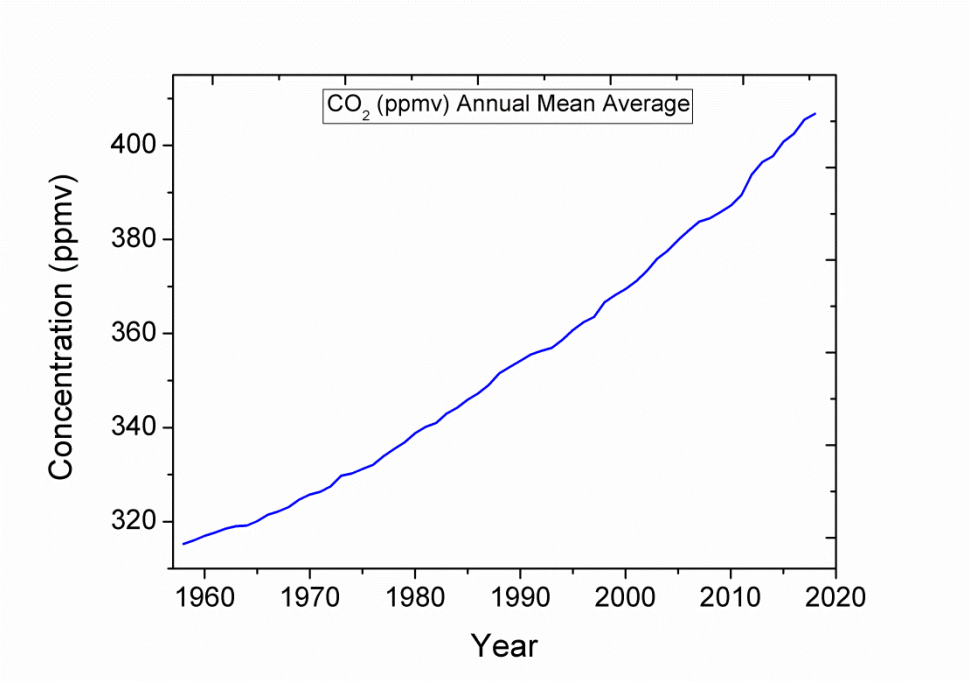

Figure 1.1: The annual mean average concentration of the CO_2 measured at Mauna Loa, Hawaii, USA.

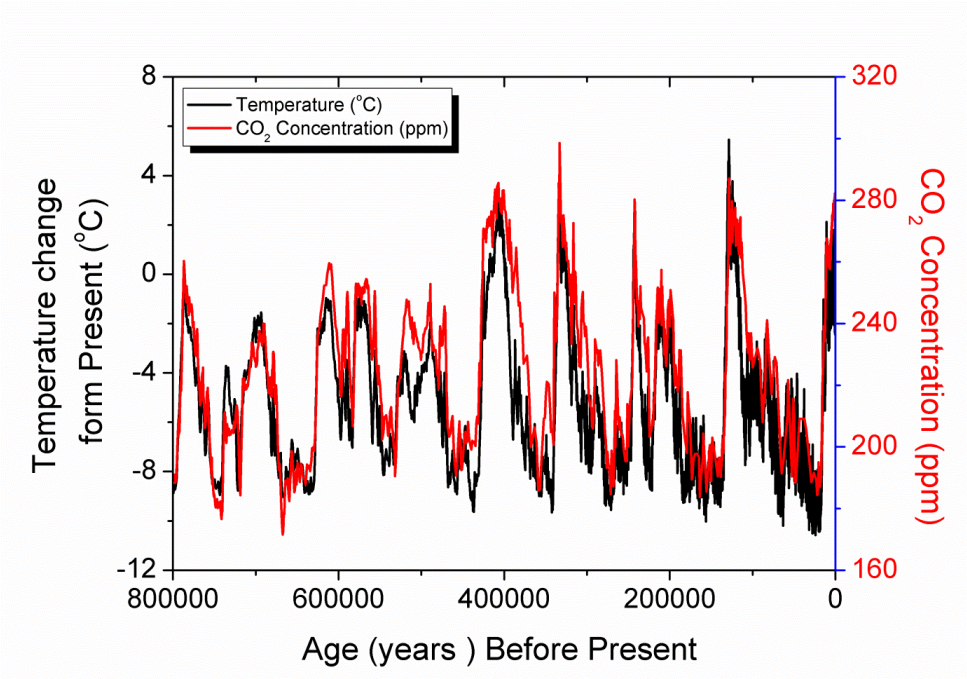

Figure 1.2 The change in the temperature and change in carbon dioxide concentration measured from the EPICA Dome C ice core in Antarctica.

1.2 Carbon Capture and Sequestration

One way to control the increase in the CO_2 concentration and avoid the effects in the form of climate change is to plant billions of trees to convert the atmospheric CO_2 to chemical energy. However, this method of planting and growing plants to trees can be a long term solution as it will take a lot of time and care, as well as precious resources in the form of land and water. Due to continuously growing population, both these resources are now becoming rare. Therefore, we have to search for the new alternatives which are short term and has potential to benefit us economically too. Consequently, it is important to find solutions where CO_2 can be captured and converted to useful products that can be processed further. A lot of attention is being paid on the capture of CO_2, storing and sequestration (carbon capture and sequestration (CCS)). In CCS, CO_2 is captured at the point of its emission from large sources such as thermal power plant using coal or natural gas as fuel. Initially, CO_2 is separated from other constituents of the combustion gases to obtain pure CO_2. The research and development in this area have been matured to an extent where almost pure CO_2 can be captured and stored, and process it for some commercial application if required. Once captured, the CO_2 thus obtained is then compressed for transportation to the application site. The CO_2 then can be disposed of by primarily four methods;

1. Pumping it in the dip well specially created, the exhausted wells of natural gas or oil to store CO_2 underground.
2. Loading the CO_2 on big ships and then discharge the CO_2 in lakes or at the bottom of the sea or dissolved in the sea water.
3. Absorbing CO_2 in materials such as (a) zeolites of porous crystalline aluminosilicates (b) activated carbon, (c) metal oxides of alkaline metal (Na_2O and K_2O) and alkaline earth metals (CaO, MgO) along with other metal oxides such as rubidium oxides, cesium oxides, barium oxides, iron oxides, etc., (d) absorption in amine solution of monoethanolamine (MEA), diethanolamine (DEA) and methyl diethanolamine (MDEA) (Choi, Drese, and Jones 2009).
4. The production of the commercially important chemicals where CO_2 can be used as feedstock.

However, these methods of carbon capture and storage have limitations regarding the high cost of storage and the possibility of leakage after storage (Metz et al. 2005). Other limitation of the CCS includes its unsuitability due to the distance of safe sites for

sequestration from the sources and low concentration of CO_2 in the exhaust gases. Further, the carbon cycle does not get completed, and potential of CO_2 as a source for the synthesis of valuable chemical or fuel remains untapped. Doing so can reduce the raw material cost of an organization, may make the whole process cheaper and certainly reduce the environmental concerns. It has been estimated that about 5 to 10% of CO_2 emitted can be recycled to produce commercially important chemicals and fuels.

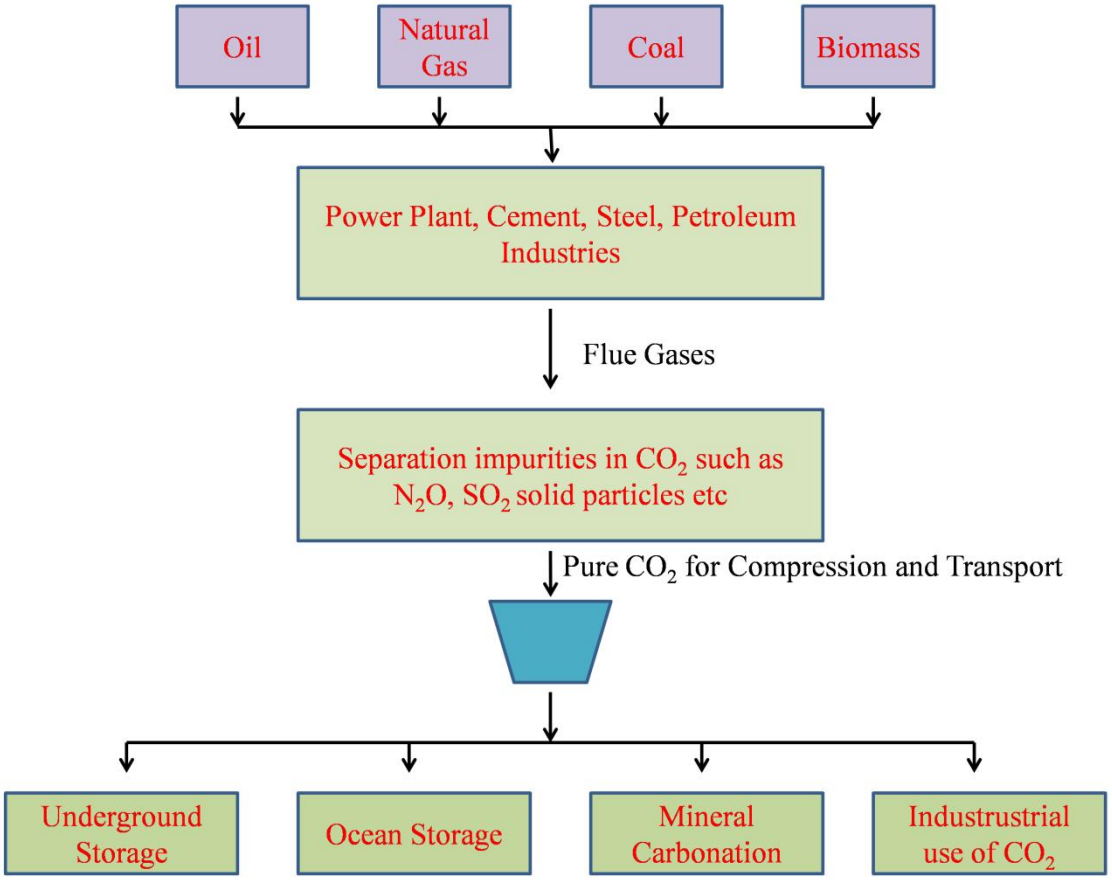

Figure 1.3 Schematic of carbon capture and sequestration (Metz et al. 2005)

Nonetheless, thermodynamically the process would involve a significant expenditure of energy. The standard molar Gibbs energy of formation (ΔG^0) of CO_2 is -393.5 kJ/mole (Wagman et al. 1982), which means that reaction converting CO_2 (reduction of CO_2) to fuel/chemical will require an external work of 393.5 kJ to make the reaction go forward leading to carbon. For other products, though the external work varies slightly, it still requires a considerable input of energy. Due to this limitation, the use of CO_2 in the production

process for fuels and chemicals is very limited. Currently, CO_2 is used as feedstock for very few processes such as the production of urea, salicylic acid, and polycarbonates. For these processes, the use of CO_2 is very small compared to the CO_2 available for the conversion. Further, the limitations of CCS (high cost, transportation to the sequestration site, etc.) can be avoided by converting CO_2 to some product by using energy from renewable sources. With this thought, different methods were explored for the conversion of CO_2 back to some commercially useful products. Table 1.1, shows the standard Gibbs free energy of formation for few chemical compounds can be produced from the reduction of CO_2.

Table 1.1: Standard Gibbs free energy of formation of few chemical compounds can be produced from the reduction of the CO_2 (Alper and Orhan 2016).

Sr. No.	Compound	Std. Gibbs Free Energy (KJ/mol)
1	Formic Acid	-361.4
2	Carbon monoxide	-137
3	Formaldehyde	-113
4	Methanol	-166.4
5	Methane	-50.8
6	Hydrogen	0
7	Ethanol	-174.9
8	Ethane	-32.9
9	Acetic Acid	-389.9

1.3 Methods for Reduction of CO_2

Following are different methods used for the reduction of the CO_2 to different commercially useful product (Scibioh and Viswanathan 2004).

1. **Radiochemical**

In this method, high energy Gamma rays are used as atomic bullets to impart the required energy for conversion. Formic acid, formaldehyde, and acetaldehyde were produced in aqueous solution from CO_2 by passing ^{60}Co γ-radiations. Further, at higher doses of the ^{60}Co γ-radiations oxalic acid and glycol were also observed. Hydrogen was also a product of this reaction along with CO which get produced at lower pH only (Getoff, Scholes, and Weiss 1960).

2. Chemical Reduction

In this method, CO_2 is reduced on metals (most commonly cobalt, iron and ruthenium) which occur at relatively high temperature. Quite frequently, CO_2 first reduces to CO and then this CO is mixed with hydrogen gas to get syngas. The syngas is then further reduced catalytically to hydrocarbons at high temperature and high pressure (Fischer Tropsch reaction) [$(2n+1)\ H_2 + n\ CO \rightarrow C_nH_{(2n+n)} + nH_2O$]. This is an important step in the production of liquid fuels from the gaseous feed. The gaseous feed is mostly generated from coal or biomass. Thus Fischer Tropsch remains an important reaction for converting the coal or biomass to hydrocarbon to be used as commercial fuel (Quinn and Jones 1936).

3. Thermo-Chemical

In this method, carbon dioxide is split into carbon monoxide and oxygen when heated to high temperature in the presence of CeO_2, Na_2HPO_4, etc. Once CO_2 is converted to CO, then it can be reduced to the hydrocarbons by reacting with hydrogen as mentioned in above method (Bamberger and Robinson 1980).

4. Photochemical

Carbon dioxide and water are reduced to a mixture of CO and H_2 by irradiating with photons in a suitable medium. For example, a solution of Ru(2-2'-bipyridine)$_3^{2+}$, cobalt (II) chloride in acetonitrile/water/triethylamine on irradiation in the presence of CO_2 leads to CO. The amount of CO and H_2 generated as a result of photochemical reduction primarily depends on the composition of the system. Further, it was observed that the addition of free pyridine in the systems increases the H_2 generation by suppressing CO generation. Moreover, by changing the tertiary amines from trimethylamine to tripropylamine increased both the quantity of CO and H_2 produced as well as the ratio of CO/H_2 (Lehn and Ziessel 1982).

5. Biochemical

In this method, methane was produced continuously from H_2, and CO_2 in a packed bed reactor made up of methanobacterium thermoautotrophicum, and diatomaceous earth was used as support for the medium The rate of conversion of the H_2 and CO_2 to methane was observed as high as 80% of the theoretical value. The highest rate of methane formation observed was 5.2 liter/(liter of bed volume×hour) (Jee, Nishio, and Nagai 1988).

6. Biophotochemical

Biophotochemical reactions fix CO_2 in two different ways. The first approach uses natural cofactors as catalyst and carboxylation reaction to fix CO_2. In the second approach, the reaction is carried out in the absence of natural cofactor, but enzyme FDH (formate dehydrogenase) is used as a catalyst. Mostly, this biocatalyst converts CO_2 to formate ions (Mandler and Willner 1988).

7. Photoelectrochemical

This method used a combination of both photon and electrical energy. Mostly a semiconductor is used to capture photons and electrochemically reduce CO_2. For example, the photoelectrochemical reduction of CO_2 on (100) plane of CdTe semiconductor electrode, in non-aqueous solution (DMF (dimethylformamide)) solution with 5% water leads to the formation of mainly CO. However, the faradaic efficiency for the formation of the CO was greater than 80% when the percentage of water went up to 25%. The reduction current was stable up to 24 hours at the reduction potential of -1.0 V versus standard calomel electrode (SCE) (Taniguchi, Aurian-Blajeni, and Bockris 1984).

8. Bioelectrochemical

In this method, CO_2 fixation was carried out in oxoglutaric acid using isocitrate dehydrogenase (ICDH) enzyme as electrocatalyst and methylviologen (MV^{2+}) as a mediator. This bioelectrochemical reaction leads to the formation of isocitric acid. The faradaic efficiency for the formation of isocitric acid was almost 100% in 0.2 M tris buffer of pH 7 at a potential equal -0.9 V versus SCE. The principle behind this reduction method is to reverse the reaction of isocitric acid oxidation to oxoglutaric acid and CO_2 (Sugimura, Kuwabata, and Yoneyama 1989).

9. Biophotoelectrochemical

In this method, CO_2 fixation carried out using p-type indium phosphide (p-InP) as semiconductor photoelectrode with formate dehydrogenase enzyme as biological catalyst. By this method, CO_2 was converted into formic acid. The electron generated in the photoelectrode due the light photon was coupled to the enzyme through a mediator. The electron can be generated even at the light of wavelength shorter than 900 nm. This makes

possible to use full spectra of the visible light for the fixation of the CO_2 (Parkinson and Weaver 1984).

10. Electrochemical

This is the most studied method for the reduction of CO_2. Electrochemical reduction of CO_2 is mostly carried out in either an aqueous solution or non aqueous solution. Due to proton deficiency in the non aqueous solvents, CO_2 competitively gets reduced to three different products, oxalate, carbon monoxide, and formate ions. In case of an aqueous solution, the availability of protons results in the evolution of hydrogen as a side reaction along with hydrocarbon, alcohols, and acids which gets generated during the reduction reaction of CO_2. Most often, the method requires a conductive catalyst, typically termed as an electrocatalyst. In aqueous solutions, a different metal such as copper, zinc, palladium, platinum, silver, gold, lead, etc. has been used as an electrocatalyst. The product of the electrochemical reduction of CO_2 and the selectivity of the product is a strong function of the electrolyte and electrode material as well as the operating conditions such as pH, potential, etc. (Amatore and Saveant 1981).

The reactions given below are for the formation of some of the products as a result of the CO_2 reduction. The values written in the bracket are the standard reduction potential at 25 ^{0}C versus standard hydrogen electrode (SHE) at a pH of 7 (Scibioh and Viswanathan 2004; Y Hori 2008).

$$CO_2 + H_2O + 2e^- \rightarrow CO + 2OH^- \quad (1.1)\ (E^0 = -0.52\ V)$$

$$CO_2 + 2H_2O + 2e^- \rightarrow HCOOH + 2OH^- \quad (1.2)\ (E^0 = -0.61\ V)$$

$$CO_2 + 2H_2O + 2e^- \rightarrow HCHO + 2OH^- + 0.5O_2 \quad (1.3)\ (E^0 = -0.48\ V)$$

$$CO_2 + 6H_2O + 8e^- \rightarrow CH_4 + 8OH^- \quad (1.4)\ (E^0 = -0.25\ V)$$

$$2CO_2 + 8H_2O + 12e^- \rightarrow C_2H_4 + 12OH^- \quad (1.5)\ (E^0 = -0.34\ V)$$

$$2CO_2 + 9H_2O + 12e^- \rightarrow C_2H_5OH + 12OH^- \quad (1.6)\ (E^0 = -0.33\ V)$$

$$3CO_2 + 13H_2O + 18e^- \rightarrow C3H_7OH + 18OH^- \quad (1.7)\ (E^0 = -0.32\ V)$$

In all the above methods CO_2 has been reduced to some useful products. The electrochemical method seems to be one of the most appealing methods for the production of chemicals such as formic acid, methanol, methane, ethylene, etc. Moreover, the coupling of the electrochemical method with electricity generated by non-conventional and intermittent

sources such as the wind and solar energy can lead to storage of the electricity in a convenient high energy density chemical form that can be transported easily(Whipple and Kenis 2010). Apart from usages of CO_2 reduction products as fuel (methanol, ethanol, etc.), products such as formic acid also have industrial application in different processes like for tanning and dyeing in leather and textile industries, as a coagulant agent in the production of latex rubber, etc. Further, formic acid can be used as feedstock to produce sodium formate, methyl formate. Salts of formic acid such as sodium formate have application in dyeing and printing of fabrics, can be used as food additive, or as a buffering agent for strong mineral acids, etc. Another derivative, methyl formate is used as fumigant, foaming agent and refrigerant. (Leitner 1995).

The advantages of the electrochemical method for CO_2 reduction are:

A. Water itself acts as a source of H^+ ions/hydrogen required in the reduction reaction.
B. The electrochemical reduction of CO_2 is carried out at room temperature, the reaction parameters which influences the electrochemical reduction of CO_2 are potential of CO_2 reduction, electrolyte and its pH, which can be easily controlled.
C. Space requirement for electrochemical reactors is small compared to traditional reactors.
D. The catalyst in any form such as foil, mesh, powder or thin film deposited on the conductive substrate can be used as an electrode for the electrochemical reduction of the CO_2.
E. Advanced membranes (cation/anion) with low resistance are available and can be integrated not only to separate the two electrodes (to avoid any oxidation reaction on the positive electrode of the products produced at the negative electrode) but also to obtain pure products without the additional step of separation and intensification.

However, the mechanism of formation of the products on electrochemical reduction of CO_2 is poorly understood, and it depends strongly on the choice of medium of electrolysis (electrolyte) as well as the electrode material (electrocatalyst). Whereas in aqueous media, the choice of electrolyte is mostly limited to bicarbonates, the electrocatalyst explored spans a wide range of materials from metals and its alloys, metals oxides, semiconductors and some

novel carbons. Thus, search for electrocatalysts occupies a greater fraction of the available work on electrochemical reduction of CO_2. We will discuss the electrochemical reduction of CO_2 in more details in next chapter.

1.4 Thesis Organization

- Chapter1 talks about the need for the CO_2 reduction and the different available methods for the reduction of the CO_2.
- Chapter 2 talks about the literature available for the electrochemical reduction of the CO_2. In which we have discussed different electrolytes and electrode used for the electrochemical reduction of the CO_2 and the kinetics of the electrochemical reduction of the CO_2. We have selected copper as our electrode material for the study of aqueous phase reaction.
- Chapter 3 discusses the electrochemical oxidation of bulk copper in 0.5 M KOH, 0.5 M Na_2CO_3 and 0.5 M $NaHCO_3$ solutions by CV. Moreover, CV of monolayer copper deposited on platinum has been obtained.
- In chapter 4, the copper foil was oxidized by three different electrochemical methods CV, LSV, and CV. Electrochemical reduction of CO_2 was then carried out at -1.6 V in 0.5 M $NaHCO_3$ solution. Further, quantification of the CO_2 reduction was carried out for all three electrodes at -1.6 V and real surface area estimated by UPD of Pb on copper.
- In chapter 5 the comparison between un-oxidized, electrochemically oxidized and thermochemically oxidized copper foils has been made for electrochemical reduction of CO_2 at the different potential in 0.5 M $NaHCO_3$ solution. Again, the real surface area of the copper foil has been estimated using UPD of Pb.
- Chapter 6 deals with the estimation of the surface area of copper powder by Cu_2O monolayer, UPD of Pb, the particle size measured by SEM images of copper powder, particle size analyzer, and BET.
- In chapter 7, electrochemical reduction of CO_2 was done on mixed metal oxides of La, Ca, and Cu. The product analysis of CO_2 reduction has been carried out on HPLC.
- Chapter 8 concludes all work.

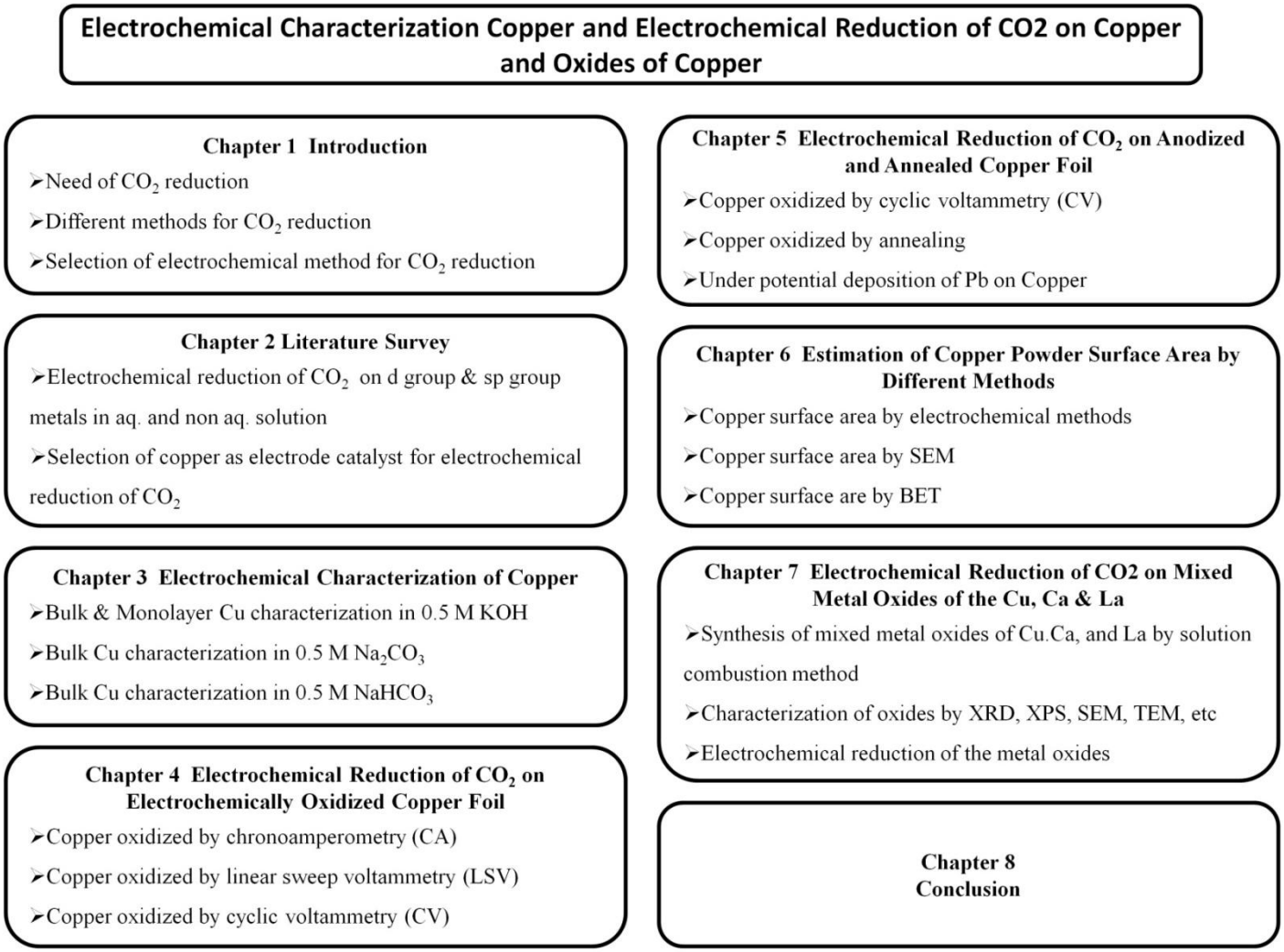

Figure 1.4: Organization of the thesis.

Chapter 2

Literature Survey on Electrochemical Reduction of CO_2

2.1 Introduction

The electrochemical reduction of CO_2 takes place at the cathode (working electrode) in an electrochemical cell, whereas at the anode (counter electrode) mostly oxygen evolution takes place. The electrochemical reduction of CO_2 leads to the formation of different compounds based on the electrolyte and electrocatalyst used for the reduction. The standard electrode potential for different products and the corresponding reduction reactions are mentioned below, the potential referred here in the reactions are versus a standard hydrogen electrode (SHE) (Lamy, Nadjo, and Saveant 1977; Bard 1976).

$$CO_2 + 2H^+ + 2e^- \rightarrow CO + H_2O \quad (E^0 = -0.105\ V) \quad (2.1)$$

$$CO_2 + 2H^+ + 2e^- \rightarrow HCOOH \quad (E^0 = -0.199\ V) \quad (2.2)$$

$$CO_2 + 4H^+ + 4e^- \rightarrow HCHO + H_2O \quad (E^0 = -0.071\ V) \quad (2.3)$$

$$CO_2 + 6H^+ + 6e^- \rightarrow CH_3OH + H_2O \quad (E^0 = -0.03\ V) \quad (2.4)$$

$$CO_2 + 8H^+ + 8e^- \rightarrow CH_4 + 2H_2O \quad (E^0 = +0.169\ V) \quad (2.5)$$

$$2CO_2 + 8H^+ + 8e^- \rightarrow CH_3COOH + 2H_2O \quad (E^0 = +0.106\ V) \quad (2.6)$$

As the products of CO_2 reduction mainly depends on electrolyte and electrocatalyst employed for the reduction of the CO_2, it is important to understand their effect on the product distribution of CO_2 reduction. Further, the product distribution also changes with the potential applied for the reduction of CO_2. For simplicity, electrolytes are classified as aqueous and non-aqueous and predominantly metals electrodes are employed for the reduction of CO_2 in these electrolytes.

2.2 Electrochemical Reduction in Aqueous Solution

The main advantages of using aqueous phase electrolyte for the electrochemical reduction of CO_2 is the requirement of hydrogen atoms which is met in-situ for the formation of hydrocarbon, alcohols and carboxylic acid (C_xH_y, $C_xH_yO_z$ etc). The water splits into hydrogen ions and oxygen at counter electrode (in acidic media) simultaneously during the electrochemical reduction of CO_2 at working electrode. Hence, a wide range of the products has been detected in an aqueous medium as a result of the electrochemical reduction of the

CO_2 including C_xH_y, $C_xH_yO_z$ along with CO and H_2. Additionally, there no need for any exotic solvent and just addition of some salt is sufficient to make deionized water conductive enough for successful CO_2 reduction. Further, separation of the reduction product is easier in the case of the aqueous solution than in case of the non aqueous solution. However, one of the major drawbacks of operating in aqueous media is the concomitant evolution of hydrogen due to the splitting of water during reduction reaction which is usually termed as the hydrogen evolution reaction (HER). The HER is a major side reaction and is responsible for the low faradaic efficiency (faradaic efficiency to form a product is defined as the ratio amount of charge consumed to form product to the total amount of charge transferred) of the CO_2 reduction product. Further, the low solubility of CO_2 in the aqueous solution indirectly supports the HER, as the amount of the CO_2 available for the reduction at any instant is significantly lower than that in case of any non aqueous solution. Although some metal electrode do show high overpotential for the HER compared to the CO_2 reduction reaction, still a fraction of the total charge will invariably be consumed by the HER. Table 2.1 summarizes some of the metal electrocatalyst used for electrochemical reduction of CO_2 in aqueous electrolytes and the products of the electrochemical reduction of CO_2.

Table 2.1: Summary of electrocatalyst and the product produced by the electrochemical reduction of CO_2.

Sr. No.	Electrode Material	Salt Solution	CO_2 Reduction Product	Authors
1	Zn	$NaHCO_3$	HCOOH	(Coehn and Jahn 1904)
2	Cu	$KHCO_3$	HCOOH, CH_4, C_2H_4, C_2H_3OH C_3H_7OH	(Y Hori 2008)
3	Cu-Zn (alloy)	$KHCO_3$	HCOOH	(Katoh et al. 1994)
4	Cu-Sn (alloy)	$KHCO_3$	HCOOH	(Katoh et al. 1994)
5	Cu-Hg (alloy)	$KHCO_3$	CH_3OH, CH_4, $C2H_4$	(Katoh et al. 1994)
6	In	$KHCO_3$	HCOOH	(Azuma et al. 1990; Ishimaru, Shiratsuchi, and Nogami 2000)
7	Sn	0.95 KCl + 0.05$KHCO_3$, $KHCO_3$	CO, HCOOH	(Kapusta and Hackerman 1983; Azuma et al. 1990)
8	Pb	$KHCO_3$	HCOOH	(Azuma et al. 1990)
9	Bi	$KHCO_3$	CO, HCOOH	(Hara, Kudo, and Sakata 1995)
10	Pt	$KHCO_3$	CO, C_2H_5OH	(Hara, Kudo, and Sakata 1995)
11	Pd	$KHCO_3$	CO, HCOOH	(Azuma et al. 1990)
12	Pd-Ru	$KHCO_3$	HCOOH, CO	(Furuya, Yamazaki, and Shibata 1997)
13	Ni	$KHCO_3$, K_2HPO_4	H_2, CO, CH_4, C_2H_4, C2H6, HCOOH	(Yoshio Hori, Kikuchi, and Suzuki 1985; Koga and Hori 1993)
14	Fe	$KHCO_3$	H_2, CO, HCOOH, C_4H_{10}	(Hara, Kudo, and Sakata 1995)
15	Ru	Na_2SO_4	CH_3OH, CH_4	(Ko W Frese and Leach 1985; Summers and Frese Jr 1988)
16	Au	$KHCO_3$	CO, HCOOH,	(Azuma et al. 1990; Hara, Kudo, and Sakata 1995)

In addition to the electrocatalyst, the anions present in the electrolytes also have a significant effect on the faradaic efficiency of products in the electrochemical reduction of CO_2. It has been observed that the presence of the CO_3^{2-}, HCO_3^- and SO_4^{2-} in the aqueous solution increases the faradaic efficiency for formic acid and other products of the CO_2 reduction. However, the presence of PO_4^{3-} ions does not enhance the faradaic efficiency. The faradaic efficiency varied from 35% to 87% for the different ions in the order $PO_4^{3-} < SO_4^{2-} < CO_3^{2-} < HCO_3^-$. Ulmann et al. speculated that the cations like HCO_3^- takes part in the reaction mechanism of CO_2. This may explain the higher faradaic efficiencies obtained in the presence of HCO_3^- (Ikeda, Takagi, and Ito 1987; Spichiger-Ulmann and Augustynski 1986; Manuel M Baizer and Henning Lund 1991; Oniciu et al. 1990).

2.3 Electrochemical Reduction in Non-Aqueous Solution

The study of electrochemical reduction of CO_2 in non aqueous solution is not as extensive as it is in aqueous solution. Though some attempts have been made to study the activity and selectivity of CO_2 reduction in non aqueous solution such as dimethyl Sulfoxide (DMSO), Acetonitrile, tetraethylammonium perchlorate (TEAP). The major advantage of using non aqueous solution for the electrochemical reduction of CO_2 is the solubility of CO_2 which is comparatively high in non-aqueous solution than an aqueous solution. Further, the investigation also showed that non aqueous solution not only increases the solubility of CO_2 but also helps for dimerization process, during which produces higher values C_2 compounds such as oxalic acid (Oniciu et al. 1990). However, the lack of hydrogen ions in the solution the major products observed in case non aqueous solution are CO and oxalates. There are some attempts to add some water to the solvent to increase the hydrogen availability and change the product distribution. Table 2.2 briefly summarizes the electrochemical reduction in non-aqueous solution on some metal electrodes in different electrolytes.

Table 2.2. Summary of electrochemical reduction of CO_2 using different metal electrodes in non aqueous solution.

Sr. No.	Electrode Material	Solvent	CO_2 reduction product	Authors
1	Au and Hg	Anhydrous DMSO (dimethyl Sulfoxide)	CO	(Haynes and Sawyer 1967)
2	Sn, In, Pb, and Hg	DMF, Acetonitrile, DMSO (dimethyl Sulfoxide)	Oxalate ions	(Vassiliev et al. 1985)
3	Sn, In	TEAP, Quaternary ammonium salt in DMSO	Oxalix acid, CO	(Ito et al. 1985)
4	Zn	TEAP, Quaternary ammonium salt in DMSO	Oxalic acid, Glyoxalic acid, CO	(Ito et al. 1985)
5	Cu	Benzalkonium chloride/methanol supporting electrolyte	CO, CH_4, and C_2H_4	(Naitoh et al. 1993)
6	Ni, Pt	TEAP tetraethylammonium perchlorate /propylene carbonate	CO, HCOOH, traces of Oxalic acid	(Ikeda, Takagi, and Ito 1987)
7	Pd	TEAP (tetraethylammonium perchlorate /propylene carbonate	Oxalic acid, trances of CO, HCOOH	(Ikeda, Takagi, and Ito 1987)
8	Ti, Nb, Cr	TEAP (tetraethylammonium perchlorate /propylene carbonate	Oxalate, Glyoxalate, and Glycolate	(Ikeda, Takagi, and Ito 1987)
9	Mo	TEAP (tetraethylammonium perchlorate /propylene carbonate	Oxalate	(Ikeda, Takagi, and Ito 1987)

2.4 Selection of Metal Electrode for CO_2 reduction

Table 2.3: Faradaic efficiency of products in CO_2 reduction at various electrodes. Electrolyte: 0.1 M $KHCO_3$, Temperature T = 18 ± 0.5 ^{0}C, reproduced from the reference Hori Y. (2008) with permission from Elsevier.

Electrode	Potential vs. SHE (V)	Current Density (mA/cm^2)	Faradaic Efficiency, %							
			CH_4	C_2H_4	EtOH	PrOH	CO	$HCOO^-$	H_2	Total
Pb	-1.63	5	0	0	0	0	0	97.4	5	102.4
Hg	-1.51	0.5	0	0	0	0	0	99.5	0	99.5
Tl	-1.6	5	0	0	0		0	95.1	6.2	101.3
In	-1.55	5	0	0	0	0	2.1	94.9	3.3	100.3
Sn	-1.48	5	0	0	0	0	7.1	88.4	4.6	100.1
Cd	-1.63	5	1.3	0	0	0	13.9	78.4	9.4	103
Bi	-1.56	1.2	-	-	-	-	-	77	-	-
Au	-1.14	5	0	0	0	0	87.1	0.7	10.2	98
Ag	-1.37	5	0	0	0	0	81.5	0.8	12.4	94.6
Zn	-1.54	5	0	0	0	0	79.4	6.1	9.9	95.4
Pd	-1.2	5	2.9	0	0	0	28.3	2.8	26.2	60.2
Ga	-1.24	5	0	0	0	0	23.2	0	79	102
Cu	-1.44	5	33.3	25.5	5.7	3	1.3	9.4	20.5	103.5
Ni	-1.48	5	1.8	0.1	0	0	0	1.4	88.9	92.4
Fe	-0.91	5	0	0	0	0	0	0	94.8	94.8
Pt	-1.07	5	0	0	0	0	0	0.1	95.7	95.8
Ti	-1.6	5	0	0	0	0	tr	0	99.7	99.7

Few review papers have very well summarized the literature on the electrochemical reduction of CO_2 in aqueous solution on various metal electrodes. Table 2.3 gives the faradaic efficiency for various products in 0.1 M $KHCO_3$ solution which has been reproduced from the work of Hori et al. It can be seen from Table 2.3; copper is one of the most promising metals for CO_2 reduction as it is capable of producing many diverse different products such as formic acid, ethanol, propanol, methane, ethylene, etc. Some of these products generated from the electrochemical reduction of CO_2 can be directly used in the present combustion system and thus completing the carbon cycle. Further, the HER overpotential is comparatively higher as indicated by faradaic efficiency for the formation of H_2 which is comparatively lower than

other metal such as Ni, Pt, Fe, Ti, etc. Hence, copper was selected for our study and further investigation.

2.5 Mechanism for CO_2 Reduction in Aqueous Solutions on Copper

The reduction potential for the different products upon electrochemical reduction of CO_2 is mentioned in the introduction section of this chapter as well as in the table (Table 2.3) of faradaic efficiency for different compounds on metal electrodes. It can be seen from the values of the reduction potential that the difference in the standard reduction potential for different products is not very high and hence the reduction of the CO_2 on copper mostly results in the formation of the mixture of the different products (Table 2.3). Therefore, it is important to understand the mechanism for the formation of different species. Literature suggests that the electrochemical reduction of CO_2 happens in two steps. First the formation of the $HCOO^-$ and CO from the reduction of the CO_2, second the reduction of CO to form alcohols and hydrocarbons.

2.5.1 Reduction of CO_2 to $HCOO^-$ and CO

The first step for the reduction of CO_2 by an electrochemical method in aqueous solution was assumed to be the formation of the anion radical of CO_2 (CO_2^-) after transfer of the first electron (Ayers 1994; Lamy, Nadjo, and Saveant 1977; Bard 1976; Jordan and Smith 1960) (reaction 2.7). The formation of the CO_2^- radical as an intermediate during the reduction of CO_2 has been demonstrated by the reaction between UV radiation and CO_2 and reaction between sodium formate crystal and γ irradiation (Aylmer-Kelly et al. 1973; Lunsford and Jayne 1965). After formation of CO_2^-, Paik et al. (Paik, Andersen, and Eyring 1969) suggested that it undergoes further reaction with water and formate radical is produced. The presence of formate radical as an intermediate was demonstrated by the galvanostatic charging curves. The galvanostatic curves were obtained in neutral solution at constant current. The time versus potential data was obtained in the galvanostatic curves.

$$CO_2 + e^- \rightarrow CO_2^- \quad \text{.....(2.7)}$$

Further, it has been concluded from the Tafel slope (118 mV/decade) of the polarization curve of CO_2 reduction, that the first electron transfer to CO_2 to form CO_2^- is rate controlling step.

The reaction for the formation of the formate radical by the reaction between a water molecule and CO_2^- radical is shown below (reaction 2.8 and 2.9).

$$CO_2^- + H_2O \rightarrow HCO_2 + OH^- \quad \text{.....(2.8)}$$

$$HCO_2 + e^- \rightarrow HCO_2^- \quad \text{.....(2.9)}$$

The optical data show that the presence of the intermediate (CO_2^-) on the electrode surface was very small (surface coverage ~ 0.02) and further confirmed by the photoelectrochemical measurements (Schiffrin 1973). This indicates that the intermediate radicals are present in the electrolyte and not on the electrode surface. This argument is in line with the fact the electrode is at negative potential hence the probability of the presence of the anion on such surface is very low. Based on these arguments, Alymer-Kelly et al. (Aylmer-Kelly et al. 1973) concluded that the reaction of the intermediate (CO_2^-) is with water and not with H^+ ions supported by the calculations of the flux of the H^+ ions from the splitting of the water in neutral pH of the electrolyte. On the other hand, in acidic solutions, H^+ ions react with CO_2 or the intermediate (CO_2^-) to form HCO_2 which then further gets converted into formic acid. Due to the large overpotential of CO_2 reduction, it very common to apply higher reduction potential for CO_2 but at this high negative potential mostly an evolution of the hydrogen takes place and very less amount of the formic acid is produced.

As mentioned in the reaction scheme above, standard reduction of CO_2 to CO potential is positive compared to the standard reduction of CO_2 to formate ions. The reason for the lower reduction potential for the formation of CO was suspected due to the attachment of the intermediate (CO_2^-) to the electrode surface, and that leads to a decrease in the overpotential. This suggests that the mechanism for the formation of CO will be different than the mechanism for the formation of $HCOO^-$. The formation of CO or $HCOO^-$ depends on whether the intermediate (CO_2^-) has been adsorbed on the copper surface or not. When formate ions is the product, intermediate (CO_2^-) is in the electrolyte near the electrode surface (as (CO_2^-) was not attached to electrode surface) and not on the electrode surface. However, the availability of the *d* electron affects the back donation of the charge results in the excess negative charge and oxygen atom which results in the C coordination of CO_2 with copper. The C coordination of CO_2 with copper surface results in the attachment of the CO_2^- on the

copper surface. Once CO_2^- get stabilized on the copper surface, it undergoes protonation reaction to give CO and OH^-.

2.5.2 Reduction of CO to Alcohols and Hydrocarbons

After the formation of these two species ($HCOO^-$ and CO) from the reduction of CO_2 in aqueous solution, the other products will form on the subsequent reduction of these two species. The experiments with already formate ions mixed in the electrolytes and the reduction of these formate ions using copper electrode show that the formate ions cannot be reduced further to any of the other possible product of the CO_2 reduction (Yoshio Hori, Murata, and Takahashi 1989; Cook, MacDuff, and Sammells 1989). On the other hand, the reduction of the CO on copper carried out by Hori et al. has resulted in the formation of hydrocarbon and alcohols (Yoshio Hori et al. 1987). Hence, it was concluded that the CO produced from the reduction of the CO_2 has been further reduced to hydrocarbons or alcohols (Peterson et al. 2010).

The product gas analysis of electrochemical reduction of CO_2 has confirmed the presence of CO along with gaseous hydrocarbon in the product stream. The reason for the incomplete reduction of CO_2 to CO and not to hydrocarbons and alcohols is the attachment of the CO to the copper surface. The bonding of the CO with the copper surface is intermediate strength (estimated for the heat of the adsorption) (Somorjai 1978; Yoshio Hori et al. 1987). For other metal electrodes, CO bind very strongly or loosely results in no further conversion of the CO. Once CO stabilizes on the copper surface it undergoes further reduction. With the transfer of H^+ ions to the adsorbed CO on copper results in the formation of the CH_2(ad). The CH_2(ad) species on further reduction results in the formation of the CH_4 and C_2H_4. The reaction of the CH_2(ad) reacts with CO results in CH_2CO(ad) which upon further reduction results in CH_2CHOH(ad) which undergoes reduction to gives CH_3CH_2OH. The reaction of CH_2CHOH with CO and followed by the reduction results in the $CH_3CH_2CH_2OH$. These steps lead to the formation of various C_1, C_2, etc. Alcohols (Gattrell, Gupta, and Co 2006; Peterson et al. 2010; Y Hori 2008).

Further, after the formation of the CO, its further reduction to give hydrocarbon/alcohol strongly depends on the electrolyte used for the reduction. In K_2SO_4, KCL, $KClO_4$ and dilute HCO_3^- the aqueous solution will give rise to the formation of alcohols and C_2H_4. On the other hand, the concentrated HCO_3^- and phosphate electrolytes will results in the formation of CH_4 specifically. The reason for this change in product distribution may be due to the pH of the solution or in other words when the hydrogen evolution is preferred;

the formation of the CH_4 may also be favoured due to the large availability of the proton (Yoshio Hori, Murata, and Takahashi 1989).

2.6 Conclusion

The two major category of the electrolytes used for the electrochemical reduction of CO_2 is aqueous and non aqueous solution. Sometimes, the non aqueous solution has been selected for the electrochemical reduction of the CO_2 due to the higher solubility of the CO_2. However, the electrochemical reduction of CO_2 in non aqueous solution mostly results in the formation of CO and oxalate due to the lack of protons in the solution. On the other hand, the splitting of the water in aqueous solution results in the formation of the required protons for the formation of hydrocarbons, alcohols and carboxylic acid. Even with the limitation of hydrogen evolution as a major side reaction, electrochemical reduction of the CO_2 in the aqueous medium is promising and has been studied extensively. The reason for selection of aqueous medium for the study lies in the wide range of products in aqueous solution. Further, the distribution of the product in aqueous solution depends on the choice of the electrocatalyst used for the reduction of the CO_2. As far as we know, only copper has shown hydrocarbons and alcohols as products upon electrochemical reduction of CO_2. Though, other metal electrodes also demonstrated the formation of CO during the reduction of CO_2. However, no hydrocarbons/alcohols have been reported.

Chapter 3

Electrochemical Characterization of Copper in Alkaline Solutions

3.1 Introduction

Among all the other metals that have been used as catalysts, copper has been investigated to a great extent primarily because of the product profile. A range of products such as methanol, ethanol, methane, ethylene, formic acid, etc. forms on copper as a result of the electrochemical reduction of CO_2. Hence copper was selected for electrochemical reduction of CO_2. In this context, it is important to understand the behaviour of copper under applied potential in both acidic and alkaline solution. Moreover, unlike other noble metals such as platinum, palladium, etc., copper has not been explored in details on its behaviour under applied potential. In acidic solution under applied potential copper dissociates to give cupric (Cu^{2+}) ions and these can be either complex with other anions present in the medium or form copper salt (like $CuCl_2$ etc.) (Crundwell 1992). However, in alkaline solution different oxides and hydroxides forms on the copper surface which are functions of the applied potential.[1] Among one of the first investigations, Mullar (1907) has reported many important aspects of oxidation of copper in alkaline media using galvanostatic measurements. Afterward, the study of the electrochemical oxidation of copper was complimented by other characterization techniques such as X-ray diffraction, electron diffraction, etc. Subsequently, it was found that the oxides produced on the surface of copper due the electrochemical oxidation were mainly Cu_2O, CuO and $Cu(OH)_2$. (Ambrose, Barradas, and Shoesmith 1973a). However, the relation between the formation of different species and applied potential was unclear until the advent of cyclic voltammetry.

By utilizing cyclic voltammetry technique, Ambrose et al. (Ambrose, Barradas, and Shoesmith 1973a, 1973b) did an extensive analysis of the copper oxides produced on the copper surface as a result of the oxidation in alkaline solution on stationary as well as a rotating electrode. They have confirmed the formation of Cu_2O, CuO and $Cu(OH)_2$ due to oxidation along with some water-soluble copper hydroxide (Cu hydroxide) which were also speculated to form. Afterward, extensive analysis of CVs of copper in NaOH was done by Abd El Haleem et al. (El Haleem and Ateya 1981). The assignment of different possible reactions on a copper surface to different peaks observed in CV of copper was done by using

[1] A portion of the work reported in this chapter has been published in J. Electrochem. Soc., **163 (3),** H252 (2016).

the slope of the line obtained by plotting peak potential (E_p) versus the logarithm of the concentration of OH^- ions. Further, by assuming that the first peak observed during oxidation of copper surface is due to the formation of a monolayer of Cu_2O, they estimated the true or electrochemical active surface area of copper. More recently, Mayer et al. (Mayer and Muller 1992) studied oxidation of copper using an in situ Raman spectroscopy and confirmed the formation of oxides and hydroxides of copper during oxidation of copper in alkaline solution. The potential sweep experiments were carried out in 1 M and 6 M KOH solution at 0.5, 1 and 10 mV/s. As the potential is moved positive at low scan rates, initially formation of Cu_2O takes place. However, the oxidation of copper and formation of Cu_2O occurs at higher potentials predicted by thermodynamics alone and as the potential moves further, $Cu(OH)_2$ get produced followed by CuO.

We have studied electrochemical behaviour of copper in three alkaline solutions viz 0.5 M KOH (pH=13.51), 0.5 M Na_2CO_3 (pH=11.14), and 0.5 M $NaHCO_3$ (pH=7.77). It was observed that the electrochemical behaviour change considerably upon changing the electrolytes. Due to increasing complexity of the reactions and the products detailed electrochemical characterizations were performed in 0.5 M KOH solutions only. Further, electrochemical behaviour was supplemented by detailed characterizations techniques such as XPS, SEM, etc. Additionally, the electrochemical characterization was performed for UPD copper on platinum, and electrochemical behaviour was compared against the bulk copper electrode in 0.5 M KOH solution.

3.2 Experimentation

3.2.1 Electrodes

Standard three electrode setup was used for all electrochemical measurements. Polytetrafluoroethylene (PTFE) shrouded bulk copper electrode was fabricated in-house. The electrode was made from 99.999 % pure copper rod of 5 mm diameter (supplied by Goodfellow Inc., Cambridge-UK). The copper rod was inserted into a core drilled PTFE rod so that only the cross-sectional area of copper rod remains exposed to the electrolyte. Commercial glassy carbon electrode 5 mm in diameter (supplied by PINE Research Instrumentation) was used for experiments of copper monolayer deposition on carbon-supported platinum nanoparticles (nominal 20 wt%, Fuel Cell Store). The copper electrode, as well as the glassy carbon electrode, was polished to mirror finish before use. The platinum electrode used for copper underpotential deposition experiments was prepared by drop casting

20 µl of the ink made by sonicating 2 ml of water along with 2 mg of 20 wt% carbon-supported platinum nanoparticles catalyst and 20 µl of Nafion solution (5 wt%, Sigma-Aldrich) till a homogeneous dark suspension was obtained. The ink was then dried under an infra-red (IR) lamp. The under potential deposition of a copper monolayer on platinum was performed in a solution of 50 mM $CuSO_4$ + 0.5 M H_2SO_4 by chronoamperometry. The potential applied during chronoamperometry was 10 mV positive to the open circuit potential (OCP) value obtained for bulk copper deposited on platinum nanoparticles in the same electrolyte for 10 minutes. After the chronoamperometry, the electrode was then rinsed in argon saturated de-ionized water and transferred to another electrochemical cell (containing either 0.5 M H_2SO_4 solution to study copper monolayer in acidic media or 0.5 M KOH to study oxidation of copper monolayer in alkaline media) for recording cyclic voltammogram.

To obtain SEM images and XPS spectra of the oxidized copper surface, the copper foil (extra pure, Loba Chemie, India) of 0.5 cm × 0.5 cm was cleaned by immersing it in 20 % (v/v) aqueous solution of HNO_3 and then washed with de-ionized water. Copper foil thus cleaned was oxidized electrochemically by linear sweep voltammetry (LSV) in Ar-saturated 0.5 M KOH solution. Surface morphology of oxidized copper surface was observed at different magnification in a JEOL JSM 7600 (FESEM) scanning electron microscope. The AXIS Ultra (Kratos Analytical made) XPS machine used for survey scan of the oxidized copper surface to ascertain different species of copper oxides and hydroxides that were formed.

A platinum mesh was used as a counter electrode for all the experiments. The reference electrode for experiments conducted in alkaline solution was Hg/HgO (0.3 M KOH), and a Hg/Hg_2SO_4 (sat. K_2SO_4) reference was used for acidic media. In this chapter, all potentials are referred versus Hg/HgO reference electrode for an alkaline solution, and for an acidic solution, these are referred versus Hg/Hg_2SO_4 reference electrode.

3.2.2 Electrolytes

Experiments in the acidic medium were carried out in 0.5 M H_2SO_4 solution which was prepared by using EMSURE grade H_2SO_4 (supplied by Merck, Germany) and de-ionized water. The 50 mM $CuSO_4$ + 0.5 M H_2SO_4 solution was prepared by adding required amount of $CuSO_4 \cdot 5H_2O$ (AR grade, 99% purity, Merck, India) and H_2SO_4 in de-ionized water. The experiments in the alkaline medium were carried in 0.5 M KOH, 0.5 Na_2CO_3 and $NaHCO_3$ solutions which were prepared by dissolving required amount KOH pellets, Na_2CO_3 and

$NaHCO_3$ (EMPLURA, Merck, India) in de-ionized water. The electrochemical cell used was a five neck vessel having a capacity of 50 ml. All glassware was washed with aqua regia and then rinsed three times with de-ionized water before use. Biologic (Model No. VSP-300) Potentiostat along with EC-Lab V10.34 software was used for all electrochemical data collection and analysis.

3.3 Electrochemical Characterization of Copper (Bulk and Monolayer) in 0.5 M KOH Solution

3.3.1 Bulk Copper Characterization in 0.5 M KOH Solution

The typical voltammogram of bulk copper electrode obtained in 0.5 M KOH at a scan rate of 50 mV/s is shown in Figure 3.1. The essential features of the voltammogram match very well with the reported voltammogram of bulk copper by several researchers (Ambrose, Barradas, and Shoesmith 1973a, 1973b; El Haleem and Ateya 1981; Mayer and Muller 1992). The cyclic voltammogram of the bulk copper electrode is defined by two prominent peaks which appear during oxidation of the copper surface, i.e. when the potential was scanned from negative to a positive potential (-1.2 V to 0.5 V) and two peaks corresponding to the reduction of the oxidized species which are observed in reverse scan. For convenience, the peaks have been marked here as A and B (oxidation), and C and D (reduction). Apart from the two prominent current peaks during oxidation, a small shoulder at approximately -0.55 V was also observed just before peak A. Although, the exact nature of the electrochemical reaction occurring during the step is not well established, the consensus is more towards the formation of (soluble species) which was first postulated by Miller (B. Miller 1969) from experiments done using a split ring-disk electrode. In those experiments the pure copper disk was oxidized galvanostatically, and currents due to both oxidation and reduction reactions of almost equal magnitude were observed simultaneously on two split Au rings kept at two different potentials (one slightly below the oxygen evolution reaction on copper and another far negative to reduce any oxidized species to metallic copper). This arrangement helps in the identification of the unsteady reaction at the electrode surface. The product produced during the small shoulder is a Cu^+ species which can be further oxidized by an electron to get Cu^{2+} and reduced to get Cu. Later Ambrose et al. proposed that the species is produced by the reaction 3.1

$$Cu + 2OH^- \rightarrow Cu(OH)_2^- + e^- \qquad \left(E^0 = -0.2913\ V\right) \text{.....(3.1)}$$

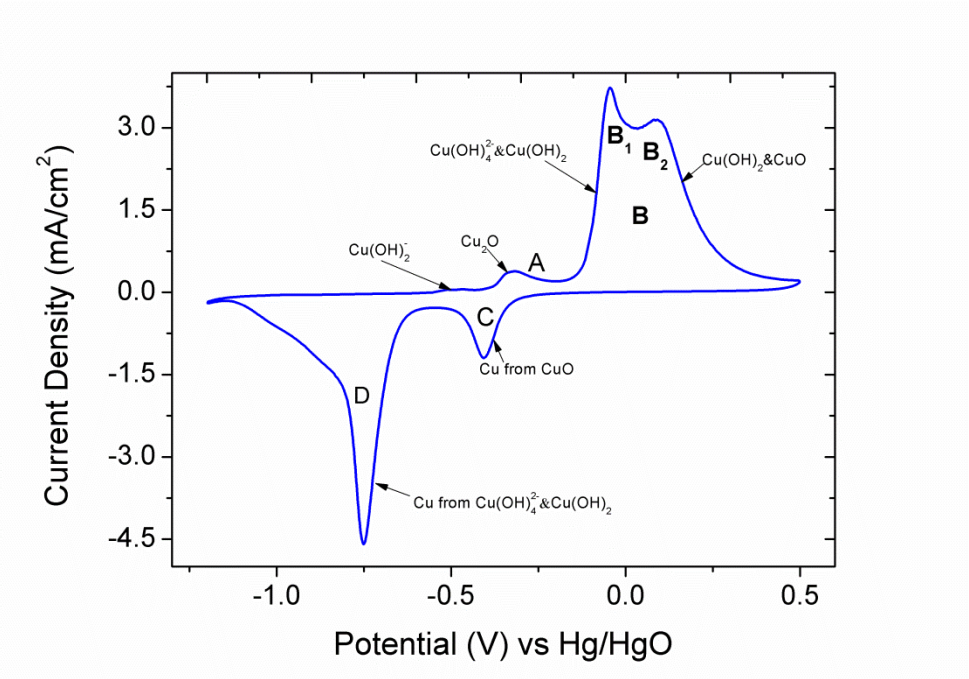

Figure 3.1: Cyclic voltammogram of the bulk copper electrode (5 mm diameter) in argon saturated 0.5 M KOH at a scan rate of 50 mV/s.

However, based on the thermodynamic data provided by Beverskog et al. (Beverskog and Puigdomenech 1997), the formation of $Cu(OH)_2^-$ by reaction 3.1 seems unlikely as the standard electrochemical potential for the above reaction (3.1) is much higher compared to the appearance of the shoulder in the cyclic voltammetry. We suspect that the formation of $Cu(OH)_2^-$ is not due to direct oxidation of copper as given in reaction 3.1, but by oxidation of Cu to Cu_2O initially (reaction 3.2) and its subsequent dissolution via the reaction 3.3. Moreover, the magnitude of K_{eq} also suggests that the extent of the dissolution reaction is very small.

$$2Cu + 2OH^- \rightarrow Cu_2O + H_2O + 2e^- \qquad (E^0 = -0.4641\,V) \text{.....(3.2)}$$

$$Cu_2O + 2OH^- + H_2O \Leftrightarrow 2Cu(OH)_2^- \qquad (K_{eq} = 1.4316 \times 10^{-6}) \text{.....(3.3)}$$

As the potential is increased beyond -0.4 V, the rate of formation of Cu_2O by electrochemical oxidation of metallic copper dominates over the dissolution of Cu_2O as given by reaction 3.3, manifesting as a peak (peak A) at around -0.4 V to -0.2 V.

Peak A

Primarily, two possible reactions pathways have been proposed for the formation of Cu_2O. Shams et al. (El Din and El Wahab 1964), Dignam et al. (Dignam and Gibbs 1970), and Hampson et al. (Hampson, Lee, and MacDonald 1971) proposed two electrons direct oxidation of copper leading to the formation of Cu_2O as given by reaction 3.2. On the other hand, Abd El Haleem et al. proposed a one-electron transfer reaction, initially leading to Cu(OH) (reaction 3.4), which again decomposes to Cu_2O via the reactions 3.5.

$$Cu + OH^- \rightarrow Cu(OH) + e^- \qquad (E^0 = 0.2635V) \text{.....(3.4)}$$

$$2Cu(OH) \Leftrightarrow Cu_2O + H_2O \qquad (K_{eq} = 4.0811\times10^{24}) \text{.....(3.5)}$$

Abd El-Haleem et al. based their conclusions on the variation of peak potential (E_p) with respect to the logarithm of the concentration of OH^- ions, which for a reversible reaction under diffusion control with insoluble products will yield a slope of 59 mV per decade change in the concentration of OH^-. However, we believe that the reaction cannot be considered to be purely under diffusion control. To verify the assertion, a plot of peak current (I_p) versus square root of scan rate (υ) was obtained, and the data were fitted to a straight line. For the conditions mentioned above, the slope of the straight line will be given by $3.67\times10^5 n^{3/2} A C_0 D^{1/2}$ (Gerischer 1956). Where, n is the number of electrons transferred in the reaction, A is the area of the electrode cm^2, C_0 is the bulk concentration of OH^- ions in mol/cm^3 and D is the diffusion coefficient in cm^2/s. Hence, once slope was found diffusion coefficient for OH^- ions can be evaluated.

Although the fit was unsatisfactory, the diffusion coefficient obtained from the slope for OH^- was 3.0×10^{-11} cm^2/s; a value too low than reported value $\sim10^{-5}$ cm^2/s,(Lide 1947) suggesting that the reaction is not controlled by the diffusion of OH^- ions. Similar, conclusions have also been drawn by Ambrose et al. for the peak A. Furthermore, the standard thermodynamic potential (E^0) for reaction 3.4 is 0.2635 V, while for reaction 3.2 it is -0.454 V, evidently pointing out that reaction 3.2 is thermodynamically much more probable as the potential is moved from -1.2 V to 0.5 V. Hence, it can be concluded that the formation of the Cu_2O is as per the reaction 3.2 only. Further, if the oxidation reactions produce a monolayer film of Cu_2O on the surface of the electrode, then charge under peak A can be used to determine the true or electrochemical active surface area of the copper

electrode using correct charge density factor. For example, it is usual to assume charge density factor equal to 210 μC/cm^2 for platinum to evaluate the true surface area using hydrogen adsorption.(Green and Kucernak 2002) In case of copper, a charge density factor equal to 352 μC/cm^2 has been reported by Fletcher et al. (Fletcher, Barradas, and Porter 1978) By assuming the value of 352 μC/cm^2, the true surface area was determined to be 0.314 cm^2 at a scan rate of 50 mV/s in 0.5 M KOH, corresponding to a roughness factor of 1.6 (real area / geometric area). The value is in a close match with those obtained by S. Fletcher et al. as well as Abd El Haleem et al.

Ideally, for monolayer oxidation, the charges would remain invariant with respect to scan rate as well as the OH^- concentration in the solution. However, charge under peak A was observed to be invariant for only a range of scan rate and exhibited dependence on pH as well. At moderate scan rates (30 mV/s and up to 100 mV/s) charge under peak A remained fairly constant (110 μC). However, at very high scan rate a small decrease in charges due to the oxidation reaction was observed. The possible reason may be errors in estimating the correct charges due to increased double layer capacitance at higher scan rates. On the other hand, at low scan rates (less than 20 mV/s) there was an increase in charges. For example at 10 mV/s the charges come to be approximately three times that of those obtained at 50 mV/s, implying a multilayer thick film of Cu_2O (Figure 3.2). Evidently, at lower scan rate the OH^- ions diffuse across the Cu_2O film to react with the underlying copper surface resulting in multilayer thick film. Similar observations have been made by Miller also where the bulk copper electrode was anodized galvanostatically at a current density of 448 μA/cm^2, and the film thickness was computed to be 57 Å. Furthermore, the charge under the peak was found to be a strong function of the concentration of OH^-. In an analogy similar to that of the scan rate, the increase in charges can be explained by the higher flux of OH^- ions, which percolates through the monolayer oxide and reacts with metallic copper leading to the multilayer film of Cu_2O. Other than the charges, the variation of OH^- concentration, does not affect the nature of the peak. However, at a lower concentration, the peak position moved further right, which reflects the dependence of the reaction on pH.

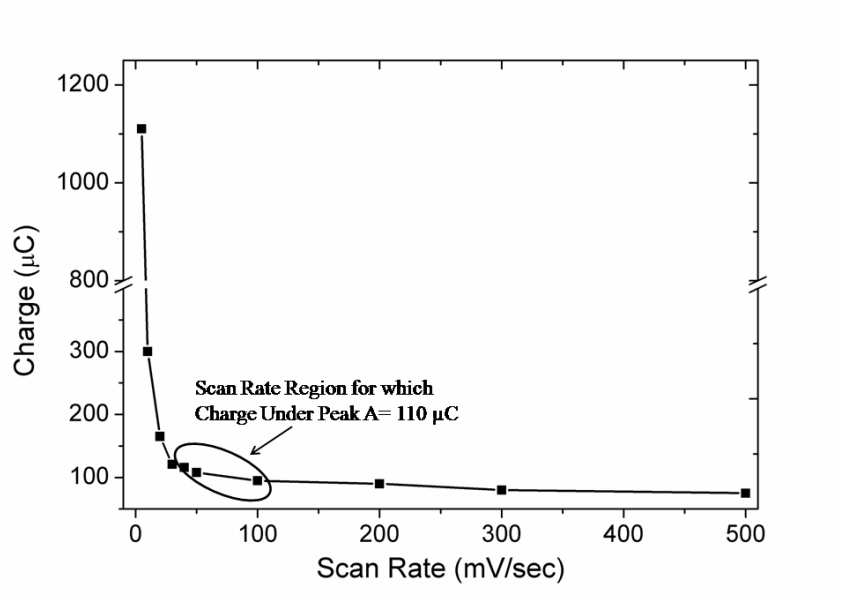

Figure 3.2: Scan rate vs. charge under the peak A in Ar saturated 0.5 M KOH solution.

Peak B

As the potential is increased further, a sharp rise in current was again observed indicating further oxidation. However, unlike peak A, where a change in scan rate does not influence the shape of the peak, the shape of peak B was found to be a strong function of scan rate. At low scan rates, a sharp peak centered at -0.020 V was observed. However, at intermediate and high scan rates instead of a well-defined single current peak, a rather broad plateau with two prominent current peaks indicating multiple reactions were observed. Here, subscripts B_1 and B_2 to distinguish between the first peak (B_1) which occurs first when we are moving from negative to a positive potential and the second peak (B_2) which occurs after the first peak were used.

The cyclic voltammetry profiles of peak B have been observed to be significantly more complicated compared to peak A. Here; one can differentiate two regimes with respect to scan rate approximately above and below 30 mV/s. At very low scan rate (10 and 20 mV/s) the intensity of peak B_2 is more prominent, and peak B_1 manifests as a small shoulder ahead of peak B_2. Surprisingly, the intensity of peak B_2 decreases with increase in scan rate. As the scan rate is increased beyond 30 mV/s, the intensity of both peak B_1 and B_2 starts increasing. At high scan rate, (> 100 mV/s) peak B_2 hardly manifests as a separate peak, and one single current peak with a long tail extending well beyond 0.5 V was observed as shown in Figure 3.3. To investigate, if the electrode reactions at peak B_1 is diffusion controlled, the

peak currents (I_p) of B_1 was plotted versus the square root of scan rate (υ) to estimate the diffusion coefficient of OH^- ions. The values come out to be 2.46×10^{-9} cm^2/s, which is again much less than the reported value $\sim10^{-5}$ cm^2/s, indicating that the reactions under B_1 are not diffusion controlled.

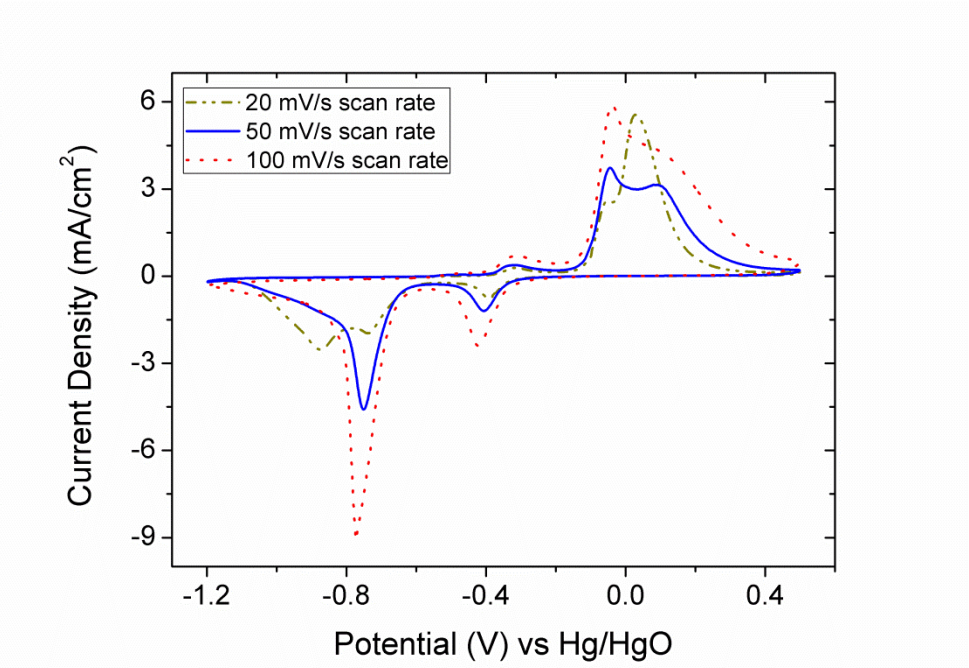

Figure 3.3: Cyclic voltammograms of the bulk copper electrode in argon saturated 0.5 M KOH at a scan rate of 20, 50, and 100 mV/s.

Other than the scan rate, the shape of peak B changes with concentration of OH^- ions as shown in Figure 3.4. When CVs were carried out at low concentration of OH^-, i.e., 0.005 M KOH, no separate peak B was observed at a scan rate of 50 mV/s. Instead, the current almost remained constant after peak A, suggesting continuous oxidation, very similar to that of oxide growth on other noble metals particularly platinum. As the concentration of OH^- in the electrolyte was increased to 0.05 M KOH, peak B_1 was observed superimposed on that continuous oxide growth suggesting another pH dependent redox reaction. At a very high OH^- concentration (5 M KOH) peak B appears as single broad peak having the very high intensity and a large peak area (not shown in Figure 3.4).

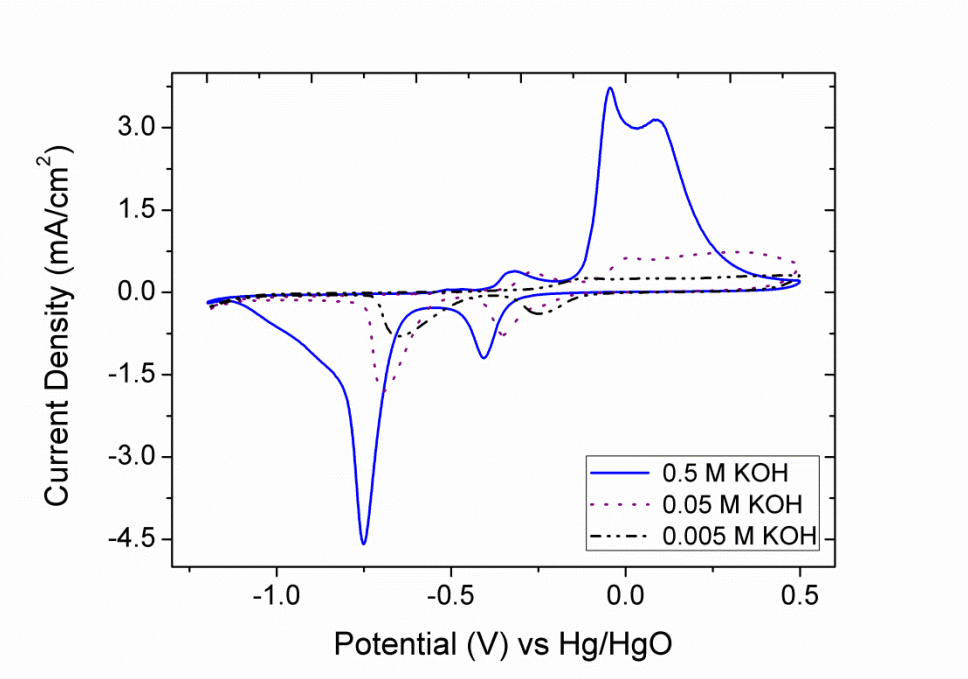

Figure 3.4 Cyclic voltammograms of the bulk copper electrode in argon saturated 0.5, 0.05 and 0.005 M KOH at a scan rate of 50 mV/s.

Primarily, two reaction schemes have been proposed (i) formation of soluble or insoluble hydroxides such as $Cu(OH)_4^{2-}$ and $Cu(OH)_2$, respectively by oxidation of Cu or Cu_2O, and (ii) formation of CuO by oxidation of metallic copper or dehydration of $Cu(OH)_2$. Abd El-Haleem et al. proposed the following two-step reaction (reactions (3.6), (3.7), and (3.8)), where the first step involves electrochemical oxidation of Cu and Cu(OH) to $Cu(OH)_2$ followed by a dehydration step leading to CuO. Here again, the argument was based on the slope of the straight line between peak potential (E_p) and the logarithm of OH^- concentration (36 mV per decade for a reversible reaction with insoluble products involving 2 electron transfer).

$$Cu + 2OH^- \rightarrow Cu(OH)_2 + 2e^- \qquad (E^0 = -0.3312\ V) \text{.....(3.6)}$$

$$Cu(OH) + OH^- \rightarrow Cu(OH)_2 + e^- \qquad (E^0 = -0.9259\ V) \text{.....(3.7)}$$

$$Cu(OH)_2 \rightarrow CuO + H_2O \qquad (K_{eq} = 20.1447) \text{.....(3.8)}$$

It needs to be pointed out here reaction 3.7 particularly may not be applicable as this would entitle prior formation of Cu(OH) which was found to be thermodynamically not feasible. Furthermore, the reaction scheme (3.6) would permit just a single redox peak, while the cyclic

voltammograms show at least two redox peaks. Evidently, the oxidation wave involves multiple redox reactions.

Another reaction scheme was proposed by Ambrose et al., where the current peak B_1 at low potential is due to oxidation of Cu or Cu_2O to insoluble $Cu(OH)_2$ and soluble $Cu(OH)_4^{2-}$ depending on the pH via reaction 3.9, 3.10 and 3.11.

At 1 M KOH

$$Cu_2O + 6OH^- + H_2O \rightarrow 2Cu(OH)_4^{2-} + 2e^- \qquad (E^0 = -0.1668\ V) \text{.....(3.9)}$$

$$Cu + 4OH^- \rightarrow Cu(OH)_4^{2-} + 2e^- \qquad (E^0 = -0.2466\ V) \text{.....(3.10)}$$

At 0.1 KOH

$$Cu_2O + 2OH^- + H_2O \rightarrow 2Cu(OH)_2 + 2e^- \qquad (E^0 = -0.1983\ V) \text{.....(3.11)}$$

While, at still higher potential (close to peak B_2), water-soluble ($Cu(OH)_4^{2-}$) produced by reaction 3.9 and 3.10 gets converted to $Cu(OH)_2$ as per reaction 3.12 accompanied by metallic copper reacting with OH^- ions to produce CuO and $Cu(OH)_2$ as per reaction 3.6 and 3.13

$$Cu(OH)_4^{2-} \Leftrightarrow Cu(OH)_2 + 2OH^- \qquad (K_{eq} = 725.6734) \text{.....(3.12)}$$

$$Cu + 2OH^- \rightarrow CuO + H_2O + 2e^- \qquad (E = -0.3697\ V) \text{.....(3.13)}$$

As per the reaction schemes mentioned above, $Cu(OH)_4^{2-}$ produced during peak B_1 by oxidation of Cu_2O gets converted into $Cu(OH)_2$, and $Cu(OH)_2$ further converts to CuO by dehydration. Additionally, metallic copper reacts with OH^- ions (reaction 3.6) leading to the formation of $Cu(OH)_2$. As the potential increases, oxidation of metallic copper by OH^- ions transported through the porous film of Cu_2O, CuO and $Cu(OH)_2$ begins, and it manifests as a separate peak (peak B_2). Whatever be the mechanism of oxidation, the final products on the electrode are likely to be CuO and $Cu(OH)_2$. But a study by Shoesmith et al. (Shoesmith et al. 1983) using X-ray Photoelectron Spectroscopic (XPS) technique and Brisard et al.(G M Brisard et al. 1995) using Probe Beam Deflection (PBD) method concluded that Cu_2O is also

present in the oxide film produced on the copper along with other oxides and hydroxides. This suggests that Cu_2O produced on the copper surface do not react completely as per reaction 3.9 and 3.11 to produce $Cu(OH)_2$ and CuO.

The behaviour of peak B_2 with respect to scan rate deviates from the usual characteristics of voltammetry where an increase in scan rate increases the peak currents. To understand the effect of scan rate on morphology, copper foils was oxidized electrochemically by LSV from -1.2 V to 0.5 V at scan rates of 10, 30 and 100 mV/s, and the oxidized surfaces were studied using SEM (Figure 3.5). The SEM images show that at a low scan rate of 10 mV/s, the copper surface gets completely covered with needles of copper oxides projecting outward from the surface (average length = 1 µm ± 0.2 µm). The effect of scan rate can be qualitatively argued by considering the morphology of the oxidized surface at low (10 mV/s), intermediate (30 mV/s) and high scan rates (100 mV/s). This type of growth of oxide on the surface increases the electrochemically active or the real surface area of the electrode. Hence at low scan rate, the peak current is high. As the scan rate increases to 30 mV/s, the density of these needles like projections decreases substantially resulting in a decrease in the real surface area. While at a scan rate of 100 mV/s no needle-like structures were observed and the real surface area of the electrode is similar to that of bare un-oxidized copper foil. A similar type of surface growth on copper was also observed by D. Reyter et al. (Reyter et al. 2007) after the copper surface was polarized at a different potential.

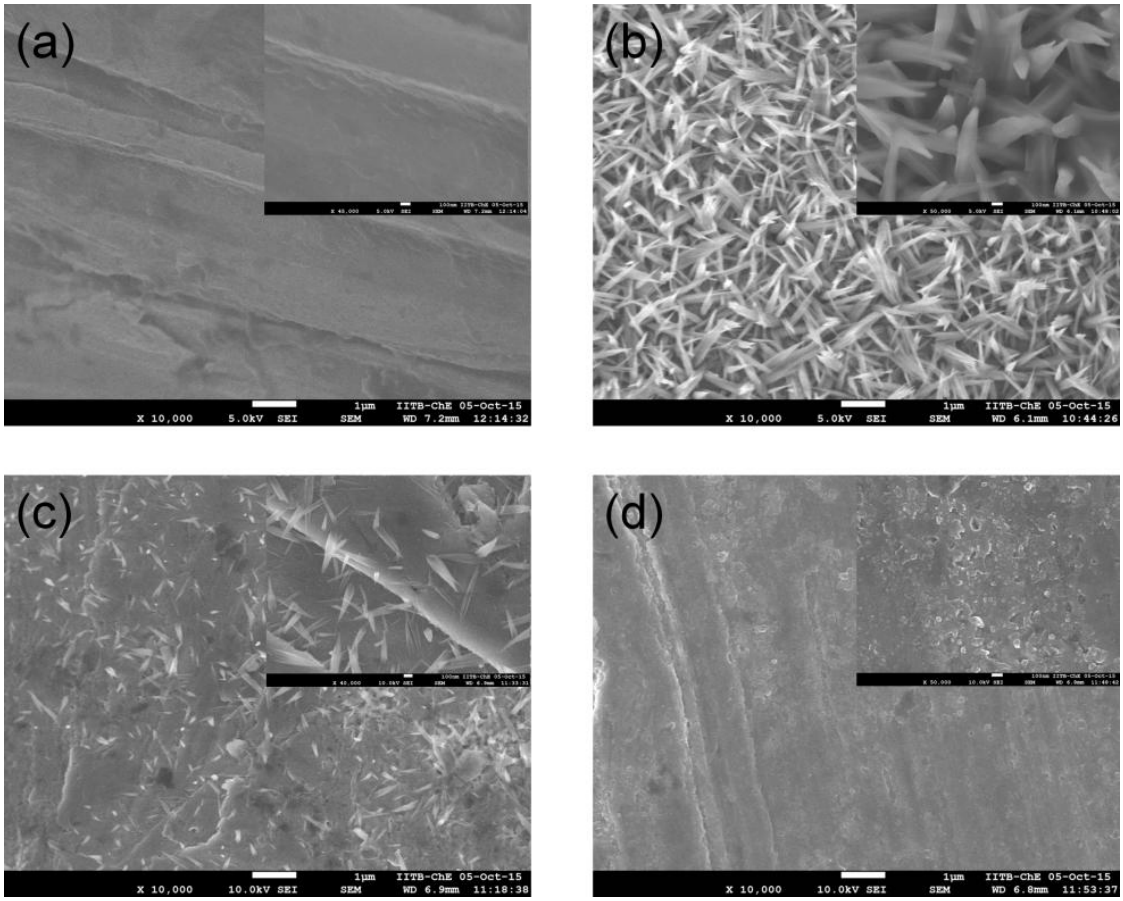

Figure 3.5: SEM images of (a) copper foil (b) copper foil oxidized by LSV (linear sweep voltammetry) at 10 mV/s scan rate (c) copper foil oxidized by LSV at 30 mV/s scan rate (d) copper foil oxidized by LSV at 100 mV/s scan rate. The inserts show the images of the same surfaces obtained at higher magnification. The LSVs were performed in Ar-saturated 0.5 M KOH.

Figure 3.6 shows the 2*p* core-level XPS profiles of the samples oxidized in the same fashion that used for SEM study (copper foils oxidized electrochemically by LSV from -1.2 V to 0.5 V at scan rates of 10, 30 and 100 mV/s). All the profiles show two main peaks corresponding to Cu $2p_{3/2}$ and Cu $2p_{1/2}$ centered at 934.5 eV and 954.1 eV, respectively. Additionally, two satellite peaks of Cu $2p_{3/2}$ and Cu$2p_{1/2}$ were also observed at 943 3 eV and 962 (±0.2) eV, respectively. All the XPS profiles were fitted by pseudo-Voigt method after background subtraction using Shirley's method. The deconvolution reveals the presence of the four different species Cu or Cu_2O, CuO and $Cu(OH)_2$ at 932.6 (±0.1) eV, 934.0 (±0.1) eV, and 935.2 (±0.1) eV, respectively (peak for both Cu and Cu_2O appears at 932.5 eV, which is indistinguishable) (Wan et al. 2013; McIntyre and Cook 1975; Deroubaix and Marcus 1992; Haber et al. 1978; McIntyre et al. 1981). The quantification results of the species Cu_2O, CuO

and $Cu(OH)_2$ as a function of scan rate is also shown in Figure 3.6. It can be clearly observed that the amount of CuO formed decreases with increasing scan rate, whereas the amount of $Cu(OH)_2$ produced increases with increase in the scan rate. This supports the earlier assertion that peak B_1 corresponds to the formation of $Cu(OH)_2$ while peak B_2 is primarily due to the formation of CuO.

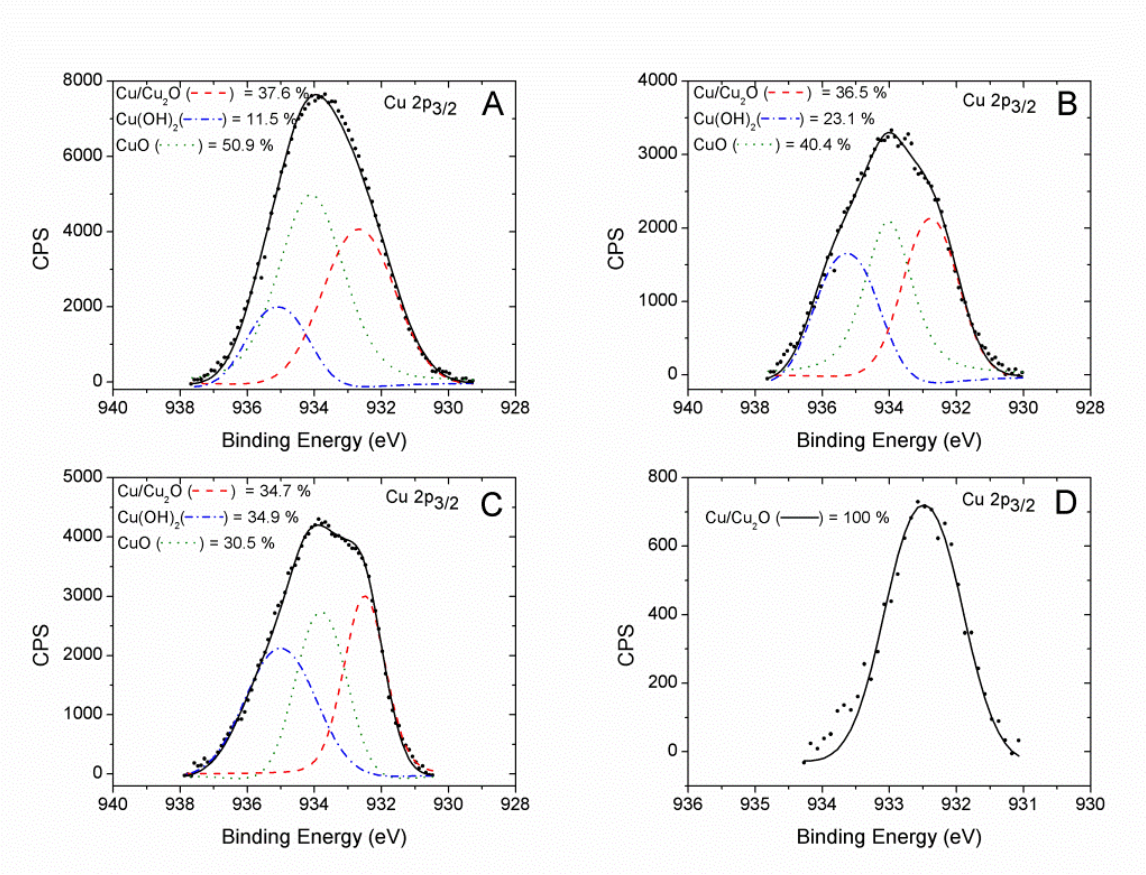

Figure 3.6 XPS profiles and fitting results of (A) copper foil oxidized by LSV at 10 mV/s scan rate (B) copper foil oxidized by LSV at 30 mV/s scan rate (C) copper foil oxidized by LSV at 100 mV/s scan rate (D) copper foil. The LSVs were performed in Ar-saturated 0.5 M KOH.

Peak C and D

In the reverse scan (i.e., from positive potential end to negative potential end), once again two peaks were observed, peak C and peak D. In the reduction regime, no major changes in shape were observed for the peak C with respect to scan rate unlike peak D, which broadened and segregated into multiple peaks at lower scan rate. Further, the shape of the peaks (C and D) also remained invariant with respect to concentration, albeit the peak

positions shifted towards negative potential and the peak intensities increased as the concentration of OH^- increases. To assign reactions to these two peaks during reduction scan, CVs were carried out by changing the turnaround potential as shown in Figure 3.7.

In the reduction regime, three distinct changes were observed with respect to turn around potential. When the potential at the positive end was reduced to 0.1 V from 0.5 V, the area of peak C started decreasing, and the peak potential moves positive without any significant changes in peak D. As the turnaround potential further moves towards more negative value (in the potential range of peak B_1, from 0.1 V to -0.1 V), peak area of peak D starts decreasing and peak C disappeared. Interestingly, continuing decreasing the turnaround potential towards more negative value (-0.1 V to -0.2 V), a new peak was observed between peak C and D (marked here as E), and more interestingly both the peak C and D disappeared. Further moving the turnaround potential towards negative value (-0.2 V to -0.3 V), shifts the peak observed between peak C and D (peak E) to a higher potential.

From the above experiments with changing turnaround potential, following qualitative arguments can be put forward:

1. From the oxidation wave corresponding to peak A and B, it can be inferred that insoluble species produced during peak B_2 (primarily $Cu(OH)_2$, and CuO) got reduced at peak C in potential range 0.1 V to 0.5 V. This is comparable to oxidation behaviour of noble metal surfaces where species with higher oxidation state formed at higher potential gets reduced first when the cycle was reversed. However, the peak area of peak B_2 is significantly more than that of peak C implying only a fraction of the oxides got reduced. Further, based on the change in Gibb's free energy, it can be concluded that the thermodynamic driving force for reduction of CuO to Cu is more than that for $Cu(OH)_2$ to Cu. Thus it can be argued that peak C is predominantly due to the reduction of CuO to metallic copper.
2. Peak D probably corresponds to the reduction of some soluble species trapped inside the pores as well as the reduction of remaining oxides. It is important here to reiterate that when the turnaround potential was between 0.1 V to 0.5 V; peak D did not manifest any significant change. It disappeared only when the turnaround potential was below -0.1 V implying a reduction of the oxidation products during peak B_1.
3. Peak E probably corresponds to the reduction of Cu_2O to metallic Cu only.

Even though the variation of turnaround potential indicates the possible reduction reactions, exact steps in mechanism remain unknown. Further, as proposed by Shoesmith et al. using XPS and Brisard et al. using PBD method, Cu_2O remains in the film along with CuO. This would necessitate another reduction wave similar to peak E, between peak C and D but no such peak observed in full potential scan (Figure 3.7).

Clearly, the reduction behaviour of oxides of copper are complicated and involve many steps similar to that of oxidation. Nonetheless, additional insights may be obtained if the number of copper atoms on the surface is known. With this thought, we have embarked on studying the redox behaviour of a copper monolayer on platinum in alkaline media and comparing it against the behaviour of bulk copper. The oxidation of copper monolayer has a great advantage as the number of copper atoms can be estimated with good accuracy and can be corroborated with the hydrogen desorption charges and based on the charges during oxidation of copper and peak position, species formed from the oxidation of metallic copper can be confirmed. Further, as only one layer of copper is available for the oxidation, a multilayered film consisting of different oxides and hydroxides will not be observed in this case, this further simplifies the study of the oxidation of copper.

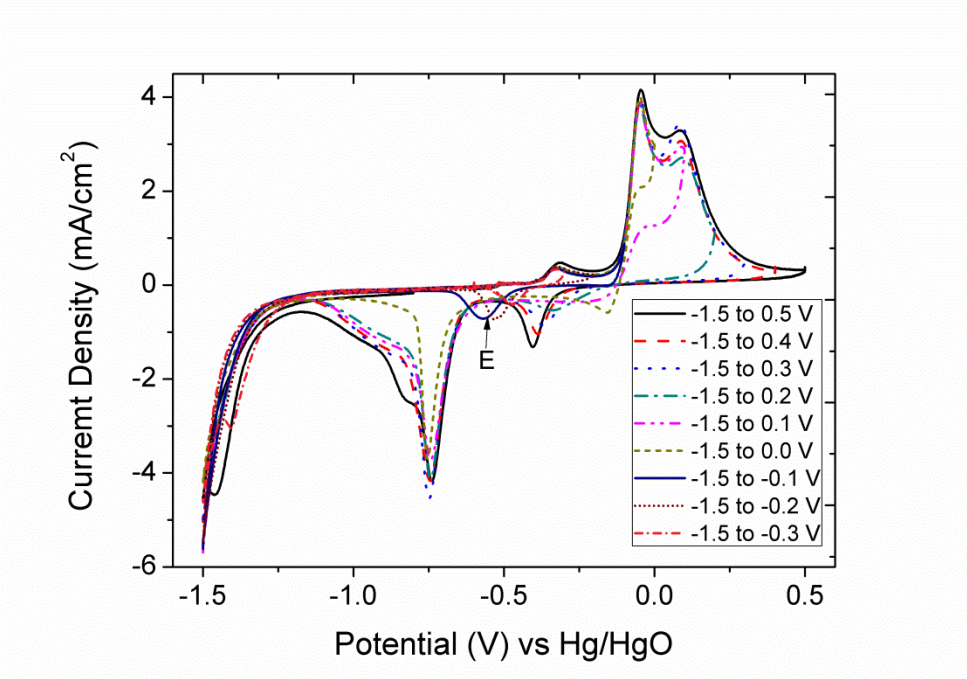

Figure 3.7: Cyclic voltammograms of the bulk copper electrode in argon saturated 0.5 M KOH at a scan rate of 50 mV/s and different turnaround potential.

3.3.2 Copper Monolayer Characterization in 0.5 M KOH Solution

The under potential deposition (UPD) of copper on platinum is a fairly well-known phenomenon for deposition of copper atoms in a monolayer fashion on the platinum surface at a potential positive to that of the Nernst potential (Green and Kucernak 2002; Trasatti and Petrii 1992). Figure 3.8 shows overlays of platinum CV and that of under potentially deposited copper monolayer CV in 0.5 M H_2SO_4. In 0.5 M H_2SO_4, the hydrogen desorption on platinum occurs in a potential range of -0.68 to -0.3 V versus Hg/Hg_2SO_4 during oxidation scan (i.e., when potential is moved to positive end from negative end). It is characterized by two prominent current peaks in the said potential range, and at still higher potential (0.1 to 0.5 V versus Hg/Hg_2SO_4) platinum surface gets oxidized (Rodríguez, Melián, and Peña 2000; Essalik, Amouzegar, and Savadogo 1995; Yamamoto et al. 1979). While for the electrode with a Cu monolayer deposited on platinum, no peaks corresponding to hydrogen desorption were observed in the range of -0.68 to -0.3 V during oxidation scan. Indeed, if copper is deposited as a complete monolayer, no platinum surface will be available for the hydrogen adsorption and as consequence hydrogen desorption peak will not be observed during oxidation scan. As the potential is moved positive (> -0.4 V), two current peaks corresponding to the stripping of copper atoms from the platinum surface were observed. Literature suggests that these two peaks correspond to site-specific desorption or stripping of Cu atoms.(Francke et al. 2008) After complete stripping of copper, a current corresponding to oxidation of platinum was again observed as well as that for hydrogen adsorption.

An accurate check for the monolayer formation of copper can be done by estimating the charge due to hydrogen desorption and copper stripping. Evaluation of platinum surface area by utilizing the charge due hydrogen desorption peaks is fairly well known, where one hydrogen atom gets adsorbed on each platinum atom by transfer of one electron. For under potentially deposited copper, one copper atom gets deposited on each platinum atom accompanied by transfer of two electrons. This implies that for the same catalyst-coated electrode, charge under copper stripping peak should be double than that of charge under hydrogen adsorption peak (Green and Kucernak 2002). Indeed, charge under hydrogen desorption peak was found to be 923 μC, while charge calculated under copper monolayer peak was found 1835 μC (~923×2). This confirms the formation of a copper monolayer on the platinum surface.

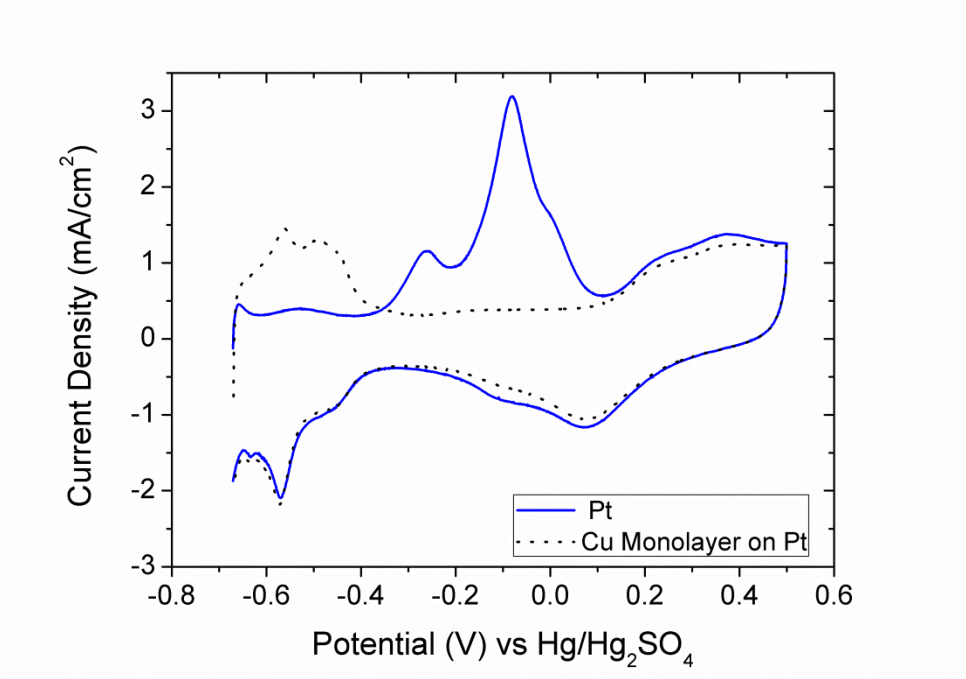

Figure 3.8: Overlay of the cyclic voltammograms of 20 wt% platinum nanoparticles supported on carbon and copper monolayer deposited on the 20 wt% platinum nanoparticles in argon saturated 0.5 M H_2SO_4 at a scan rate of 50 mV/s.

Similar to the cyclic voltammogram of platinum in acidic media, cyclic voltammogram of platinum in alkaline solution also shows the usual features of hydrogen desorption and platinum oxidation as the potential is moved from -1.0 to 0.35 V versus Hg/HgO. Further, akin to the cyclic voltammogram of copper monolayer deposited on platinum in acidic media, no peaks were observed in the hydrogen desorption region in basic media. However, as the potential is moved beyond hydrogen desorption potential range of -1 to -0.6 V versus Hg/HgO, a small hump was observed similar to the pre-wave shoulder observed in the cyclic voltammogram of bulk copper. As the potential is moved further in the same direction, a current peak of significantly higher intensity than that of platinum surface oxidation was observed in potential region -0.3 to 0.0 V. Evidently, the peak corresponds to oxidation of copper to Cu_2O similar to peak A in case of bulk copper, but much broadened and the peak potential is shifted towards positive potential as shown in Figure 3.9. The shift in peak potential for under potentially deposited copper probably manifests the greater affinity of copper atoms to underlying platinum atoms and imparts a degree of nobility vis-a-vis oxidation. One of the key advantages of monolayer deposition being that the oxidation state of Cu can be determined by simply comparing the charges as the amount of Cu on Pt is known beforehand. However, the charge under this peak would correspond to both oxidations

of copper and platinum. In a rather simple way, if it is assumed that the oxidation of Pt and Cu are independent, the charges due to oxidation of pure Cu can be obtained by subtracting the charges due to oxidation of platinum. The charge evaluated was 892 μC, which is approximately half that required to deposit a monolayer of Cu and close to that for hydrogen adsorption. This indicates that oxidation of copper follows a one-electron transfer reaction suggesting monolayer film formation of Cu_2O. Furthermore, the peak current of this oxidation peak was plotted against scan rate as shown in the inset in Figure 3.10. The data shows a good fit to a straight line implying chemisorptions of OH^- ions and a pseudocapacitive behaviour.

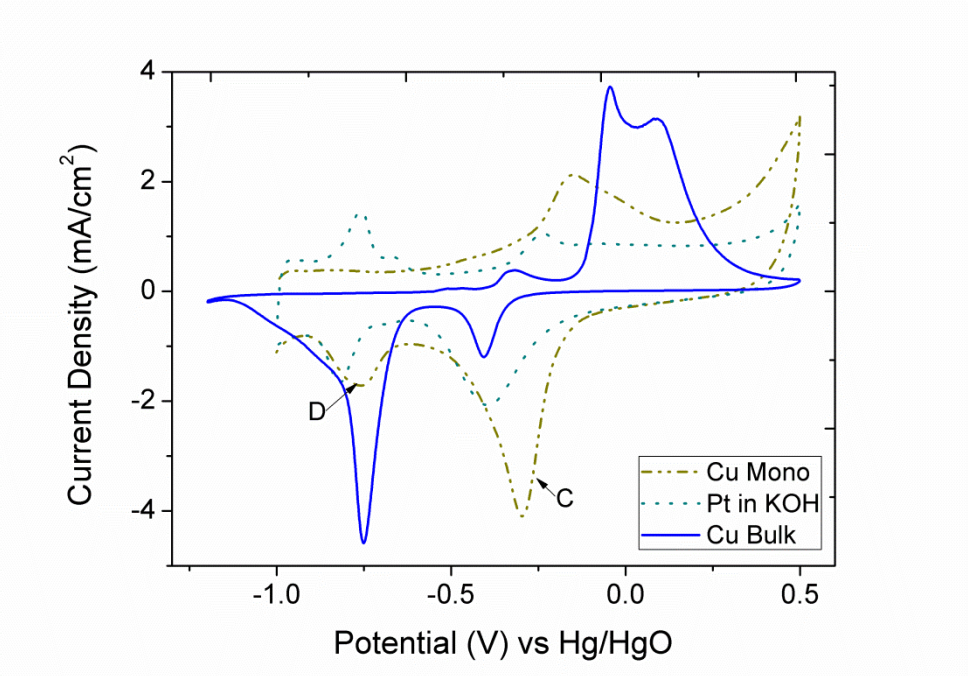

Figure 3.9: Overlay of the cyclic voltammograms of 20 wt% platinum nanoparticles supported on carbon electrode, copper monolayer deposited on the 20 wt% platinum nanoparticles supported on carbon electrode and a bulk copper electrode in Ar saturated 0.5 M KOH at a scan rate of 50 mV/s.

Interestingly, while the cyclic voltammogram of copper monolayer deposited platinum electrode in alkaline solution indicates no hydrogen desorption peak, repeated cycling reveals the gradual appearance of hydrogen desorption peaks again, and the signal intensity increases with the cycle number (Figure 3.11). It indicates that the oxidation of copper atoms produces some soluble species probably, which dissolves in the solution to free some platinum surface for adsorption of the hydrogen. The potential cycling data further indicate that the extent of formation of soluble species is maximum in the first cycle. From evaluation of the charges under the hydrogen adsorption peak, approximately 4.66% copper get dissolved in the

electrolyte in the form of water-soluble species in the first cycle, after that the dissolution percentage drops. After few cycles, the familiar CV of platinum was obtained again albeit with a smaller value of charges due to hydrogen desorption.

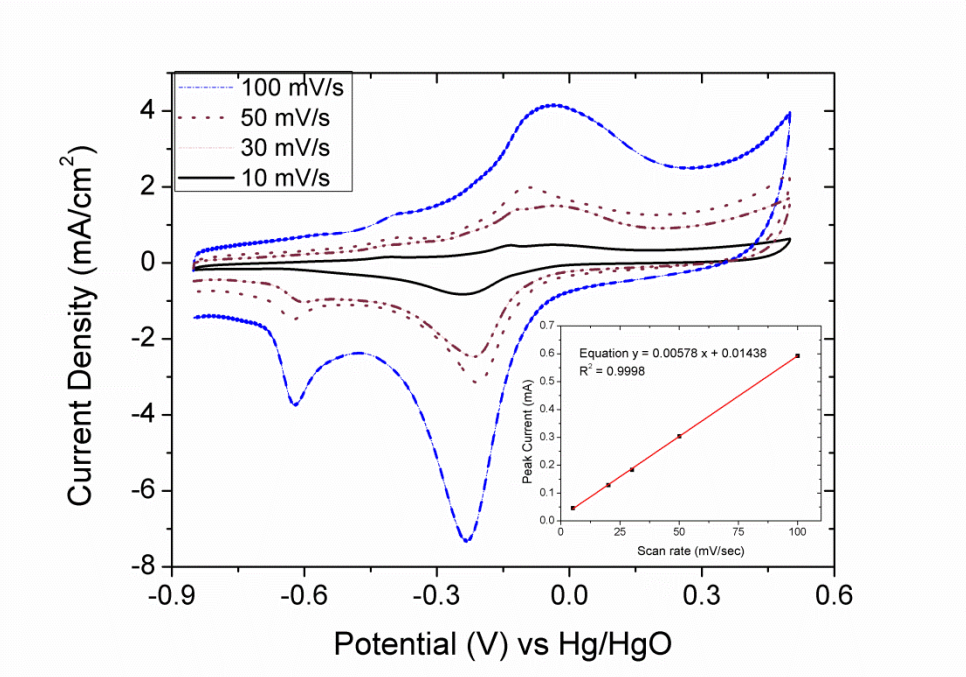

Figure 3.10: Cyclic voltammograms of a monolayer of copper on 20 wt% platinum nanoparticles on carbon electrode in argon saturated 0.5 M KOH solution at a scan rate of 10, 30, 50 and 100 mV/s. The inset shows the peak current vs. scan rate, and a straight line fit obtained.

Similar to the bulk copper electrode, during the reverse scan (i.e., reduction), two current peaks were observed peak C and peak D initially, and a third peak was observed after few cycles. The third peak (peak E) probably corresponds to hydrogen adsorption as the peak position is same as shown in Figure 3.11. The two other peaks namely C and D qualitatively look similar to that of bulk copper but for the amount of charge under first peak C which is much more than peak D, unlike the reduction wave in bulk copper electrode.

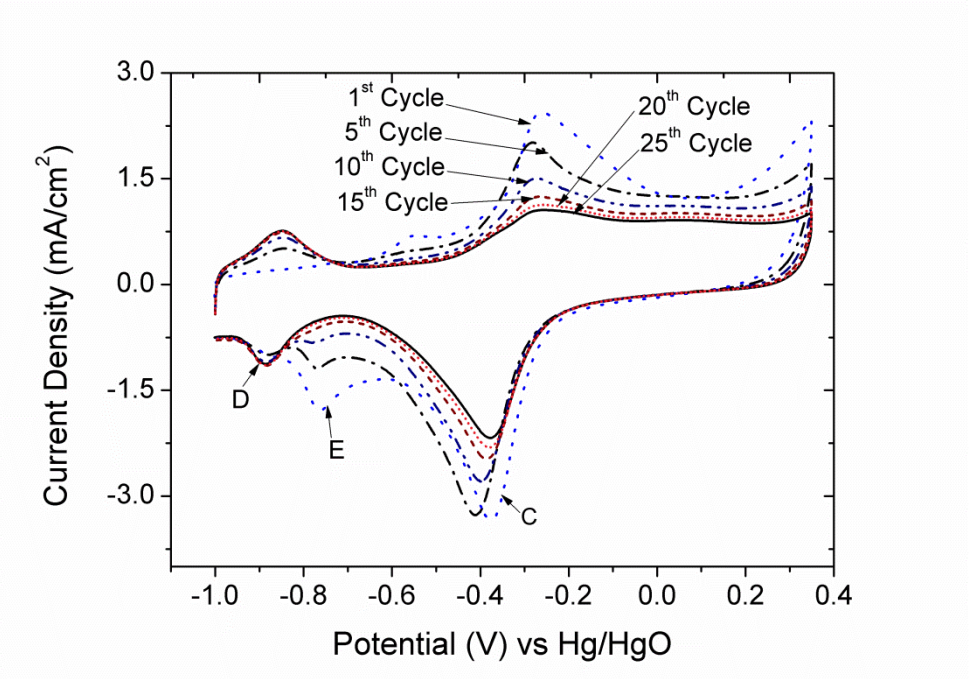

Figure 3.11: Different cycles of cyclic voltammograms of a monolayer of copper on 20 wt% platinum nanoparticles on carbon electrode in argon saturated 0.5 M KOH solution at a scan rate of 50 mV/s.

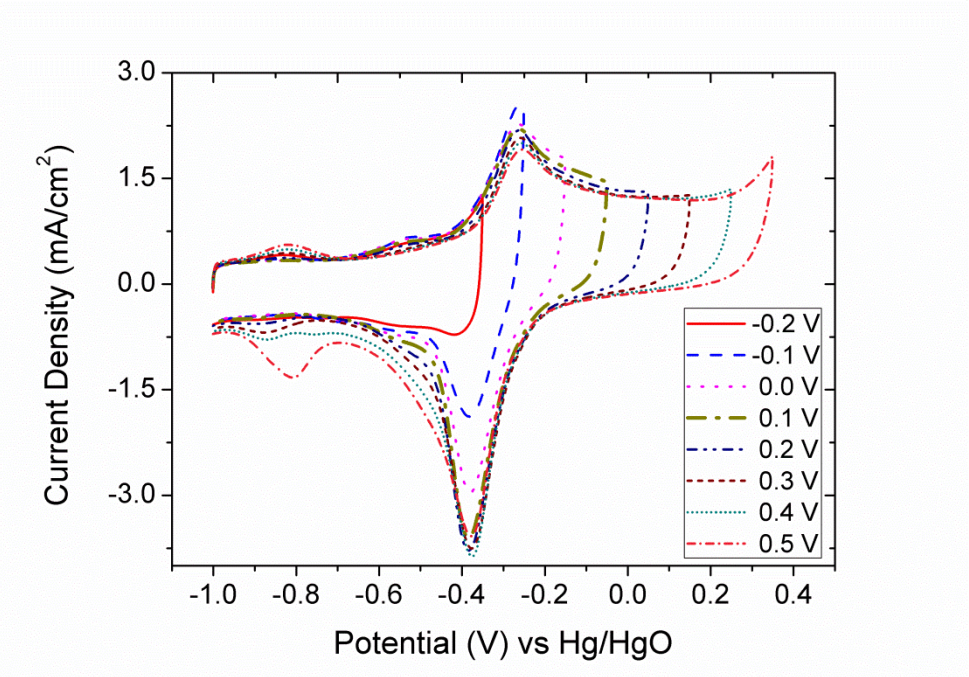

Figure 3.12: Cyclic voltammogram of copper monolayer deposited on 20 wt% platinum nanoparticles on carbon electrode in argon saturated 0.5 M KOH at a scan rate of 50 mV/s and different turnaround potential.

To investigate further and assign reaction to these peaks, CVs were obtained by changing the turnaround potential from the positive potential end as shown in Figure 3.12. As the potential is moved toward negative (i.e., from 0.5 to -0.3), the intensity of peak D start reducing and at 0.1 V peak D disappears completely as shown in Figure 3.12. However, hardly any change in the intensity of peak C was noticeable. This suggests that peak D is probably due to the reduction of $Cu(OH)_2$/ $Cu(OH)_4^{2-}$ species produced at higher potential via oxidation of Cu_2O. Whereas, evaluation of charges under peak A and peak C suggest that the peak C is due to the reduction of Cu_2O to Cu. It is interesting to note that the CVs of copper monolayer upon repeated cycling shows no change if the turnaround potential is below 0.1 V. Evidently, for copper monolayer, soluble species ($Cu(OH)_4^{2-}$) get produced only at potential higher than 0.1 V in contrast to bulk copper electrode where it is produced at fairly lower potential in the range of the peak B_1. Further, there is hardly any effect of a change in turnaround potential on the charges under peak C as long as turnaround remains more than 0.1 V, suggesting a reduction of a complete monolayer of Cu_2O produced during oxidation scan.

3.4 Electrochemical Characterization of Copper in 0.5 M Na_2CO_3 Solution

The CV of Bulk Cu in 0.5 M Na_2CO_3 at 50 mV/s scan rate is shown in Figure 3.13. Two peaks during anodic scanning were also observed in 0.5 M Na_2CO_3 similar to 0.5 M KOH solution. However, the intensity of the peak B is much lower than observed in KOH solution. After peak B, a flat steady current can be seen, indicating continuous growth the oxide film. This flat current may due to the adsorption of CO_3^- ions on the copper surface. This adsorption results in the formation of a passive film on the copper surface which prevents the further oxidation of the copper surface and may contribute to the low anodic current observed in this electrolyte as compared to voltammetry in the 0.5 M KOH solution. The total charge under both the anodic peaks (~200 µC) is much less than the total charge observed under two anodic peaks in 0.5 M KOH solution (~3500 µC). In the cathodic scan of bulk copper again two peaks were observed similar to the peaks observed in 0.5 M KOH solution. However, in a reversal of trends, the peak intensity for peak C is higher than that observed for of 0.5 M KOH while the peak intensity of the peak D is much smaller than that observed in KOH solution.

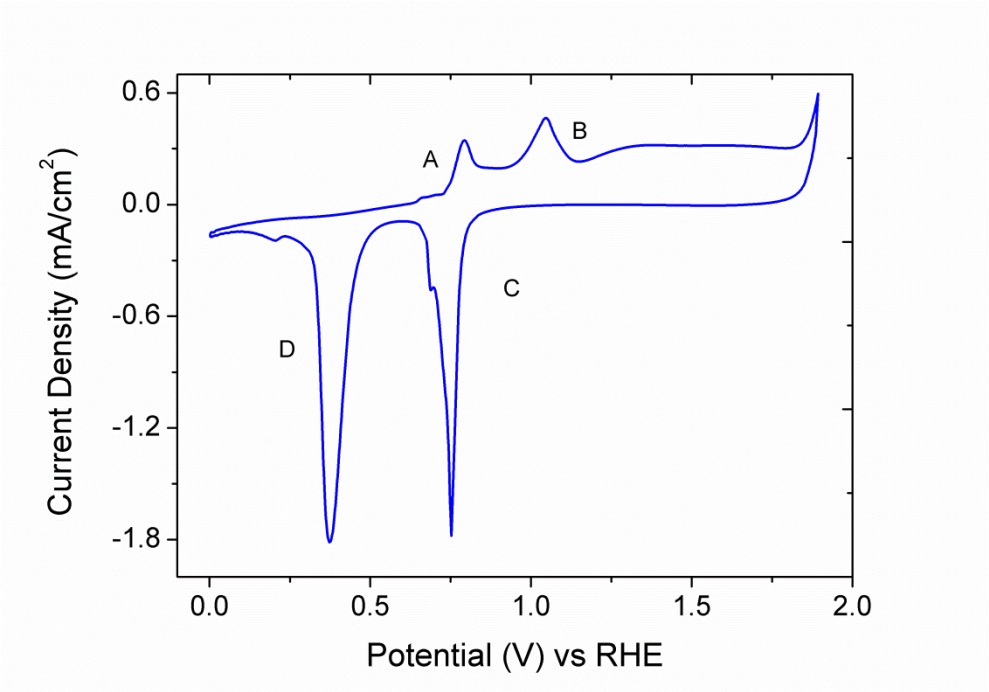

Figure 3.13: Cyclic voltammogram of the bulk copper electrode in Ar saturated 0.5 M Na_2CO_3 solution at 50 mV/sec scan rate.

The comparisons of the anodic and cathodic peaks charges suggest that the charge under the cathodic peaks (~570 µC) is more than that of anodic peaks (~200 µC). The higher cathodic charge observed in Na_2CO_3 solution compared anodic charge may be due the flat current observed after peak B during oxidation due to which true anodic charge was not able to calculate. It is has been reported that flat current profile may be due to the adsorption of CO_3^- ion on the surface and formation of copper carbonate species. These copper carbonate species generates a passive film on the electrode surface. The possible reactions of CO_3^- ions with copper are shown in reaction 3.14, 3.15 and 3.16. The pKs values of the reaction show the thermodynamically it possible to form copper carbonate along with copper oxides under applied potential and were further confirmed by the XPS (Gonzalez et al. 1998). Figure 3.14 shows the CV of copper at a scan rate of 20, 50 and 100 mV/s in 0.5 M Na_2CO_3 solution. It can be seen from the Figure 3.14, with an increase in the scan rate the peak currents are increases.

$$Cu^{2+} + 2OH^- + CO_3^{2-} + 2Na^+ \rightarrow Cu(OH)_2(CO_3)Na_2 \quad \text{.....(3.14)}$$

$$2Cu^{2+} + 2OH^- + CO_3^{2-} \rightarrow Cu(CO_3)Cu(OH)_2 \quad \text{.....(3.15)}$$

$$3Cu^{2+} + 2OH^- + 2CO_3^{2-} \rightarrow 2Cu(CO_3)Cu(OH)_2 \quad \text{.....(3.16)}$$

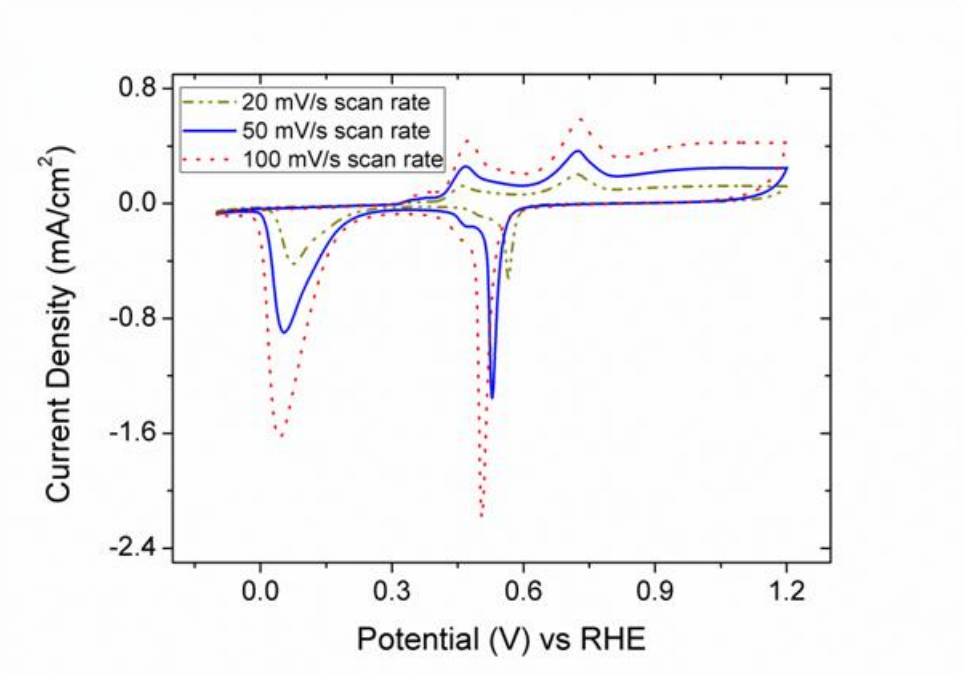

Figure 3.14: Cyclic voltammogram of the bulk copper electrode in Ar saturated 0.5 M Na_2CO_3 solution at 20, 50, 100 mV/sec scan rate.

3.5 Electrochemical Characterization of Copper in 0.5 M $NaHCO_3$ Solution

The CV of the bulk copper electrode in 0.5 M $NaHCO_3$ at 50 mV/s scan rate is shown in Figure 3.15. Similar to the voltammograms of bulk Cu in KOH and Na_2CO_3 solution, two current peaks along with a current plateau at a high potential during anodic scanning of potential were also observed in 0.5 M $NaHCO_3$ at low scan rates. However, as the scan rates increased, the separate peak was no longer discernible and peak A and B merged. Charge under peak A (30 µC) is very less than expected for a monolayer of Cu_2O at a scan rate 50 mV/s. Further, peak B does not appear to be a separate peak and get immersed into the plateau of current observed at a high potential, similar to peak A with getting immersed in peak B. and the long plateau.

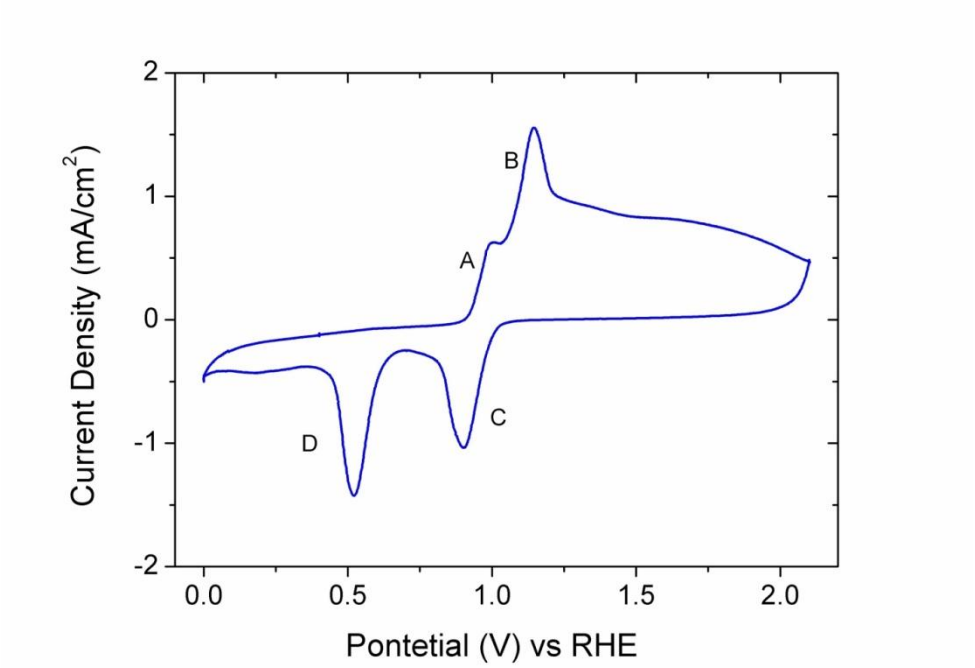

Figure 3.15: Cyclic voltammogram of the bulk copper electrode in Ar saturated 0.5 M $NaHCO_3$ solution at a scan rate of 50 mV/sec.

In reverse scan, two distinct peaks (peak C and peak D) were observed. However, the charge under these two peaks is much lower than peak A and peak B and charge under the plateau put together. This behaviour can be explained similarly to that for the carbonate ions present in the solution will get adsorbed on the copper surface to form copper carbonate. As mentioned above, bicarbonate ions will produce a passive film with mostly consists of copper oxides and copper carbonate with prevents further oxidation of the copper. This passivation may be the possible reason for the less anodic current that has been observed in 0.5 M $NaHCO_3$ solution compared to those observed in 0.5 M KOH solution.

The cyclic voltammogram of bulk copper CV in 0.5 M $NaHCO_3$ at three different scan rate viz 20, 50 and 100 mV/s is shown in the Figure 3.16. As scan rate is increased from 20 mV/s to 100 mV/s, increase in the current was observed like 0.5 M Na_2CO_3 solution unlike in 0.5 M KOH solution, higher oxidation current was observed at low scan rate than 30 mV/s. Further, the comparison between the CV of bulk copper electrode in these electrolytes shows that in the case of 0.5 M $NaHCO_3$ solution peak position for anodic peaks in CV of copper shift towards positive potential compared to 0.5 M Na_2CO_3 for which the anodic peaks in CV of bulk copper also shifted to positive potential compared to 0.5 M KOH solution (Figure 3.17). This may due to the lower pH of these two solutions compared to the 0.5 M KOH.

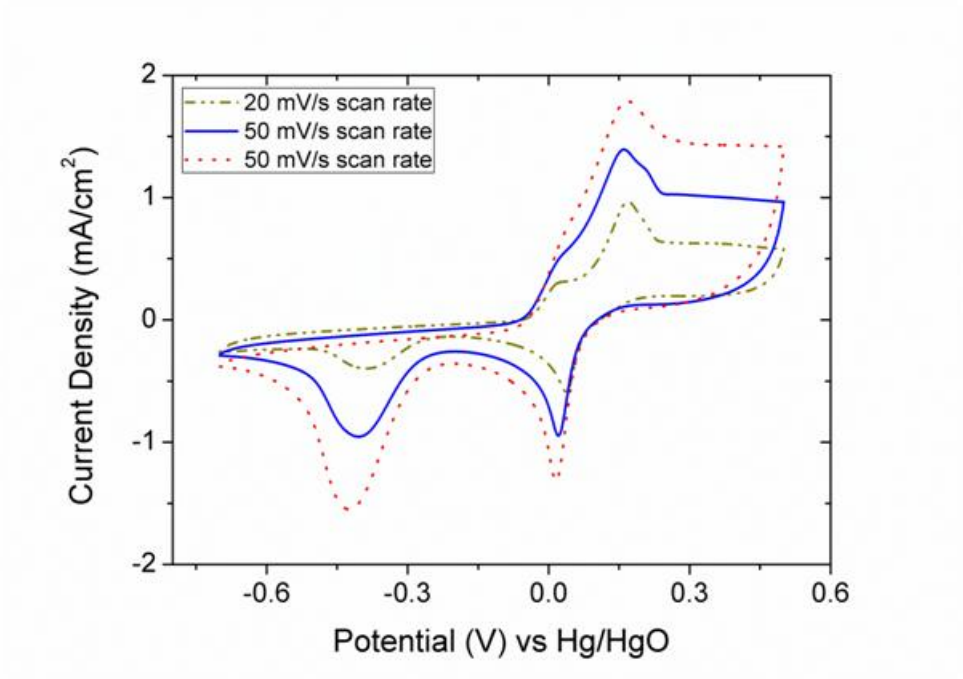

Figure 3.16: Cyclic voltammogram of the bulk copper electrode in Ar-saturated 0.5 M NaHCO3 solution at 20, 50, 100 mV/sec scan rate.

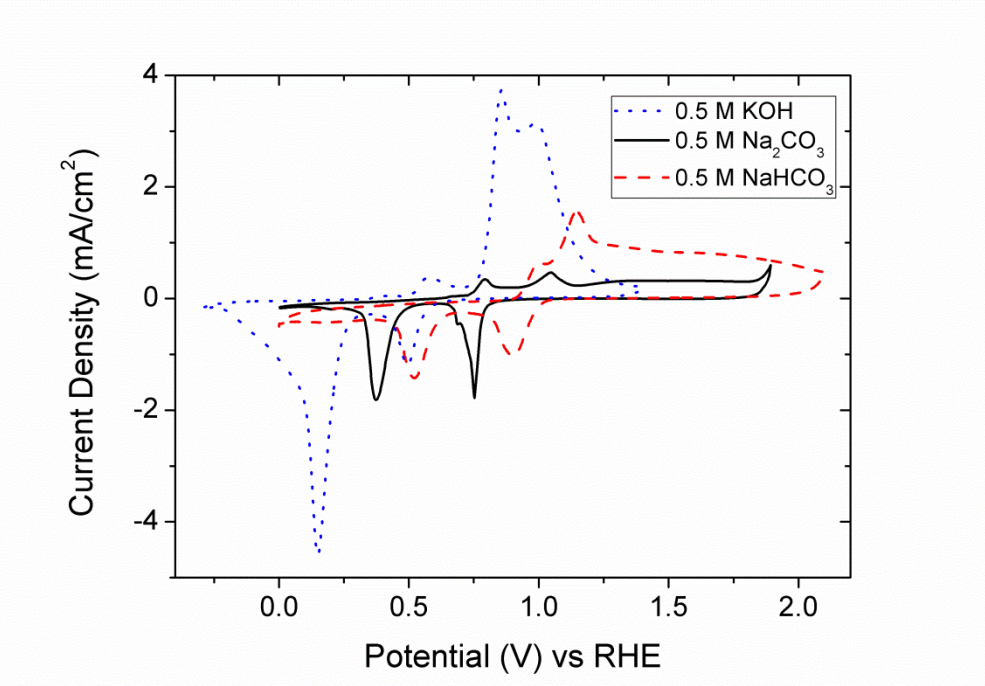

Figure 3.17: Cyclic voltammogram of the bulk copper electrode in Ar saturated 0.5 M $NaHCO_3$ solution at a scan rate of 50 mV/sec.

3.6 Conclusion

Electrochemical studies on oxidation of both the bulk copper electrode and under potentially deposited copper atoms have been performed in alkaline media. The experiments done here confirms that Cu_2O produced by initial oxidation of copper results in the formation of a monolayer film for certain range of scan rate and pH. Upon increasing the potential, copper atoms oxidizes to form $Cu(OH)_2$ along with soluble. Further, increase in potential results in the formation of CuO. These charge transfer reactions manifest as two peaks in the cyclic voltammograms. The SEM images of the electrochemically oxidized copper foils indicate the formation of needle-like structures which might explain the atypical relation between the peak currents and scan. Voltammetry data suggest that the final product of oxidation is a mix of CuO, $Cu(OH)_2$ and $Cu(OH)_4^{2-}$. This has been verified further by XPS analysis of the oxidized copper foils. Subsequent reduction of the final products of oxidation proceeds in two stages (i) initially only a fraction of CuO gets reduced to metallic Cu and (ii) the rest of oxidized species gets reduced at still lower potential.

By comparing the behaviour of bulk copper with copper monolayer deposited on platinum, several key aspects have been noted. Evaluation of charges suggests that the primary oxidation product is Cu_2O. Although, dissolution of copper indeed takes place, but at significantly higher potential and only a fraction of Cu_2O reacts further to $Cu(OH)_2$ and $Cu(OH)_4^{2-}$. While the initial stages of oxidation of copper seem to mimic that for bulk copper, the onset potential is significantly higher. Similar features have also been observed during later stages of oxidation. This suggests that the underlying platinum layer imparts a degree of nobility to copper monolayer with respect to oxidation.

Further, cyclic voltammogram of copper in 0.5 M Na_2CO_3 solution shows a different signature than that of in 0.5 M KOH solution. The shape, as well as the charge under peaks, is less than that observed in the CV of 0.5 M KOH. This may be due to the formation of a passive oxide layer produced due to the interaction with carbonate ions present in the solution. Unlike CVs in 0.5 M KOH solution, peak current increases with increase in scan rate in the studied potential range. Moreover, cyclic voltammogram of copper in 0.5 M $NaHCO_3$ solution shows slightly different signature than that of in 0.5 M KOH as well as in 0.5 M Na_2CO_3. In case of this electrolyte also, the peak currents increase with scan rate, unlike 0.5 M KOH.

Chapter 4

Electrochemical Reduction of CO_2 on Copper Foil Activated by Electrochemical Methods

4.1 Introduction

As mentioned earlier in the literature review, the main requirement for successful electrochemical reduction of CO_2 is the large negative potential. In aqueous media, at these reduction potentials, hydrogen evolution reaction (HER) ($2H_2O + 2e^- \rightarrow H_2 + 2OH^-$) competes with the desired electrochemical reduction of CO_2 reaction (Y Hori 2008; Scibioh and Viswanathan 2004; Jitaru et al. 1997). Due to the HER, the selectivity of the CO_2 reduction reaction decreases. Thus, there is a need for efficient and selective catalysts. In general, bare metals often need to be activated before being utilized for CO_2 reduction. Search for better methods to activate the electrocatalysts that can significantly reduce the overpotential compared to bare metals is an ongoing area of research. It may be interesting to note that activation of the electrodes for faster kinetics is required not just for electrochemical reduction of CO_2 but also for other reactions where copper is used, and frequently non copper electrodes also need to be activated for specific reactions.[2]

Literature suggests the activation of the metal electrode can be done by oxidizing the electrode surface deliberately and subsequently reducing it to metal. Typically, the oxidation can be achieved both by thermal as well as electrochemical means. As reported by Córdova et al. (Martins and Arvia 1980) the activity of gold electrode increases for HER when the gold electrode was subjected to the potentiodynamic perturbation in the form of intermediate repetitive triangular potential scan (RTPS) at a different scan rate and duration of the intermediate perturbation. Similarly, Vuković et al. (Vuković, Angerstein-Kozlowska, and Conway 1982) have reported the increase in the activity of ruthenium for the evolution of both Cl_2 and O_2 when ruthenium electrode was subjected to the anodic and cathodic potential cycling. Later Martins et al. (Martins and Arvia 1984) subjected copper electrode to potential scanning between hydrogen evolution potential to the potential for Cu_2O formation. The electrode thus activated, showed increased activity for HER. On similar lines, Reyter et al. (Reyter et al. 2007) showed that the activity of electrochemically activated copper surface increases for reduction of nitrate in alkaline solution. The electrochemical treatment of the

[2] A portion of the work reported in this chapter has been published in ECS Transactions 75.48 (2017): 19-31 and presented at PRiME 2016, Honolulu, Hawaii, USA.

copper surface was carried out by two different techniques. First, by cyclic voltammetry (CV) at a scan rate of 10 mV/s for 3000 cycles from the hydrogen evolution potential to the oxygen evolution potential and second by chronoamperometry (CA) at -0.1 V for 15 minutes (6). Both these electrochemical treatment resulted in the formation of a thick layer of copper oxides consisting primarily of Cu_2O and $Cu(OH)_2$. However, when the oxides thus produced were reduced to metallic copper electrochemically during the reduction reaction, a superior activity for both the HER as well as for the reduction of nitrate was observed.

In this context, there have been several works published on the electrochemical reduction of CO_2 using copper oxide and copper reduced from copper oxides as an electrocatalyst to produce methanol, methane, ethylene, and formate ions. Typically, copper foils were pre-treated by a combination of thermal and electrochemical treatments and the change in activity for the reduction of the CO_2 was investigated. Frese et al. (Karl W Frese 1991) investigated the effect of pre-treatment of copper foils such as anodization and annealing in air, and both anodization and annealing in the air on copper deposited electrochemically on titanium foils on electrochemical reduction of CO_2. The main product obtained was methanol, and the highest rate of production was on oxidized copper on titanium foil. Among thermal treatments, a thick layer of Cu_2O was also produced on the polycrystalline copper surface by annealing in the air by Li et al. (Li and Kanan 2012). The oxides thus produced was reduced to copper and then utilized for CO_2 reduction. It was found that copper reduced from Cu_2O reduction is more active for CO_2 reduction, and major product of CO_2 reduction was formate ions. Moreover, the current density and faradaic efficiency for the activated copper was higher than that obtained for polycrystalline copper. Recently, Kas et al. (Kas et al. 2014) deposited Cu_2O on copper surface electrochemically and CO_2 reduction was carried on this electrode. The major product of CO_2 reduction was ethylene. More recently Yadav V. and Purkait M. studied the electrochemical reduction of CO_2 on Cu_2O with Co_3O_4 as an anode. The major products were formic acid, formaldehyde, propanol, acetic acid, methanol, and ethanol (Yadav and Purkait 2016). Evidently, both thermal and electrochemical pre-treatments result in the form of activated copper. However, the nature of the activated copper is not well understood. Moreover, these treatments may result in an increase in electrochemical surface area, and the influence of an increase in the area on the rate of formation of products and the faradaic efficiency is not clear in the literature.

In this chapter, the effect of electrochemical pre-treatment in the form of oxidation and reduction on the activity of polycrystalline copper foils for reduction of CO_2 has been

discussed. In the subsequent chapter, specifically, an attempt is made to ascertain the effect of both thermal/thermochemical/annealing and electrochemical/anodization on the electrochemically active surface area and its relation to the rate of product formation and the faradaic efficiency. Electrochemical oxidation was carried out by linear sweep voltammetry (LSV) at 0.5 mV/s scan rate, cyclic voltammetry (CV) at a scan rate of 0.5 mV/s scan rate (5 cycles) and chronoamperometry (CA) at -0.1 V for 30 minutes in Ar saturated 0.5 M KOH solution. These were subsequently evaluated for CO_2 reduction. The oxidized and reduced copper foils were studied using scanning electron microscope (SEM) and X-ray photoelectron spectroscopy (XPS). The analysis of the products formed due to the reduction of CO_2 was done using high performance liquid chromatography (HPLC) and gas chromatography (GC). Further, the hypothesis on the increase in the roughness of the electrode surface (or electrochemically active surface area (EASA) or real surface area) due to the oxidation and subsequent reduction was verified by the measurement of the surface area before oxidation and after reduction of the oxidized surface by AFM and charge under the Cu_2O peak. These methods, however, were found to be unreliable as explained later and subsequently the measurement of EASA was performed by under potential deposition (UPD) of lead (Pb) on copper.

4.2 Experiments

4.2.1 Electrode

The standard three electrode system (working, reference and counter electrode) was used for all the electrochemical experiments in an electrochemical cell made up of a glass vessel of 50 ml capacity (It is common to use H-cell arrangement to separate cathode (working electrode) and anode (counter) by cation exchange membrane for the electrochemical reduction of the CO_2. Such arrangement is preferred as the products produced by the electrochemical reduction of CO_2 on cathode will not get oxidize on the anode. But in our case, the limitation imposed by the potentiostat on the higher value of potential difference that can be applied for the electrochemical reduction of CO_2 was not enough to carry out reduction reaction at a significant rate. Using an H-cell for the electrochemical reduction of the CO_2 will put extra resistance due to the significantly large distance between the anode and cathode.) Along with the electrochemical cell, all other glassware were washed once with aqua regia and then thoroughly rinsed with de-ionized water to avoid contamination. The working electrode was made up by a 2 cm × 2 cm piece of copper foil (extra pure, supplied by

Loba Chemie), cleaned by immersing in 20 % (v/v) aqueous solution of HNO_3 and then washing thoroughly with de-ionized water. The counter electrode used was a platinum mesh for copper oxidation studies in 0.5 M KOH and a gold foil for used for CO_2 reduction experiments in 0.5 M $NaHCO_3$. Reference electrode used was Hg/HgO in 0.3 M KOH solution. All potentials referred here are versus the Hg/HgO reference electrode.

4.2.2 Electrolyte

The 0.5 M KOH solution was prepared by dissolving the required quantity of KOH pellet (AR grade, 99% purity, Merck, India) in de-ionized water. For the electrochemical oxidation of copper foil by CV, LSV, and CA, 0.5 M KOH solution was first saturated by bubbling high purity argon (Ar) gas for 30 minutes. The 0.5 M $NaHCO_3$ solution was prepared by dissolving required amount of $NaHCO_3$ in de-ionized water. Electrochemical reduction of CO_2 was carried out at the different potential in high purity CO_2 purged 0.5 M $NaHCO_3$ solution. Electrochemical oxidation of copper was carried out by LSV at a scan rate of 0.5 mV/s, CV at 0.5 mV/s scan rate from -1.2 V to 0.5 V for 5 cycles, and CA at -0.1 V for 30 min. Figure 4.1 shows the potential versus time program employed during these three methods for copper oxidation. After CV/LSV/CA in argon saturated 0.5 M KOH solution, the oxidized copper foil was taken out from the electrochemical cell and washed thoroughly with deionized water. In case of oxidation by CV, the 5^{th} cycle was stopped just after the anodic scan.

For the UPD of Pb (lead) on copper, a 0.01M $HClO_4$ + 1 mM $PbCl_2$ solution was prepared by adding required quantity of the concentrated $HClO_4$ and $PbCl_2$ in de-ionized water. For the subtraction of capacitive charges in UPD, cyclic voltammetry of copper foils was carried out in 0.01 M $HClO_4$ + 2mM KCl. Both the solution was saturated with argon gas before performing the electrochemical experiments. To obtain the potential for the monolayer deposition of the lead, the lead was deposited on copper in bulk fashion, and open circuit potential (OCP) was measured. The OCP was observed to be -850 mV against Hg/Hg_2SO_4 reference electrode. After the OCP measurement, CV at a scan rate of 10 mV/s was obtained in the potential range of 50 mV negative to OCP to 310 mV positive to the OCP. In these range of the potential peak corresponding to the monolayer adsorption and desorption of lead appears. The charge under the lead desorption peak has been selected for the estimation of the surface area as this reaction will be free from the mass transfer limitations.

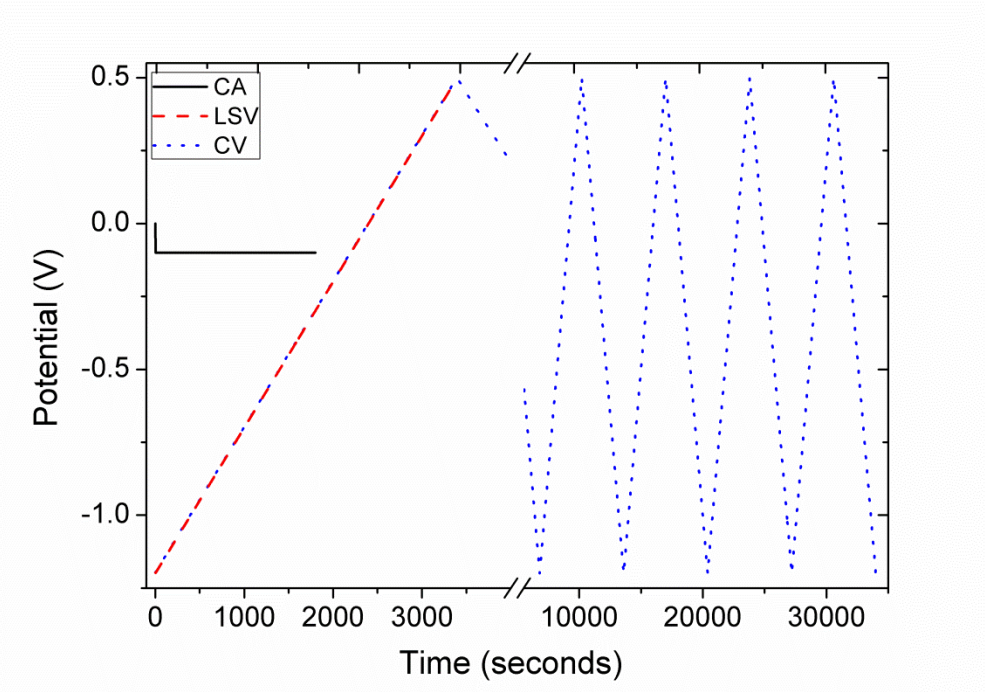

Figure 4.1: Potential versus time program employed for the electrochemical methods CA, LSV and CV used for the oxidation of the copper in Ar saturated 0.5 M KOH solution.

4.2.3 Equipment

Biologic (Model No. VSP-300) Potentiostat along with EC-Lab V10.34 software was used for all electrochemical data collection and analysis. The XPS analysis and SEM images were obtained on a small piece cut from the oxidized copper foils as well as on reduced copper foils. The XPS analysis was carried out on AXIS Supra (Kratos Analytical, UK) XPS machine. The SEM images at different magnification were captured by JEOL JSM 7600 (FEG-SEM) scanning electron microscope. Further, UV-Visible spectroscopy analysis of oxidized and reduced copper foil was carried out by dissolving the oxide layer produced on the copper foil in 0.05 M HCl solution. Since the concentration of copper ions generated due to the dissolution of oxides in acidic solution was quite low; ammonium hydroxide was used to complex the cupric ions to increase the accuracy of the measurement. UV-Visible spectroscopy analysis was carried out on a Shimadzu spectrophotometer (Model-UV-1650 PC). The wavelength selected for the concentration analysis was in visible range (560 nm). The spectrophotometer was calibrated by diluting 0.5, 1, 2, 3 and 4 ml of 0.05 M $CuSO_4$ solution to 10 ml by adding 0.05 HCl solution. In all the standard samples, 1 ml of ammonium hydroxide was added. The 0.05 M $CuSO_4$ solution was made by dissolving the required quantity of $CuSO_4 \cdot 5H_2O$ in de-ionized water. Additionally, atomic force microscopy (AFM)

analysis of copper foil reduced for 5 minutes during CO_2 reduction was carried out in an Origin, Asylum/Oxford instruments AFM machine (Model: MFP3D) to estimate the surface roughness.

Both the liquid and gaseous products of CO_2 reduction were collected at an interval of 30 minutes. High performance liquid chromatography (HPLC) (1260 infinity series) supplied by Agilent Technologies (USA) with Aminex HPX-87H column (Bio-Rad, USA) was used for the quantification of the liquid products. The mobile phase used in the analysis was 13 mM H_2SO_4 aqueous solution prepared by adding required volume of concentrated H_2SO_4 (18 M) in de-ionized (DI) and subsequently sonicating it for 30 minutes to remove any dissolved gases. As the pH of the electrolyte is higher than the operating pH range of the HPLC column (1 to 3), all the samples were acidified by adding required volume of 1 M H_2SO_4 solution to bring down the pH. For gaseous samples, gas chromatography GC) supplied by Nucon Engineers (India, model 5700) with PORAPAK column was used. High purity argon (Ar) gas was used as carrier gas for all the sample analysis.

4.3 Results and Discussions

4.3.1 Characterization of the Electrode

The CV of copper in 0.5 M KOH solution shows two oxidation peaks and two reduction peaks (Giri and Sarkar 2016). The first peak (when moving from negative potential to positive potential) which appeared during the oxidation is very small as compared to the second peak. It was suggested that the first peak is primarily due to oxidation of copper to Cu_2O and the second peak is due to the oxidation of the copper and Cu_2O to CuO and $Cu(OH)_2$ along with some water soluble species. Unlike, the CVs of noble metals (such as platinum) where the charges during anodic scan remain constant for different scan rate, the charges for copper change with scan rate. The charges under oxidation peaks remain constant with scan rate for scan range 30 mV/s to 100 mV/s, but when the scan rate was reduced below 30 mV/s, the charge under oxidation peaks starts increasing. Moreover, the charge (300 µC) under the first oxidation peak at 10 mV/s was observed to be 3 times than that observed at 50 mV/s (110 µC). This increase in charges suggests that the oxidation of copper at lower scan rate is not just restricted to surface oxidation. Instead, a multilayer film of oxides gets produced. Hence low scan rate (0.5 mV/s) was selected for the CV and LSV to form a thick layer of oxides on the copper surface. In CA experiment, -0.1 V potential was selected as the highest oxidation charge (Figure 4.2) was observed at this potential consistent with the

available literature (Reyter et al. 2007). The highest current would also mean the thickest film of oxides on the copper surface. The possible reason ascribed for this behaviour is the faster growth of the oxide in the ascending region of the peak B than at the descending region due to the formation of the passivating film of Cu(II) produced at a higher potential (refer to chapter 3, Figure 3.1).

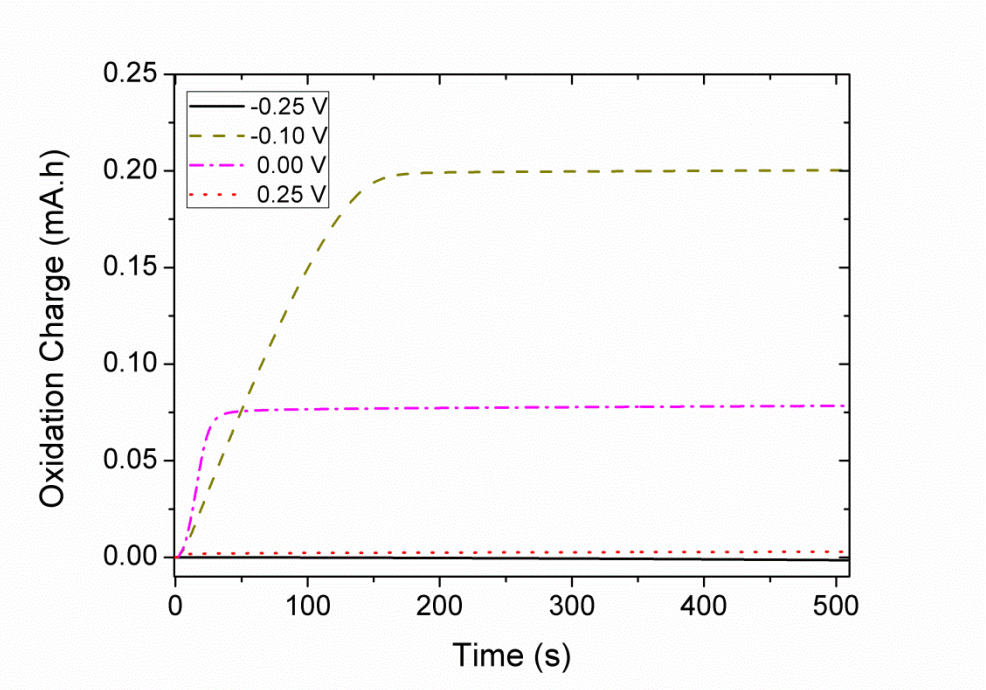

Figure 4.2: Oxidation charge for CA at potentials -0.25 V, -0.1 V, 0.0 V and 0.25 V vs. Hg/HgO in Ar saturated 0.5 M KOH solution.

The SEM images of copper surface oxidized by CA at -0.1 V for 30 min, LSV at 0.5 mV/s scan rate and CV 5 cycles at 0.5 mV/s scan rate in Ar saturated 0.5 M KOH solution and electrochemically reduced copper foil at -1.6 V initially oxidized by CA at -0.1 V for 30 min, LSV at 0.5 mV/s scan rate, and CV (5 cycles) at 0.5 mV/s scan rate are shown in Figure 4.3. The needles produced on the surface observed showed a multilayer growth of oxides similar to those reported earlier at a scan rate 10 mV/s (Giri and Sarkar 2016).

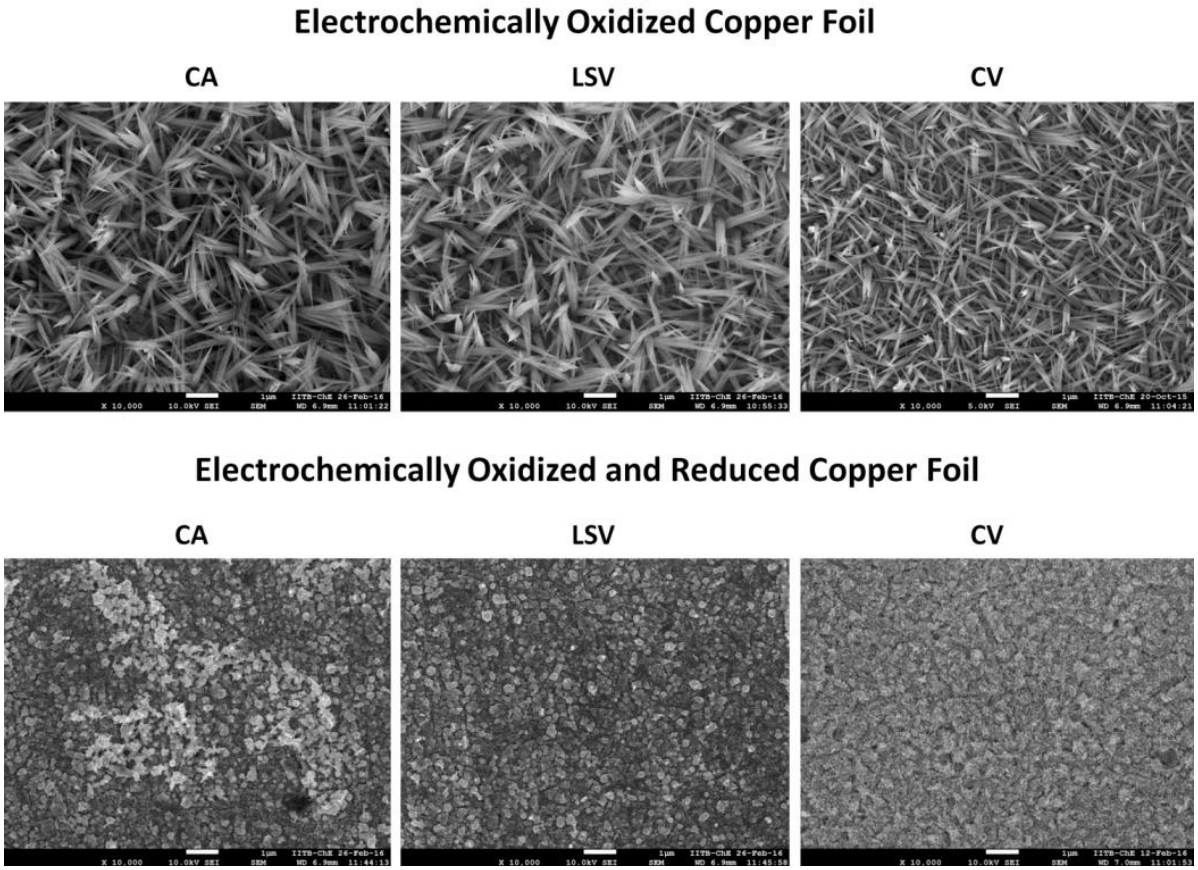

Figure 4.3: SEM images of copper foil oxidized by CA at -0.1 V for 30 min, LSV at 0.5 mV/s scan rate and CV 5 cycles at 30 mV/s scan rate. Electrochemically reduced copper foil at -1.6 V initially oxidized by CA at -0.1 V for 30 min, LSV at 0.5 mV/s scan rate and CV (5 cycles) at 0.5 mV/s scan rate The oxidation experiments were performed in Ar saturated 0.5 M KOH and the reduction was carried out in CO_2 purged 0.5 M $NaHCO_3$.

The deconvolution of the Cu $2p_{3/2}$ peak observed in XPS spectra of copper oxidized by CA at -0.1 V for 30 min, LSV at 0.5 mV/s scan rate and CV 5 cycles at 0.5 mV/s scan rate are shown in Figure 4.4. The deconvolution of the Cu $2p_{3/2}$ peak reveals the presence of Cu or Cu_2O, CuO and $Cu(OH)_2$ at 932.6 eV, 934.0 eV, and 935.2 eV, respectively. Before the deconvolution, the data was corrected by taking the reference of carbon (C 1s) peak (284.8 eV). However, deconvolution of the XPS spectra of reduced copper foil shows the presence of only Cu/Cu_2O. As the peak for Cu_2O and Cu is indistinguishable, most likely the peak corresponds to Cu^0 as thermodynamically at the potential for CO_2 reduction only metallic copper is stable (Wan et al. 2013; McIntyre et al. 1981; Deroubaix and Marcus 1992; Haber et al. 1978; McIntyre and Cook 1975). To confirm that the XPS peak at 932.6 eV correspond to copper only, spectrophotometric analysis was done for (a) copper foil initially oxidized by CA

at -0.1 V for 30 minutes and (b) oxidized by CA at -0.1 V for 30 minutes and then reduced at -1.6 V in CO_2 purged 0.5 M $NaHCO_3$ solution.

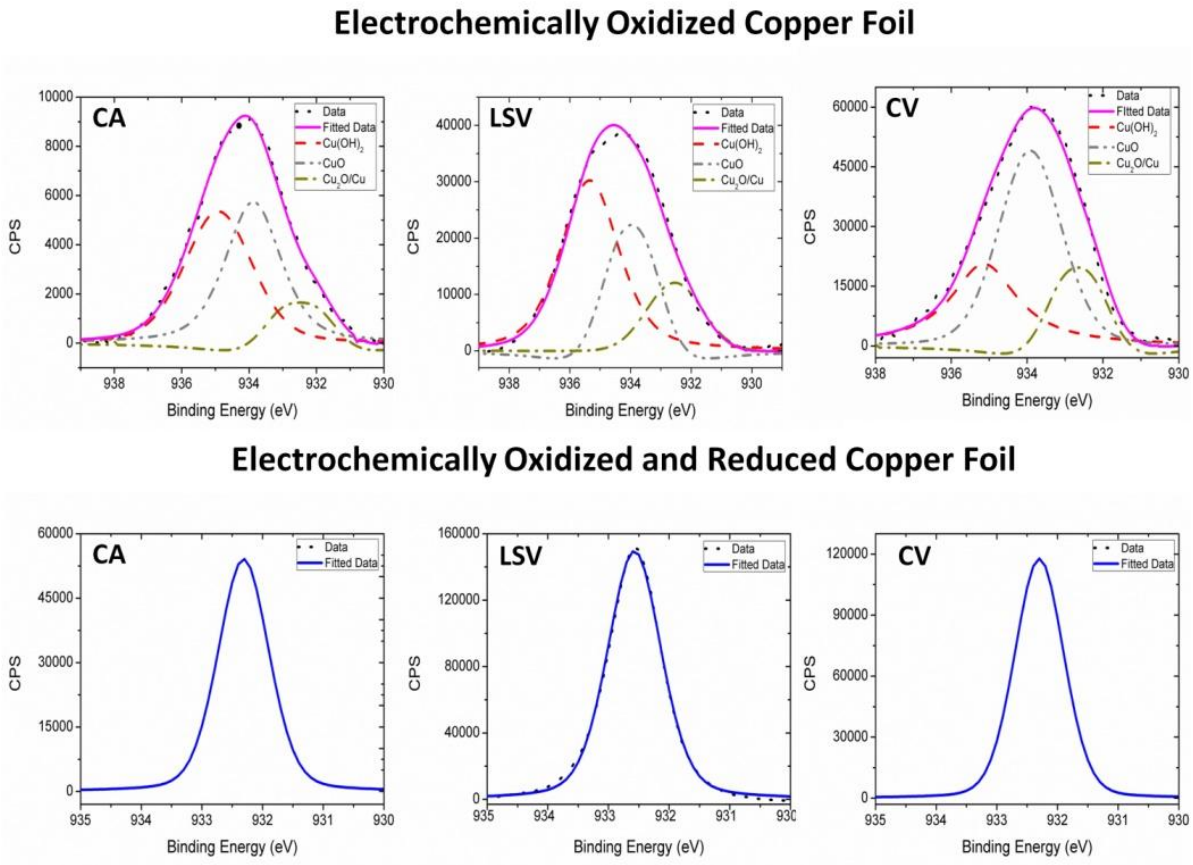

Figure 4.4: XPS analysis of copper foil oxidized by CA at -0.1 V for 30 min, LSV at 0.5 mV/s scan rate and CV (5 cycles) at 0.5 mV/s scan rate. Electrochemically reduced copper foil at -1.6 V initially oxidized by CA at -0.1 V for 30 min, LSV at 0.5 mV/s, and CV 5 cycles at 5 mV/s.

Table 4.1: Spectrophotometric analysis of cupric ions liberated after reduction of CO_2 at -1.6 V for 5 minutes in CO_2 purged 0.5 M $NaHCO_3$ on oxidized copper foil (oxidation carried out by CA at -0.1 V in Ar 0.5 M KOH solution). (* No electrochemical reduction of CO_2 was performed for this sample).

Sr. No.	Reduction Time (minutes)	Moles of Cu in Oxides (Before Reduction by Charge Calculation)	Moles of Cu in Oxides (After Reduction by Spectrophotometry)	% of Copper Oxides Reduced
1	0	1.623×10^{-5}	$1.46\times10^{-5*}$	-
2	5	1.623×10^{-5}	0.22×10^{-5}	86.44
3	10	1.623×10^{-5}	0.1×10^{-5}	93.84
4	15	1.623×10^{-5}	0.08×10^{-5}	95.09

Spectrophotometric analysis was carried out by immersing the reduced oxidized copper foil in dilute H_2SO_4 (0.05 M) solution for 1 minute so that if any oxides are present on the foil will dissolve in the dilute acid. Further, ammonium hydroxide solution was added to dilute H_2SO_4 solution to neutralize the acid and form an amine complex with the cupric ions (tetraamminediaquacopper(II) ions $[Cu(NH_3)_4(H_2O)_2]^{2+}$). Tables I shows the amount of oxide present on the copper foil after reduction for a different time interval at -1.6 V in CO_2 purged 0.5 M $NaHCO_3$ solution. It is interesting to note that the number of moles of Cu oxides (Cu^{2+}) as evaluated from the charge correspond to moles of Cu oxides obtained from the spectrophotometry data obtained after dissolution of the oxides. Further, it can also be seen that for a reduction of oxidized copper foil at -1.6 V for only 5 minutes, ~86% of oxides are reduced back to metallic copper. This value is less than that predicted by the XPS, which suggest all oxides reduced back to the copper. This may be due to the small overestimation of the oxidation charge to determine the exact amount of the oxides produced; probably due to the inclusion of the capacitive charges also which have not been subtracted. However, both methods do indicate that the reduction of CO_2 occurs on metallic copper and not on copper oxides. Further, the SEM images are shown in Figure 4.3, clearly shows that the within five minutes all the needles of the oxides goes to extinction leaving back small spherical particles of copper. Once all the needles have converted back to copper, further morphological changes do not occur for the rest of the CO_2 reduction process.

4.3.2 Estimation the Surface Area

As shown in Figure 4.3, after the reduction of the oxides produced due to the electrochemical oxidation small spherical particles. This results in an increase in the surface roughness/real surface area/EASA (electrochemically active surface area).

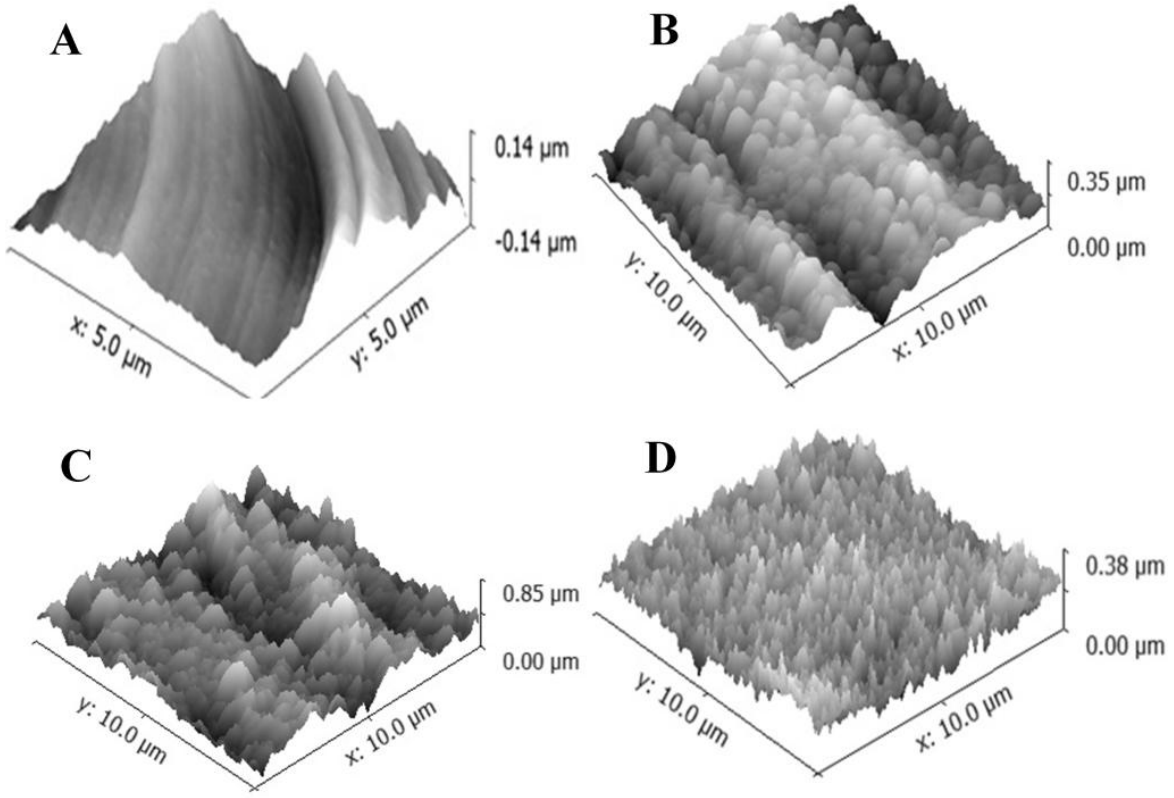

Figure 4.5: Atomic force microscopy images of the A) un-oxidized copper foil, copper foil oxidized by B) CA, C) LSV and D) CV and then reduced at -1.6 V for 5 minutes in CO_2 purged 0.5 M $NaHCO_3$ solution.

The roughness (EASA) of the surface was measured by two methods, AFM (atomic force microscopy) and electrochemical methods. The AFM was carried out in tapping mode to get the surface image and roughness of the surface was estimated in root mean square (RMS) roughness. It can be expected that as the roughness increases, the current for reduction of CO_2 will also increase (typically for a kinetics controlled reaction, the kinetic current increases proportionally to the real or electrochemical surface area). However, in this case, the highest CO_2 reduction current was observed in case of copper oxidized by the CV, and the highest roughness was observed for copper oxidized by LSV. Clearly, the roughness estimated by the AFM which measures the RMS roughness (standard deviation of the elevation in given area

(J. D. Miller et al. 1996)) does not corroborate well with the CO_2 reduction current data. One possible reason for the miss match may be due to the rolling operation on the foil while manufacturing (Figure 4.5). The copper foil surface (even un-oxidized) is not flat, and there is curvature to the rolling.

In case of the electrochemical surface, where roughness is defined as the ratio of real surface area to geometric surface area (EASA), a better match was observed. The real area can be estimated using the charge under the first oxidation peak observed during oxidation of copper ($Cu \rightarrow Cu_2O$) when the potential was moved in the positive direction. At scan rates from 30 to 100 mV/s, charge under this peak remains almost constant and was assumed to be due to formation for a monolayer of Cu_2O (Giri and Sarkar 2016; Fletcher, Barradas, and Porter 1978). For the charge density of 352 $\mu C/cm^2$, the real surface was estimated to be 0.314 cm^2 for a disk electrode with a diameter of 0.5 cm (see chapter 3).

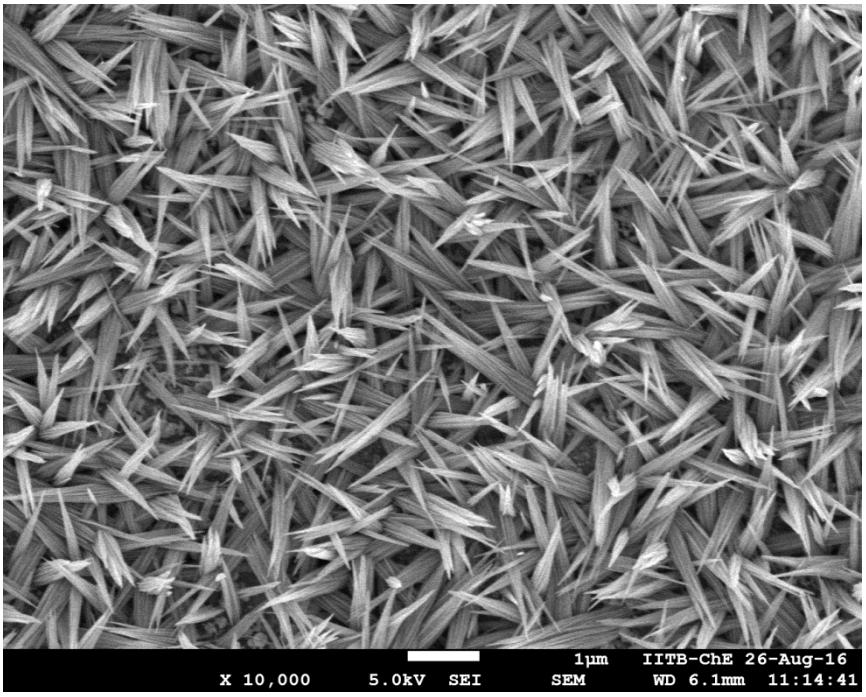

Figure 4.6: SEM image of copper foil sample after oxidation by LSV at 50 mV/s in Ar saturated 0.5 M KOH. The sample was initially oxidized in Ar saturated 0.5 M KOH at 0.5 mV/s followed by reduction at -1.6 V in CO_2 purged 0.5 M $NaHCO_3$ solution.

In the same fashion, EASA of the electrochemically oxidized and reduced copper foil was estimated and compared with un-oxidized copper foil to get the relative increase in the $EASA_{Cu2O}$. It was found that the highest $EASA_{Cu2O}$ was observed in case of copper oxidized

by CV (15.7), then followed by LSV (9.0) and CA (2.85) in consonance with the observed trend in reduction currents for CO_2 at -1.6 V. Although, the electrochemical $EASA_{Cu2O}$ data seem to corroborate with the pattern of currents per unit geometric area observed during CO_2 reduction (CV > LSV > CA), the currents per unit real area ($EASA_{Cu2O}$) shows opposite trend. To investigate further, the SEM images of the activated copper foil oxidized by LSV at 50 mV/s in Ar saturated 0.5 M KOH were obtained, and they show the formation of copper oxides needles (Figure 4.6). The activation was done by initially oxidizing the copper foil electrochemically in Ar saturated 0.5 M KOH at 0.5 mV/s followed by reduction at -1.6 V in CO_2 purged 0.5 M $NaHCO_3$ solution. Remarkably, this particular feature of needle like growth was not observed for pristine Cu foil samples at 50 mV/s (chapter 3). Hence, it is suspected that this method of evaluation of surface area by the formation of a monolayer of Cu_2O, overestimated the copper surface area.

Further, another electrochemical technique to estimate the EASA used was the UPD of Pb on the copper. The UPD of copper on platinum is one of the most well established methods for the estimation of the surface area of the platinum and well reported in the literature. In the same fashion, lead (Pb) can also be under potentially deposited on the copper to estimate the real surface area of the copper. The UPD is Pb on the copper is reported in the literature with detail analysis (Siegenthaler and Jüttner 1984; Vilche and Jüttner 1987; G M Brisard et al. 1995; Gessie M Brisard et al. 1997; Moffat 1998; Wu and Yau 2001). The UPD of Pd on copper was carried out in Ar saturated 0.01M $HClO_4$ + 1 mM $PbCl_2$ solution. Figure 4.7 shows two peaks when scanned from negative potential towards zero potential. The first peak is for the stripping of the bulk deposited Pb and the second peak is for the stripping of the monolayer of the Pb. Due to the large size of the lead atom than copper, the monolayer maximum theoretical coverage of lead atoms will be 0.53 for Cu (111) plane was estimated from the crystal lattice information of copper and lead. And the charge transfer for the maximum coverage will be 300 $\mu C/cm^2$. However, in case of polycrystalline copper by assuming equal contribution from three basic planes (100), (110) and (111) plane, the monolayer maximum theoretical coverage will be again 0.53 but the average amount of charge transferred to form this monolayer will be 250 $\mu C/cm^2$ (see appendix for detail calculation). For the calculation of the real surface area, charge under the Pb monolayer stripping peak was considered. The Pb stripping curve was first subtracted from the CV of copper in lead free 0.01M $HClO_4$ + 2 mM KCl solution to negate the effect of the interference of Cl^- ions.

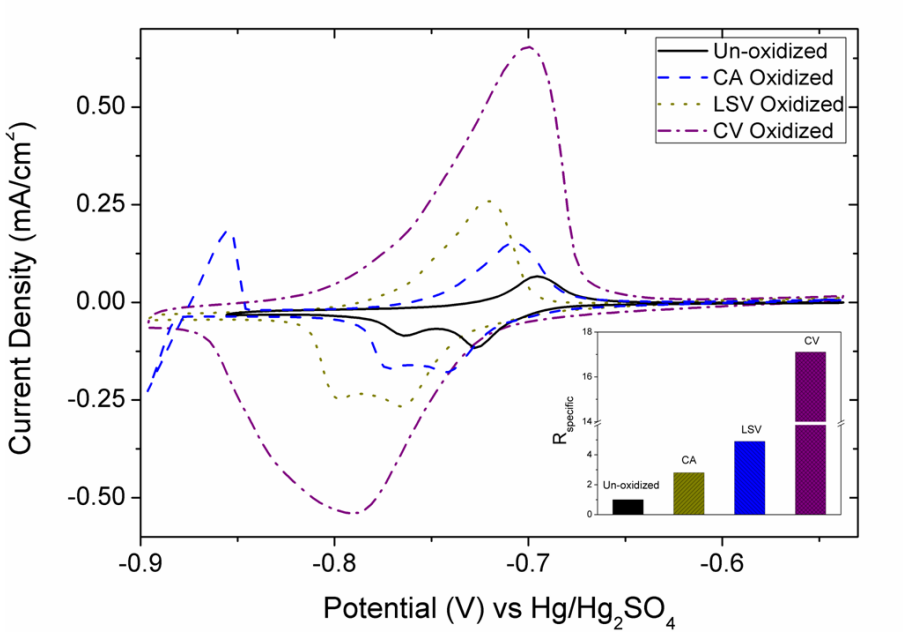

Figure 4.7: The under potential deposition (UPD) of lead (Pb) on un-oxidized copper foil, copper foil oxidized by CA at -0.1 V for 30 minutes, LSV at 0.5 mV/s and CV (5 cycles) at 0.5 mV/s in Ar saturated 0.01 M $HClO_4$ + 1 mM $PbCl_2$ solution at a c\scan rate of 10 mV/s. Figure in the inset shows a relative increase in the EASA of copper foil due to oxidation.

A copper foil of 1 cm × 0.5 cm geometric area was cleaned by immersing in 20% (v/v) aqueous nitric acid solution and then washed thoroughly with de-ionized water, and then transferred in Ar saturated 0.01 M $HClO_4$ + 1 mM $PbCl_2$. A CV at a scan rate of 10 mV/s was recorded in the potential range of -0.9 V to -0.58 V vs. Hg/Hg_2SO_4 electrode as shown in Figure 4.7. Again, the same copper foil of 1 cm × 0.5 cm geometric area was cleaned (by immersing in 20% (v/v) aqueous nitric acid solution and then washed thoroughly with de-ionized water) and then oxidized by CA using the same protocols as mentioned earlier. After electrochemical oxidation, the copper foil was transferred to the CO_2 purged 0.5 M $NaHCO_3$ solution and CO_2 reduction experiment was carried out at a potential of -1.6 V for 5 minutes during which along with CO_2 reduction copper oxides will also reduce back to the copper. After this reduction step, the copper foil was washed and transferred again in Ar saturated 0.01 M $HClO_4$ + 1 mM $PbCl_2$ for UPD of Pb. The same procedure was repeated for electrochemical oxidation by CV and LSV also using the same foil.

The Pb UPD on un-oxidized copper foil shows a charge under the stripping peak approximately 245 $\mu C/cm^2$ (total area = 2 X the foil dimensions) which very close to the theoretical value of 250 $\mu C/cm^2$ for polycrystalline copper. However, for copper foil oxidized

by CA, LSV and CV and reduced copper foil, the charge from Pb UPD for the copper foil of 1 cm^2 geometric surface area was 688.41 µC, 1199.49 µC, and 4192.10 µC, respectively. The relative increase in the $EASA_{UPD}$ for the CA, LSV and CV oxidized and reduced copper foil is 2.81, 4.90 and 17.11 times, respectively than that of the un-oxidized copper foil. These values of Pb UPD shows that the copper foil oxidized by the CV has more $EASA_{UPD}$ compared to copper foil oxidized by CA and LSV. This is in agreement with the fact that the CV has produced thicker oxides film as estimated from the total oxidation charges (charge transfer during oxidation for 1 cm^2 surface area for CV was 0.402 C, while for CA and LSV it were 0.0637 C and 0.325 C, respectively). Here after, the $EASA_{UPD}$ estimated by Pb UPD has been used for the calculations of the current density and rate of formation of format ions per unit real surface area.

4.3.3 Electrochemical Reduction of the CO_2 on Oxidized Copper Foils

Figure 4.8 shows the current density for electrochemical reduction of CO_2 on these four different electrodes at -1.6 V vs. Hg/HgO. As can be seen from the Figure 4.8, the current density for all the oxidized copper electrodes is almost 3 times more than that for the un-oxidized copper electrode. This suggests that the electrochemical oxidation and reduction yields a form of active copper which is superior compared to polycrystalline copper for electrochemical reduction of CO_2. When the current density obtained by dividing geometric surface area was normalized by a relative increase in the $EASA_{UPD}$, current density profile changes significantly. As shown in Figure 4.9, the current density for un-oxidized copper foil and copper foil oxidized by the CA shows same current density. However, for copper foil oxidized by LSV the current density is almost half of the current density observed for un-oxidized copper foil. In case of copper foil oxidized by CV, the lowest value compared to all oxidized and un-oxidized copper foil was obtained.

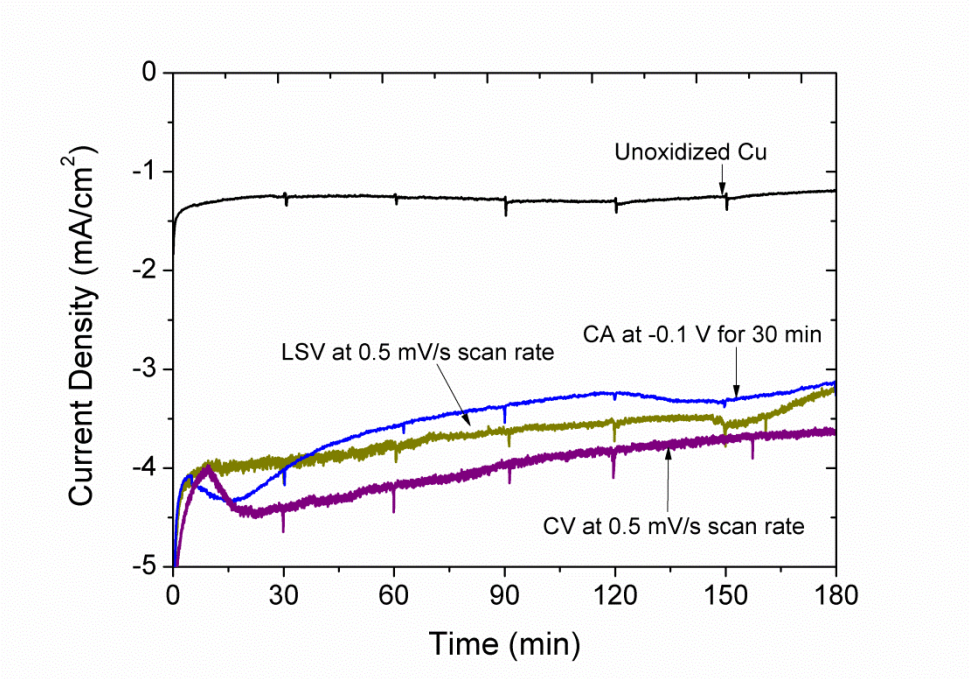

Figure 4.8: Current per unit geometric surface area vs. time at -1.6 V for a CO_2 reduction in CO_2 purged 0.5 M $NaHCO_3$ solution on un-oxidized copper and copper oxidized by three different electrochemical methods viz. CA at -0.1 V for 30 min, LSV at 0.5 mV/s scan rate and 5 cycles of CV at 0.5 mV/s scan rate in Ar saturated 0.5 M KOH solution.

The major products obtained for the electrochemical reduction of CO_2 was formate ions in aqueous phase and hydrogen in the gas phase. Figure 4.10 shows the amount of formate ions produced with time on three different oxidized electrodes at a reduction potential of -1.6 V. The amount of formate ions produced was highest for the copper oxidized by CV, while that for un-oxidized copper foil it was very small (not shown in Figure 4.10, amount of formate ions on un-oxidized copper foil has been compared with oxidized (electrochemical and thermochemical) copper foil in next chapter. Here a comparison between only the electrochemically oxidized copper foil has been done.). The second highest amount of formate ions produced is for CA activated and then followed by LSV activated. However, the amount of the formate ion produced on all these electrodes when normalized by $EASA_{UPD}$ shows a different picture. The highest amount of the formate ions has been now observed in case of copper foil oxidized by CA followed by LSV and then CV. Figure 4.11 shows the faradaic efficiency for formate ions production on these electrodes. Evidently, the faradaic efficiency is highest for the copper oxidized by CV.

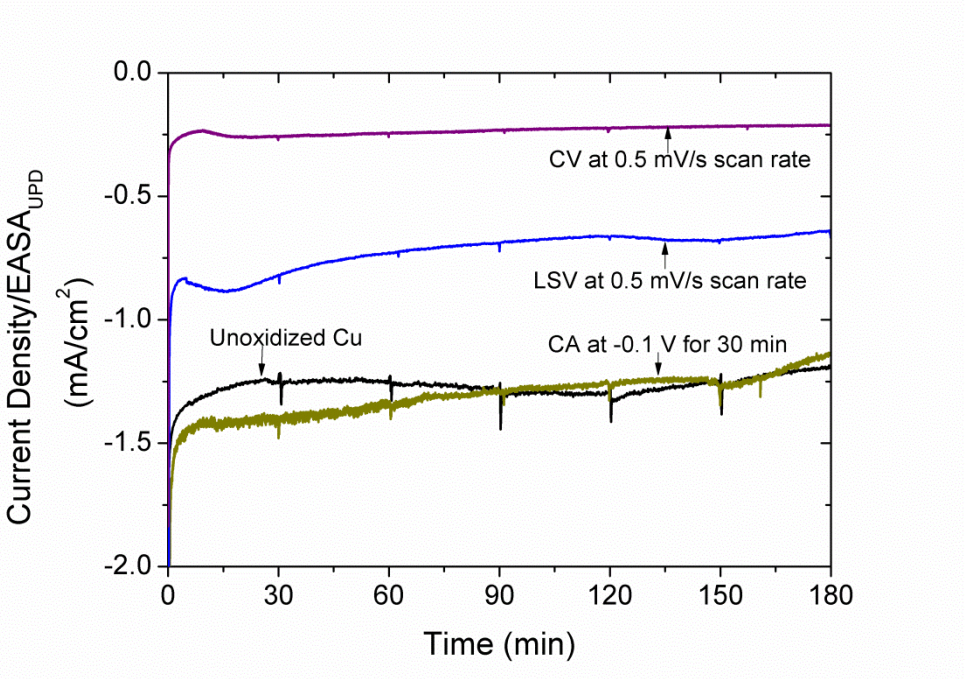

Figure 4.9: Current density normalized by $EASA_{UPD}$ vs. time at -1.6 V for CO_2 reduction in CO_2 purged 0.5 M $NaHCO_3$ solution on un-oxidized copper and copper oxidized by three different electrochemical methods viz. CA at -0.1 V for 30 min, LSV at 0.5 mV/s scan rate and 5 cycles of CV at 0.5 mV/s scan rate in Ar saturated 0.5 M KOH solution.

The highest increase in $EASA_{UPD}$ was observed for the copper foils oxidized by the CV, and it also showed the highest yield of formate ions as well as higher faradaic efficiency. However, the faradaic efficiency decreased with time for all the three samples. This decrease in faradaic efficiency may due to the deactivation of the copper electrode surface due to the CO_2 reduction. Hori Y. et al. (Y Hori et al. 2005) did extensive analysis on the deactivation of the electrode copper electrode surface during CO_2 reduction. They found that the major reason for the deactivation of the electrode is due to the deposition of heavy metals present in the electrolyte. The Fe and Zn present in electrolyte deposit on the copper surface during CO_2 reduction. This deposition is mostly sub monolayer. When the electrolyte was purified by electrolysis using platinum as an electrode, and all Fe and Zn removed, no deactivated of the electrode surface was observed. Hence they concluded that the deactivation of the electrode surface during CO_2 is not due to adsorption of the intermediates of reaction but due to the deposition of the metal on the electrode surface. We suspect that the deactivation in our case may be the same where the impurities most likely like came as leachant from the glass vessel.

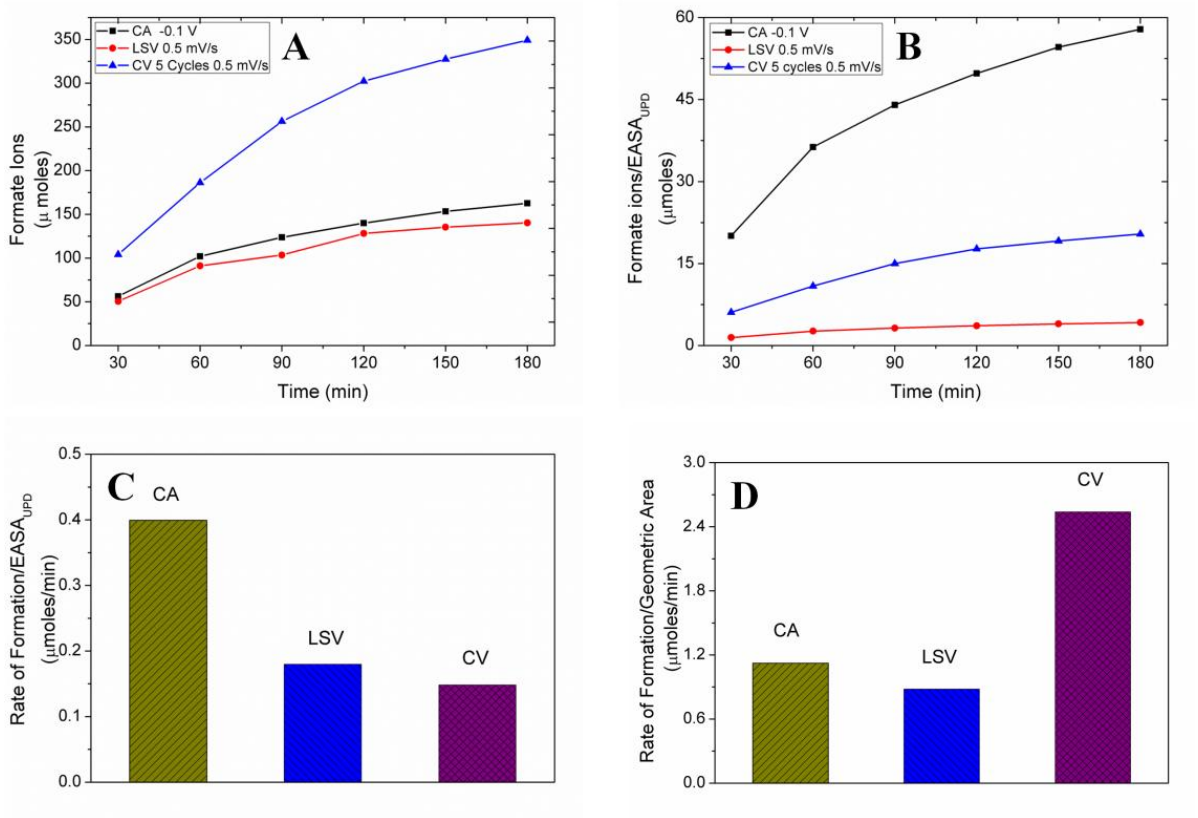

Figure 4.10: The amount of formate ions produced with time during reduction of CO_2 in CO_2 purged 0.5 M $NaHCO_3$ solution on electrochemically oxidized copper by CA at -0.1 V for 30 min, LSV at 0.5 mV/s scan rate and 5 cycles of CV at 0.5 mV/s scan rate after normalizing with $EASA_{UPD}$.

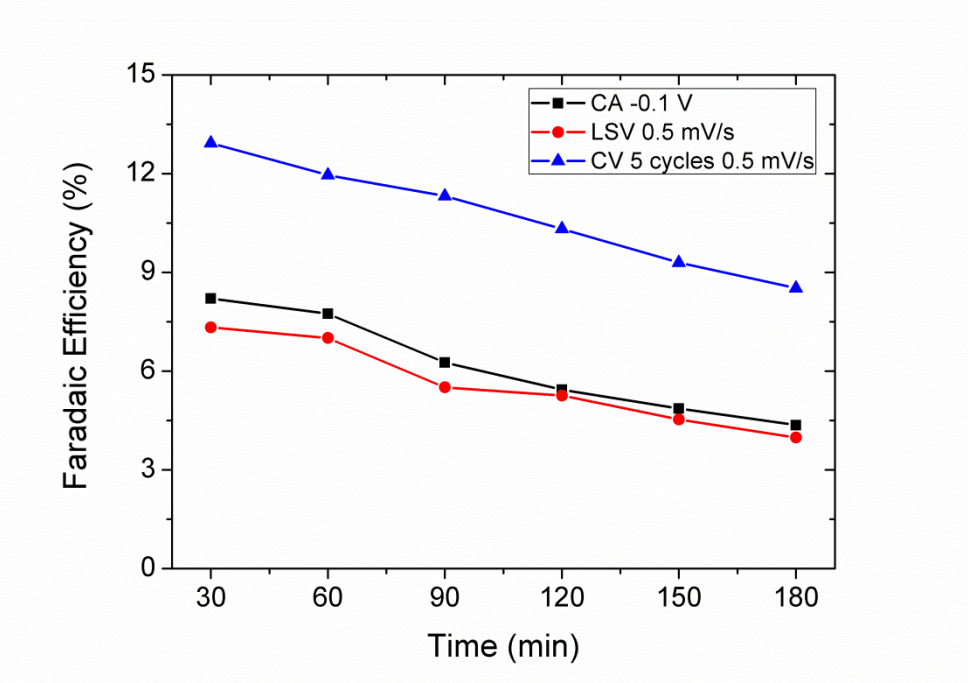

Figure 4.11: Faradaic efficiency of formate ions produced with time during reduction of CO_2 in CO_2 purged 0.5 M $NaHCO_3$ solution on electrochemically oxidized copper by CA at -0.1 V for 30 min, LSV at 0.5 mV/s scan rate and 5 cycles of CV at 0.5 mV/s scan rate.

4.4 Conclusion

The XPS analysis shows that the oxides produced on the copper surface by electrochemical methods reduce back to copper in first few minutes. This assertion was further verified by spectrophotometric analysis of the reduced copper foil. The SEM images also show that the oxides needles go to extinction within five minutes of the CO_2 reduction. Hence, it can be concluded that the increased activity of the catalyst due to oxidation and reduction was not due the copper oxides but the due to the metallic copper only. Further, the copper formed due to the reduction of the copper oxides was found to have a significantly higher surface area as well as more active for the electrochemical reduction of the CO_2 As more of the oxides forms on the surface, more active copper is produced on the surface during reduction. In this study the oxidation of copper by CV results in more oxidation of copper as compared to LSV and CA, hence more amount of active copper and higher activity for CO_2 reduction. This manifests as higher yields of formate ions (~2 times) on electrode oxidized by CV as compared to LSV and CA. However, for all the electrodes the highest value of faradaic efficiency was observed in the first hour of CO_2 reduction which then slowly decreases as the CO_2 reduction proceeds.

The copper oxidized by potential sweep seems to be the most efficient and better method of activating the Cu electrodes for the reduction of CO_2 probably due to two reasons (i) larger increase in EASA as compared to other electrochemical techniques (LSV and CA) and (ii) the amount of formic acid produced by this method is significantly higher than the other two methods. Hence, this technique has been selected to compare the activity and selectivity with copper foil oxidized by annealing (thermochemical method). However, the scan rate has been increased to 5 mV/s from 0.5 mV/s as the time required for the later scan rate was more compared to former (~9.5 hours 5 cycles at 0.5 mV/s and ~4.7 hours 25 cycles at 5 mV/s), but the number of cycles in CV has been increased to 25 from 5 to achieve the same degree of oxidation (which manifests as similar EASA produced by these two methods). In next chapter, the activity and selectivity of the copper foil oxidized by the anodization (CV at a scan rate of 5 mV/s, total 25 cycles) and annealing (annealed at 400 ^{0}C for 10 hours) have been compared.

Chapter 5

Electrochemical Reduction of CO_2 on Copper Activated by Anodizing and Annealing in Air

5.1 Introduction

As mentioned in the previous chapter, deliberate electrochemical oxidation of copper electrodes and subsequent reduction of the oxidized electrodes results in an increase in the EASA compared to the un-oxidized copper electrode. Further, the increase in the electrochemically active surface area (EASA) for CA (-0.1 V for 30 minutes) was almost 3 times, for LSV (at a scan rate of 0.5 mV/s) was almost 5 times and for CV (at a scan rate of 0.5 mV/s, 5 cycles) it was almost 17 times the un-oxidized copper surface. Evidently, potential cycling (repeated oxidation and reduction) is far more effective in increasing the surface area. This increase in EASA also results in an increase in the CO_2 reduction currents on these oxidized copper electrodes. Consequently, the rate of formation of the formate ions was also found to be higher on these oxidized electrode surfaces compared to the un-oxidized copper electrode.

In this chapter, we have compared the activity of the copper electrode oxidized by anodization/electrochemical oxidation (CV at a scan rate of 5 mV/s, 25 cycles) and air annealing/thermochemical oxidation at 400 ^{0}C for 10 hours. The anodization by CV was considered, as the highest increase in the EASA was observed for this electrochemical method as compared to other two. However, the scan rate used is more than that used in the previous case, but the number cycles have been increased to get same oxidation of the copper electrode. As will be shown later in this chapter the increase in EASA for both these CV methods is almost same. Moreover, the time required for the oxidation was reduced to the almost half.

The characterization of the oxidized copper foil before CO_2 reduction as well as reduced copper after reduction of CO_2 was done by XPS, SEM, XRD, etc. The activity and selectivity of anodized and annealed copper foil was measured by carrying out CO_2 reduction at -1.4 V, -1.6 V, -1.8 V and -2.0 V in CO_2 purged 0.5 M $NaHCO_3$ solution. Further, EASA was estimated using UPD of Pb on oxidized copper foil after reduction of the oxides to copper on both anodized and annealed copper foil. The analysis of the CO_2 reduction products was carried out to estimate the rate of formation of products on the oxidized electrode which was

further compared with a un-oxidized copper electrode on the basis of the geometric surface area as well as EASA.

5.2 Experimentation

5.2.1 Electrodes

The standard three electrode system was used for all the electrochemical experiments. The electrochemical cell used was a 50 ml five neck vessel. All the glassware were washed once with aqua regia and then thrice with de-ionized water to avoid contamination. The working electrode was made from a copper foil (extra pure, supplied by Loba Chemie) of 2 cm × 2 cm dimension and was cleaned by immersing in 20% (v/v) aqueous solution of nitric acid and then washed thoroughly with de-ionized water before undergoing oxidation treatment. The counter electrode used was a platinum mesh for copper oxidation experiments in 0.5 M KOH, and a gold foil was used for CO_2 reduction experiments in 0.5 M $NaHCO_3$. Reference electrode used was Hg/HgO in 0.3 M KOH solution. All potentials referred here are versus the Hg/HgO reference electrode.

The anodized copper electrode was prepared by 25 cycles of CV of cleaned copper foil of 2 cm × 2 cm dimension in Ar saturated 0.5 M KOH solution at a scan rate of 5 mV/s in the potential range -1.2 to 0.5 V vs. Hg/HgO electrode. For the characterization of anodized copper foil, the 25th cycle was stopped after completion of the oxidation scan. On the other hand, the annealed copper foil was prepared by heating the cleaned copper foil of 2 cm × 2 cm dimension in a furnace at 400 ^{0}C for 10 hours. A small piece was cut from these copper foils and used for XPS, SEM and XRD analysis.

5.2.2 Electrolytes

An aqueous solution of KOH with a concentration of 0.5 M was used as the electrolyte. The 0.5 M KOH solution was prepared by dissolving the required quantity of the KOH pellet (AR grade, 99% purity, Merck, India) in de-ionized water. For the CV experiments, the 0.5 M KOH solution was first saturated by bubbling high purity argon (Ar) gas for 30 minutes. Electrochemical reduction of CO_2 was carried in 0.5 M $NaHCO_3$ solution prepared by dissolving the required quantity of $NaHCO_3$ salt in de-ionized water. High purity CO_2 gas was bubbled into the solution during the reduction experiments. Biologic (Model No. VSP-300) Potentiostat along with EC-Lab V10.34 software was used for all electrochemical data collection and analysis.

For the under potential deposition (UPD) of Pb (lead) on copper, a 0.01 M $HClO_4$ + 1 mM $PbCl_2$ solution was prepared by adding required quantity of the concentrated $HClO_4$ and $PbCl_2$ in de-ionized water. For the subtraction of capacitance charges in UPD, copper cyclic voltammetry was carried out in 0.01 M $HClO_4$ + 2 mM KCl. Both the solution was saturated with argon gas before performing the electrochemical experiments. To obtain the potential for the monolayer deposition of the lead, the lead was deposited on copper in bulk fashion, and open circuit potential (OCP) was measured. The OCP was observed to be -850 mV against Hg/Hg_2SO_4 reference electrode. After the OCP measurement, CV at a scan rate of 10 mV/s was obtained in the potential range of -50 mV negative to OCP to 310 mV positive to the OCP. In these range of the potentials, peaks corresponding to the monolayer adsorption and desorption of lead appears. The charge under the lead desorption peak has been selected for the estimation of the surface area as the desorption reaction will be free from the mass transfer limitations.

5.2.3 Equipments

As mentioned above, the anodization of copper foils was done is 0.5 M KOH after the electrochemical treatment, the copper foil was taken out from the electrochemical cell and washed thoroughly with de-ionized. Moreover, annealing of the copper foil was done by heating in the air by at 400 ^oC for 10 hours. A small piece of these oxidized copper foils was then cut and used for SEM imaging and XPS. The XPS analysis and SEM imaging were also carried on the copper foil reduced for 5 minutes, with similar reduction potential used for CO_2 reduction. The SEM images of oxidized copper were obtained at different magnification in a JEOL JSM 7600 (FEG-SEM) scanning electron microscope. An AXIS Supra (Kratos Analytical) XPS machine was used to obtain the XPS profile for all the samples.

Liquid and gas samples were collected from the electrochemical cell at an interval of 30 minutes. The analysis of liquid products of CO_2 reduction was carried out on a 1260 infinity series high performance liquid chromatography (HPLC) supplied by Agilent Technologies (USA) with Aminex HPX-87H column (Bio-rad, USA). The mobile phase used for the analysis was an aqueous solution of 13 mM H_2SO_4 prepared by adding required volume of concentrated H_2SO_4 (18 M) in de-ionized (DI) water and then sonicated for 30 min to remove any dissolved gases. All liquid samples were first acidified to obtain a pH of approximately 2 by adding required amount of 1 M H_2SO_4 solution. The analysis of the gaseous products was carried out on a 5700 model gas chromatography supplied by Nucon

Engineers (India) with PORAPAK column High purity argon (Ar) gas was used as carrier gas for all the GC experiments.

5.3 Results and Discussion

5.3.1 Electrode Surface Characterization

The electrodes used for the electrochemical reduction of CO_2 were prepared by oxidizing copper foil by cyclic voltammetry in alkaline solution and by annealing in air. X-ray diffraction (XRD) of copper foil oxidized by annealing shows that the oxide layer consists of copper oxide with different oxidation state (Figure 5.1(A), Reference: ICDD powder diffraction data file Cu:00-002-1225, Cu_2O:01-078-2076, CuO:01-080-1961, Cu_4O_3:01-083-1665). Further, as shown in Figure 5.2 (A), XPS analysis of the annealed copper surface shows that the electrode surface consists of CuO. The discrepancy in the composition of the film may be due to the formation of CuO (the most stable copper oxide) on the outer surface and which covers the other oxides below it. Meanwhile, in case of the electrode anodized by CV, oxides produced during the oxidation scan gets reduced back to copper in reduction scan. Hence, when electrode completes a full cycle, there will be very less or no oxides left on the surface. But to observe the structure of the oxides grows on the copper surface, 24 cycles of CV were completed and 25^{th} cycles was stopped just after the oxidation scan at 0.5 V. The XRD of anodized copper foil shows a similar pattern like copper and unlike for the annealed copper foil no peaks were observed for copper oxides (Figure 5.1 (C) and (D)). The reason for reflections corresponding to copper oxides not appearing in XRD for anodized copper foil may be the thickness of the oxide layer produced by anodizing which is very small. However, XPS analysis of this oxidized copper shows that the layer of oxides is made up Cu_2O, CuO and $Cu(OH)_2$ (Figure 5.2 (C)).

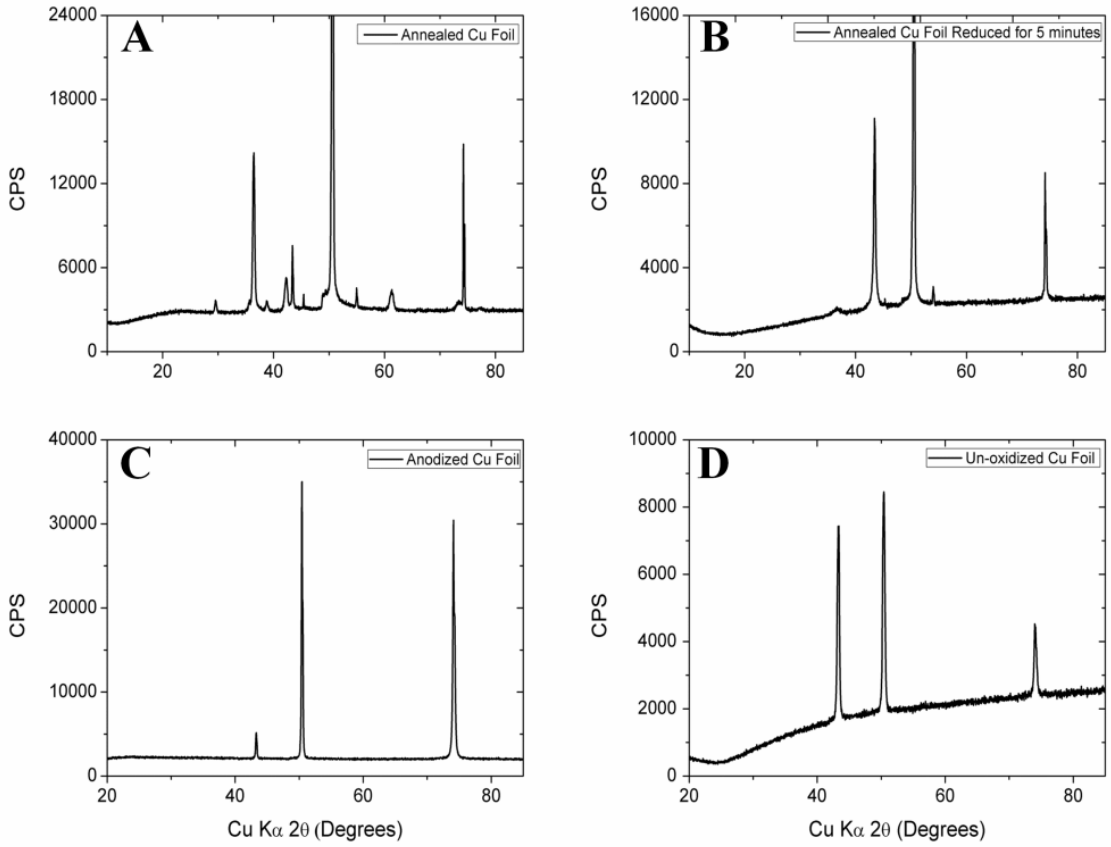

Figure 5.1: XRD pattern of copper foil after (A) Annealed in the air at 400 ^{0}C for 10 hours and (B) reduction of the oxidized foil for 5 minutes at -1.6 V for 5 minutes in CO_2 purged 0.5 M $NaHCO_3$ solution (C) Anodized copper foil (D) Un-oxidized copper foil.

The SEM images of the annealed copper foil show a layer of oxides formed on the foil surface (Figure 5.3 (A)), while the SEM images of the anodized copper foil show that the growth of the oxides takes place in the form of needles projecting outwards (Figure 5.3 (C)). However, at the potentials used for the CO_2 reduction, the oxides produced by both methods will not be thermodynamically stable and will reduce back to copper. The reduction of these oxides to copper takes place during first few minutes of CO_2 reduction (which can be observed by huge reduction current at the start of CO_2 reduction reaction, later stabilized to lesser current value). To verify this reduction of the oxides taking place in first few minutes of the CO_2 reduction, copper foil oxidized by anodizing was subjected to CO_2 reduction only for 5 minutes, and then XPS spectra for this electrode was obtained (Figure 5.2 (D)). The deconvolution of the XPS spectra shows Cu and/or Cu_2O is present on the surface. A similar analysis of annealed copper foil was also carried out along with XRD analysis. Both XPS

spectra (Figure 5.2 (B)) and XRD analysis (Figure 5.1 (B)) shows that oxides present on the foil surface get reduced back to the copper.

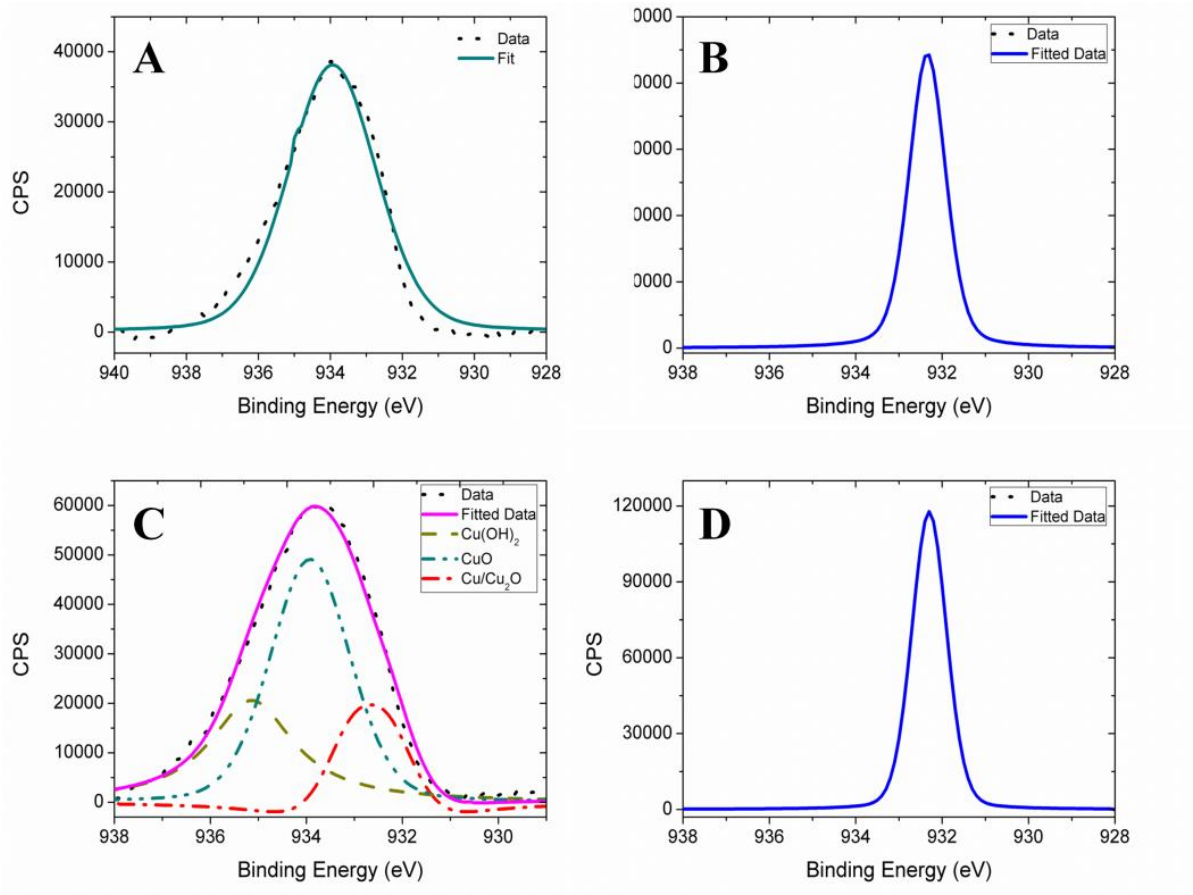

Figure 5.2: XPS profiles and fitting results of copper foils (A) oxidized by annealing in air at 400 ^{0}C for 10 hours (B) reduced subsequently during CO_2 reduction in CO_2 purged 0.5 M $NaHCO_3$ at -1.6 V for 5 minutes, and copper foils (C) oxidized by CV at 5 mV/s in Ar saturated 0.5 M KOH (25 cycles) and (D) reduced subsequently during CO_2 reduction in CO_2 purged 0.5 M $NaHCO_3$ at -1.6 V for 5 minutes. (The XPS profiles were fitted to a Gaussian Lorentzian mix (30% Gaussian) after background subtraction by Shirley's method) with the help of casa XPS software.)

In case of copper foil oxidized by anodizing and then reduced during CO_2 reduction, only one peak was obtained after deconvolution of the Cu *2p2/3* peak. This deconvoluted peak corresponds to the Cu and/or Cu_2O. The experiments done and reported in chapter 4 has concluded that the only Cu^0 is present on the electrode surface during the reduction of the CO_2 and all the oxides get reduced to Cu^0 in first few minutes only.

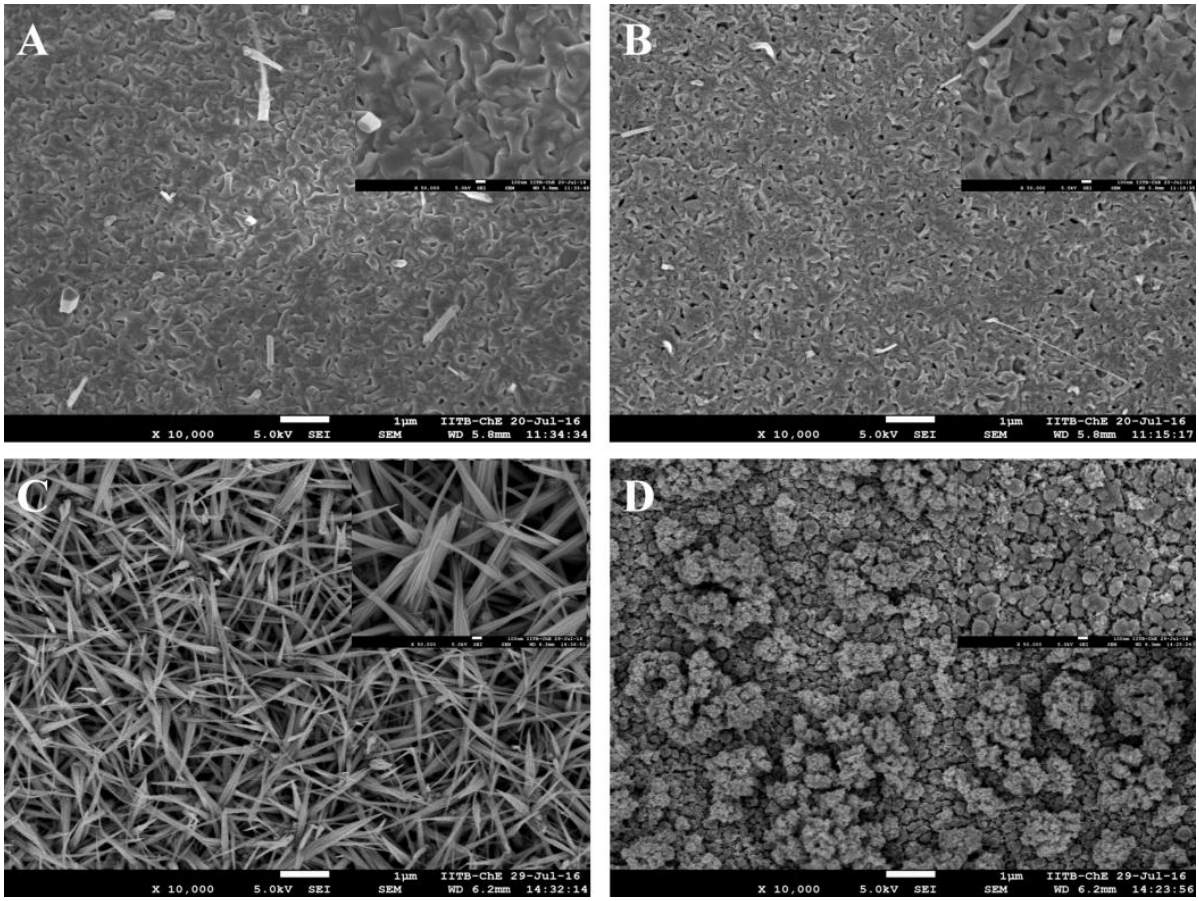

Figure 5.3: SEM images of (A) copper foil oxidized by annealing in air at 400 ^{0}C for 10 hours (B) reduced subsequently during CO_2 reduction (C) copper foil oxidized by CV at 5 mV/s in Ar saturated 0.5 M KOH (D) reduced subsequently during CO_2 reduction.

5.3.2 Under Potential Deposition of Lead on Copper

The cyclic voltammograms of the under potentially deposited Pb on copper foils which were annealed/anodized and subsequently reduced in 0.5 M $NaHCO_3$ at -1.6 V for 5 minutes along with that obtained for pristine Cu foil is shown in Figure 5.4. The cyclic voltammograms were obtained at a scan rate of 10 mV/s in Ar saturated 0.01 M $HClO_4$ + 1 mM $PbCl_2$ solution. From the Figure 5.4 two distinct current peaks can be identified when the potential is scanned from a negative potential of -0.93 V to towards -0.45 V The first peak approximately at -0.85 V is due to the stripping of the bulk Pb that was deposited and the second peak is for the stripping of the under potential deposited Pb.

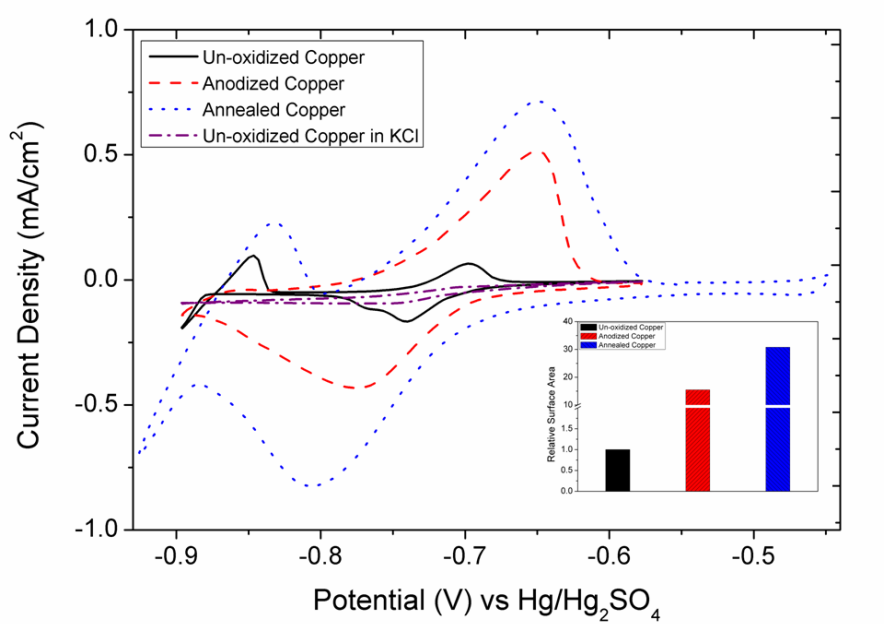

Figure 5.4: Overlay of CVs of lead (Pb) under potential deposition (UPD) on un-oxidized, anodized and annealed copper foil (after reduction in CO_2 purged 0.5M $NaHCO_3$ solution) at a scan rate of 10mV/s in Ar saturated 0.01M $HClO_4$ + 1 mM $PbCl_2$ solution.

It may be instructive to evaluate the real surface area of the Cu foil electrodes using the correct charge density factor but in this particular case, a comparison of the surface areas before annealing/anodization and its subsequent reduction in 0.5 M $NaHCO_3$ at -1.6 V for 5 minutes after annealing/anodization will be sufficient. To do so, we have evaluated the charge corresponding to the stripping of Pb atoms from the copper surface for all the three copper foil samples and determined the relative increase in surface area of the anodized/annealed samples compared to the pristine Cu foil. The increase in the EASA for the anodized copper foil is 15.5 ($S_{anodized}$ = 3800 µC/245 µC) times than un-oxidized copper foil, and for annealed copper foil this increase is 30.82 ($S_{annealed}$ = 7550 µC/245 µC) times. These values clearly show that both the oxidation treatment results in an increase in surface area. Moreover, copper foils oxidized by annealing produces far more EASA compared to copper foil oxidized by anodizing. This is also in agreement with the visual observation where the annealing treatment had produced thicker oxides films compared to the anodizing treatment. Once a reasonable estimate of the increase in electrochemically active surface area has been obtained, a meaningful comparison of the activities and product formation rates for electrochemical reduction of CO_2 can then be made.

5.3.3 Electrochemical Reduction of CO_2

Electrochemical reduction of CO_2 on copper electrode activated by anodizing and annealing is compared with un-oxidized polycrystalline copper foil at different potential as shown in Figure 5.5. For the estimation of the current density, the geometric surface area was used. It can be seen from the Figure 5.5 that copper obtained from the reduction of both anodized and annealed copper foil electrode is more active than untreated polycrystalline copper. Comparison between two pre-treated electrodes shows that the copper foil annealed in the air had a higher activity for CO_2 reduction than copper pre-treated by anodizing. The main product of CO_2 reduction was formate ions in liquid phase and hydrogen in the gas phase. The quantification of the formate ions produced was carried out by HPLC.

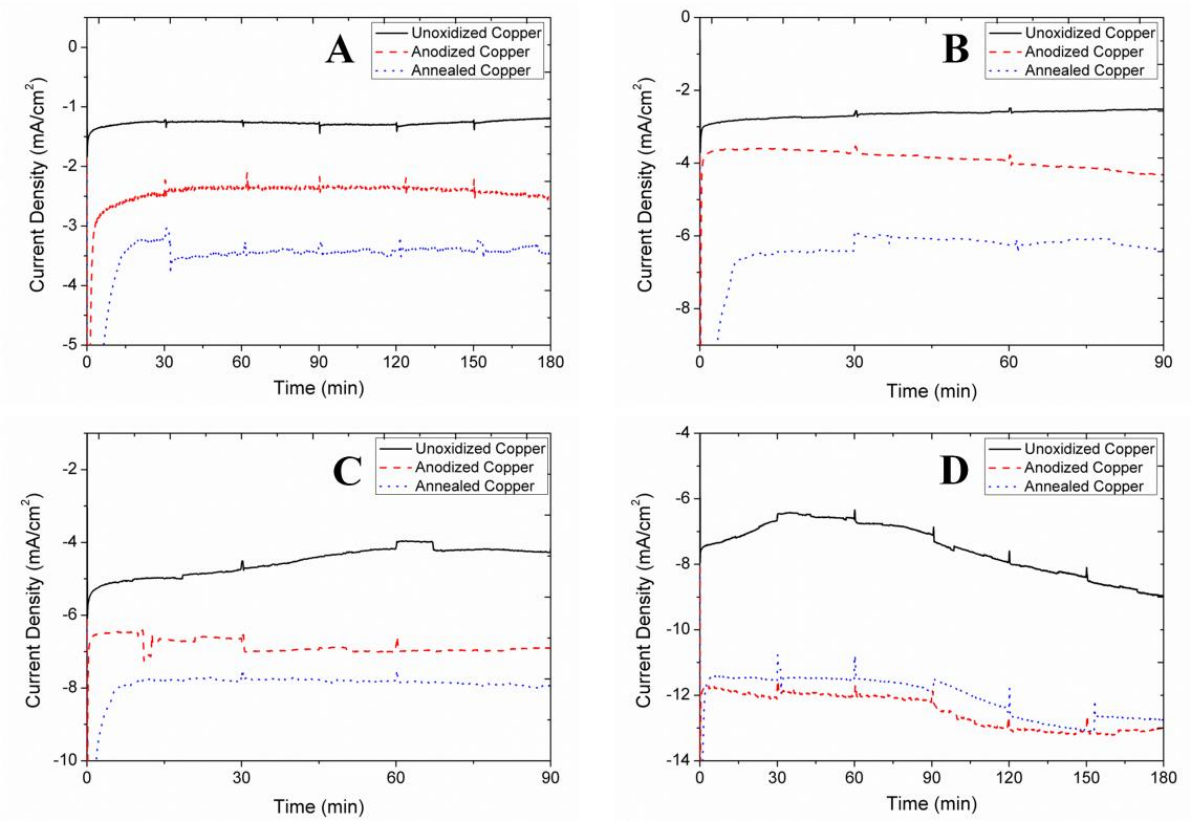

Figure 5.5: Electrochemical reduction of CO_2 on un-oxidized copper foil, copper foil oxidized by CV at 5 mV/s in Ar saturated 0.5 M KOH solution (25 cycles) and copper foil oxidized by annealing in air at 400 ^{0}C for 10 hours at reduction potential of (A) -1.4 V, (B) -1.6 V, (C) -1.8 V, and (D) -2.0 V vs Hg/HgO reference electrode in CO_2 purges 0.5 M $NaHCO_3$ solution using geometric surface area.

Few important observations need to noted from the chronoamperometry (current-time graphs) at different potentials.

- The current density for CO_2 reduction remains almost constant through the three hours of reduction at less negative reduction potentials (-1.4 V, -1.6 V), but at more negative potentials (-1.8 V, -2.0 V) current density increases for copper oxidized by anodizing.
- For copper foils oxidized by annealing in air, the current density was constant at -1.4 V only and then increases for all the more negative potentials.
- The increase in apparent activity of copper surface results in almost double the increase in current density for copper oxidized by anodizing at all reduction potentials. However, for annealed copper foil almost three times increase in the current density at less negative potential (-1.4 V and -1.6 V) and two times increase in current density at more negative reduction potentials (-1.8 V and -2.0 V) as compared to un-oxidized copper foil was observed.

The trends in current vs. time profile drastically change when the current density was computed using the relative increase in the surface area (the area of un-oxidized copper foil is taken as 1.0, and the area of the anodized and the annealed copper foils have been multiplied by $S_{anodized}$ and $S_{annealed}$, respectively). As shown in Figure 5.6, marginal difference in the current density was observed for the copper foils oxidized by the annealing and the copper foil oxidized by the anodization signifying that the net effect of both the activations procedures is similar. Interestingly, although the currents normalized with respect to the relative surface area for both the annealed and the anodized are similar, the currents density for the untreated/un-oxidized Cu foil is far higher. This is in sharp contrast with the expectation of same current density per unit electrochemically active surface area for all the three electrodes. We suspect that this is primarily due to mass transport limitations due to the porous nature of the annealed as well as the anodized electrode. On decreasing the potential of CO_2 reduction down to -1.8 V, large evolution of hydrogen was also observed, but the trends in currents were similar to that observed for -1.6 V. Thus it can be concluded that the increase in the reduction currents observed for the oxidized copper foils compared to the un-oxidized foil is not due the increase in the intrinsic change in activity of the copper surface, but it is merely due the increase in the surface area available for the reduction of CO_2.

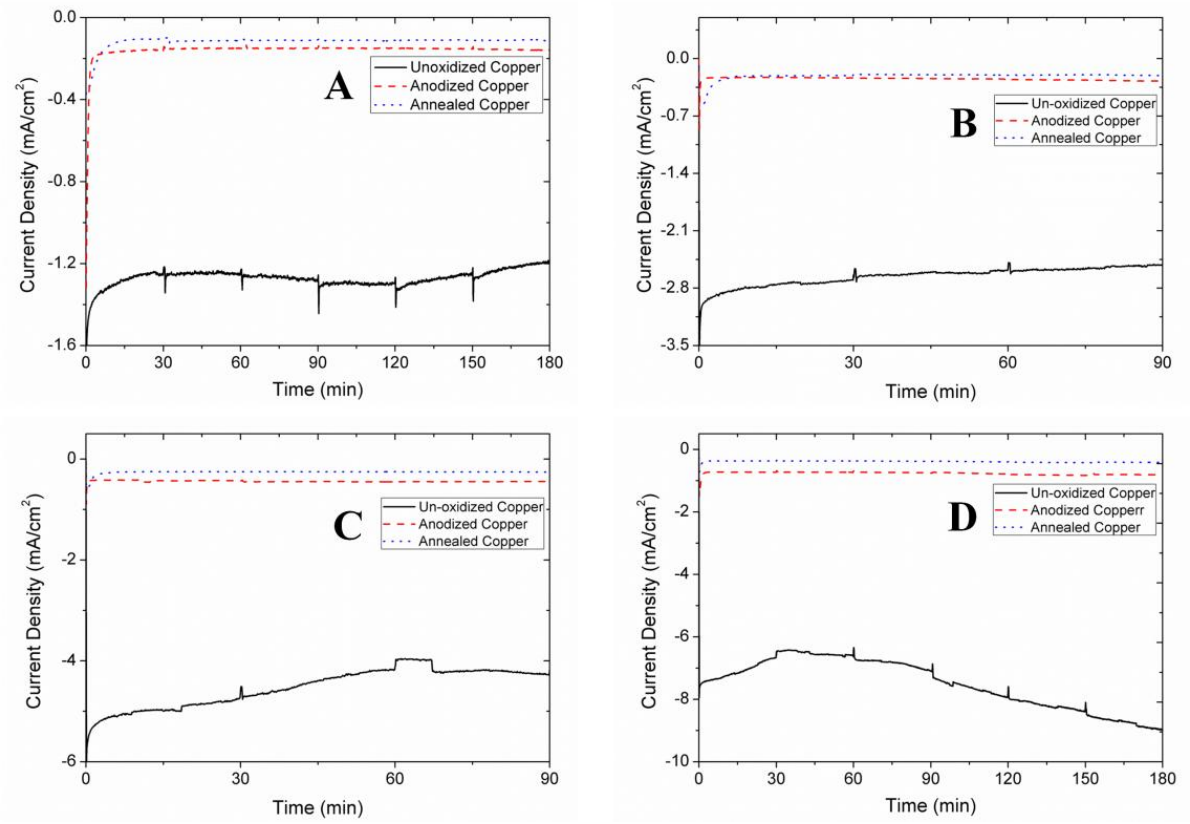

Figure 5.6: Electrochemical reduction of CO_2 on un-oxidized copper foil, copper foil oxidized by CV at 5 mV/s in Ar saturated 0.5 M KOH solution (25 cycles) and copper foil oxidized by annealing in air at 400 ^{0}C for 10 hours at reduction potential of (A) -1.4 V, (B) -1.6 V, (C) -1.8 V, and (D) -2.0 V vs Hg/HgO reference electrode in CO_2 purges 0.5 M $NaHCO_3$ solution using relative increase in EASA.

The amount of formate ion produced due to the electrochemical reduction of the CO_2 is shown in Figure 5.7. At all potential, the amount of CO_2 produced on oxidized copper foils is significantly more than that of produced on un-oxidized copper foil. This indicated that the oxidation and subsequent reduction of these oxides to copper had increased the selectivity of the copper towards the formation of formate ion. The comparison between two oxidized copper foils (annealed and anodized), at -1.4V, -1.6 V and -1.8 V, suggesting that the amount of formate ions produced on the annealed copper foil is more than the anodized copper foil. This is agreement with the increase in the surface area resulting in more formation of the formate ions. However, at -2.0 V more amounts of formate ions have been produced on copper foil oxidized by anodization than annealing. One possible reason for the may be due to the high overpotential; HER is taken the preceding at higher rates than CO_2 reduction on annealed copper due to the large surface area.

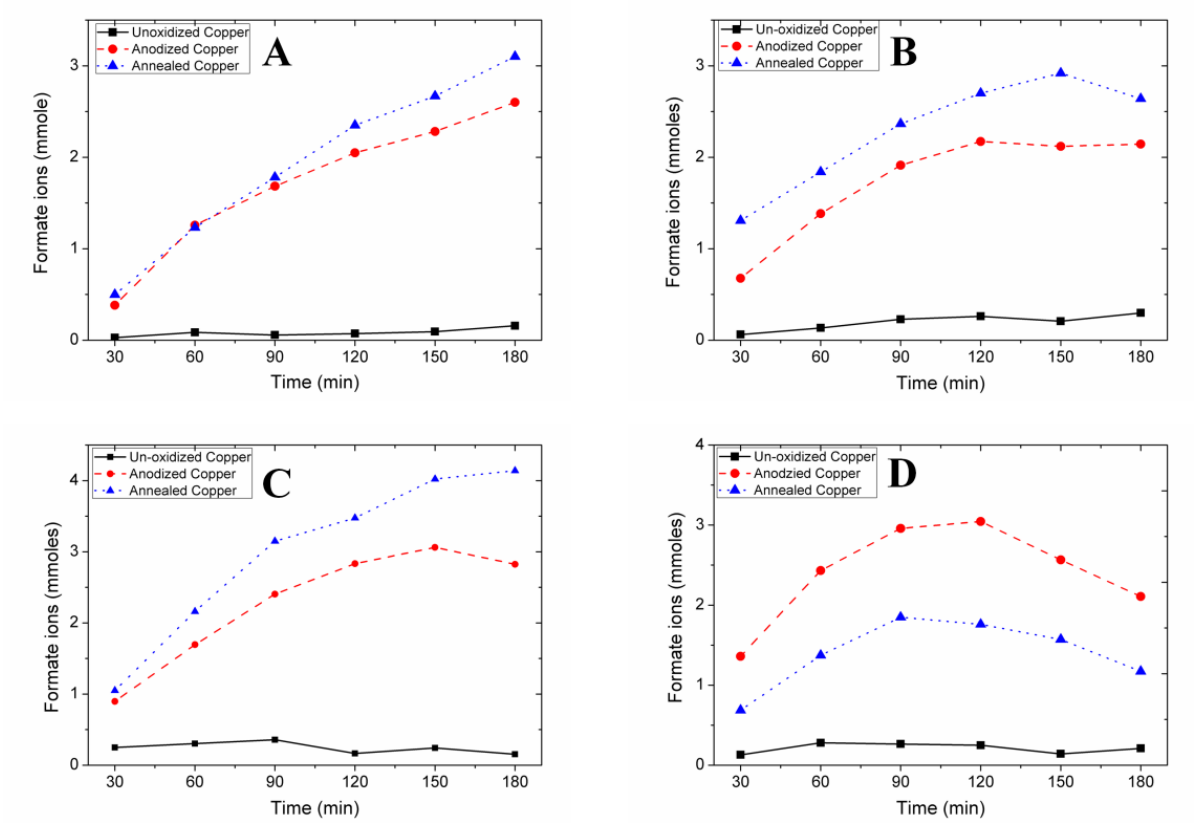

Figure 5.7: Formate ions production for electrochemical reduction of CO_2 on un-oxidized copper foil, copper foil oxidized by CV at 5 mV/s in Ar saturated 0.5 M KOH solution (25 cycles) and copper foil oxidized annealing in air at 400 ^{0}C for 10 hours at reduction po potential of (A) -1.4 V, (B) -1.6 V, (C) -1.8 V, and (D) -2.0 V vs. Hg/HgO reference electrode in CO_2 purges 0.5 M $NaHCO_3$ solution.

The faradaic efficiency for formate ions was calculated by taking the ratio of charge consumed to produce formate ions to the total charge transferred. Highest faradaic efficiency was observed in case of copper oxidized by anodizing at -1.4 V as shown in Figure 5.8. However, the amount of formate ions produced during reduction was higher for copper oxidized by the annealing in air at all reduction potential expect -2.0 V. Faradaic efficiency increase as the potential increases from -1.2 V to -1.4 V, but further increase in the reduction potential results in the decrease in the faradaic efficiency. Moreover, the rate of formation of formate ions was high initially which decrease with time at all the potentials for both oxidized electrode. The decrease in the rate of the formation with time may be due to the deactivation of catalyst surface.

The mechanism for the formation of the formate ions in aqueous solution on the copper electrode during electrochemical reduction of CO_2 has been well investigated. Two

electrons are necessary to reduce CO_2 to formate ions. Generally, it is accepted that the two electrons are transferred in two different steps. In the first step, the first electron is transferred to an adsorbed CO_2 molecule (CO_2(ad)) to form an intermediate radical CO_2^-(ad). This intermediate radical reacts with the H_2O will generate and OH^-. In the second step, another electron reacts with HCO_2(ad) to produce the formate ion ($HCOO^-$(aq)). Probably, the rate for first electron transfer is lower than the transfer of the second electron as the Tafel slope of the reduction curve is 116 mV/decade and this value corroborates with the Tafel slope with the reported literature (Figure 5.9).

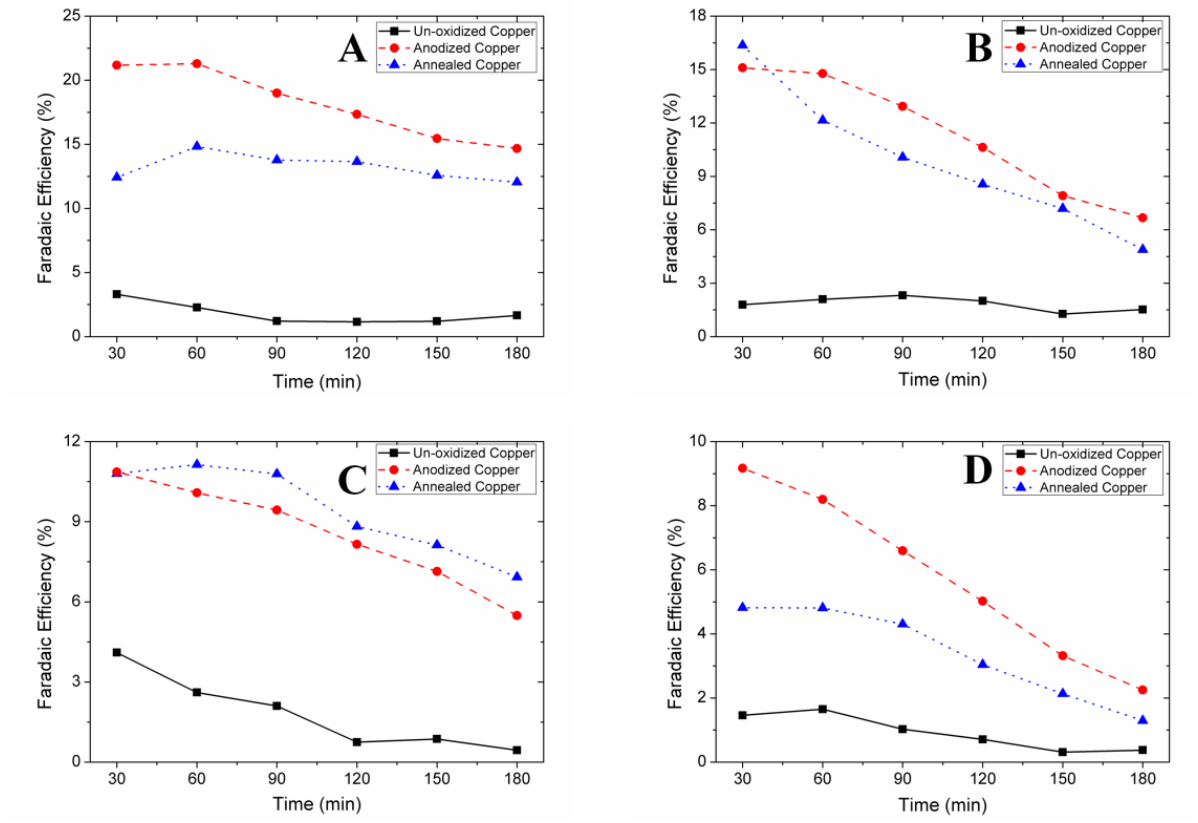

Figure 5.8: Faradaic efficiency for electrochemical reduction of CO_2 on un-oxidized copper foil, copper foil oxidized by CV at 5 mV/s in Ar saturated 0.5 M KOH solution (25 cycles) and copper foil oxidized annealing in air at 400 ^{0}C for 10 hours at reduction potential of (A) -1.4 V, (B) -1.6 V, (C) -1.8 V, and (D) -2.0 V vs. Hg/HgO reference electrode in CO_2 purges 0.5 M $NaHCO_3$ solution.

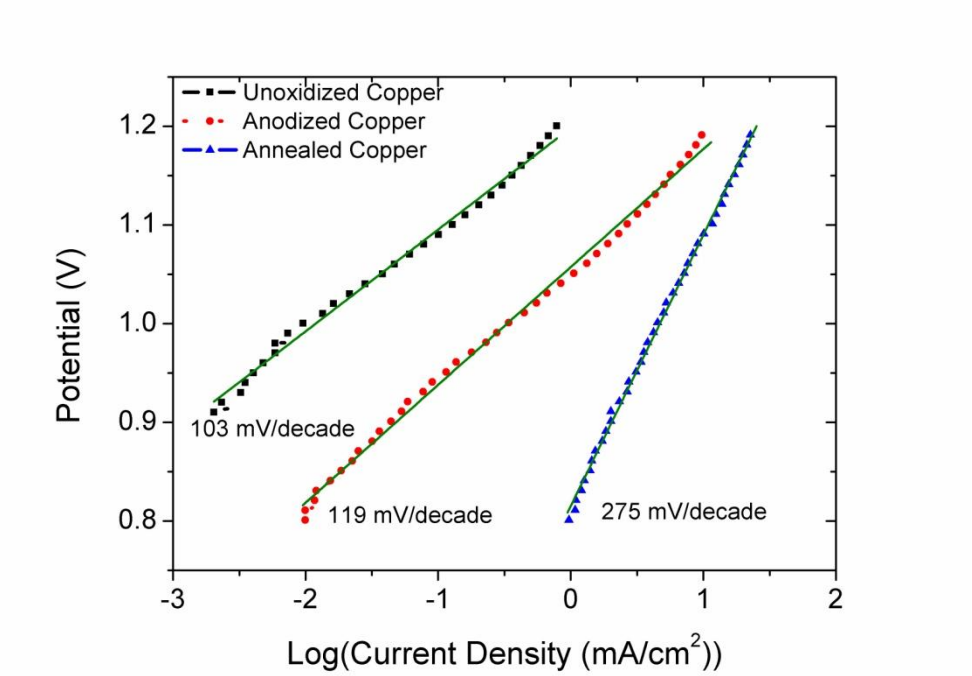

Figure 5.9: Tafel plot for a CO_2 reduction on un-oxidized copper, anodized copper and annealed copper electrode in CO_2 purged 0.5 M $NaHCO_3$ solution.

5.4 Conclusion

The comparison between the oxidation method for the activity for CO_2 reduction shows that the copper foil oxidized by the annealing produces a thick layer of oxides on copper foil compared to the anodized copper foil. This thick layer of oxides upon reduction results in the higher electrochemically active surface area as compared to the anodized copper foil. Further, the higher EASA for annealed copper foil manifests as higher currents due to electrochemical reduction of CO_2 which is more than that obtained for the anodized copper. Meanwhile, with an increase in the reduction potential, the difference between the reduction current densities of anodized and annealed copper foil decreases drastically. However, the selectivity of the formate ion formation from electrochemical CO_2 reduction increases with the pretreatment/activation (oxidation in air or electrochemical followed by the reduction while reducing CO_2 electrochemically). Further, a comparison of the selectivity, manifested by faradaic efficiency, for the formation of formate ion between anodized and annealed copper reveals that anodization of copper is more effective than annealing.

Chapter 6

Estimation of Copper Powder Surface Area by Different Methods

6.1 Introduction

Copper is one of the most studied electrocatalysts for the electrochemical reduction of CO_2. The unique characteristic of the copper to produce hydrocarbon, carboxylic acid, aldehydes/ketones and alcohols as CO_2 reduction products has persuaded many researchers to investigate the effects of different parameters on the activity and selectivity of copper for electrochemical reduction of the CO_2 ((Y Hori 2008; Scibioh and Viswanathan 2004; Gattrell, Gupta, and Co 2006)). As mentioned in the last two chapters, deliberate oxidation of the copper foil has changed the activity and selectivity of the copper for electrochemical reduction of the CO_2. Further, it was found that the oxidation and reduction of the oxides produced due to the oxidation results in the increase in the surface roughness or surface area or electrochemically active surface area (EASA). Estimation of the increased surface has helped to conclude few important facts on the electrochemical reduction of CO_2 on deliberately oxidized copper surfaces. Moreover, copper and supported copper based heterogeneous catalysts are widely employed both as chemical catalysts as well as electrocatalysts. Commercially, copper on alumina is an important system for synthesis of methanol from CO and low-temperature water-gas shift reactions (Newsome 1980). Additionally, many industrial processes such as wet oxidation of phenol in refinery wastewater (Santos et al. 2005; Mohite and Garg 2017), selective hydrogenation of organic compounds, dehydrogenation of cyclohexane (Gliński, Ulkowska, and Iwanek 2016), etc. are catalyzed by supported copper catalysts. In case of heterogeneous catalysis, it is very important to have a good estimate of the surface area of the catalyst to be used in the process.

As introduced in the last two chapter UPD of Pb can be used for the estimation of the surface area of the copper. Further, as mentioned in chapter 3, for particular scan rate in 0.5 M KOH solution a monolayer of Cu_2O get produced on the copper surface and can also be used to estimate the surface area of the copper. In addition to these electrochemical methods for the estimation of the copper surface area, in this chapter surface area of the copper powder was estimated by using SEM (scanning electron microscopy), particle size analyzer, optical microscopy and BET (Brunauer-Emmett-Teller), etc. These methods will also give further validation to the surface area estimated by the electrochemical methods. The surface area

estimation using electrochemical methods is very fast (within few minutes) compared to few hours required for the BET analysis. Further, the specialized machine used in case of BET, SEM is not required in the electrochemical method. Moreover, these methods will fail in estimating surface area if copper is monolithic or supported on carbon or some other material. The electrochemical method can be used for monolithic copper as well as supported copper as long as the support is conductive. Further, the requirement of solvents and chemicals is minimum. If the electrochemical methods protocols are fixed, then it can be used for the estimation of the surface area instead of the other methods.

6.2 Experimentation and Methods

6.2.1 Electrolytes

The required quantity of the KOH pellets (analytical grade, supplied by Merck, India) was dissolved in deionized water to make 0.5 M KOH solution. To make 0.01 M $HClO_4$ + 1 mM $PbCl_2$ solution, required quantities of concentrated $HClO_4$ (analytical grade, supplied by Merck, India) and $PbCl_2$ (analytical grade, supplied by Loba Chemie, India) was added to deionized water. The solutions thus prepared was purged for 30 minutes with high purity argon (Ar) (supplied by Mars Gas and Equipment, India) in a five neck flask having a capacity of 50 mL to be used for the electrochemical measurements.

6.2.2 Electrodes

A standard three electrode system was used for all electrochemical measurements. Copper powder of spherical shape particles of 10 micron size was obtained from Alfa Aesar (specifications: spherical particle, APS 10 micron, 99.9 % (metal basis), Lot No. Z17B008). Fifty milligrams of the copper powder was dispersed in 5 mL of deionized water, and after that 50 µL of basic nafion (5% nafion solution obtained from Sigma Aldrich was added to an alkaline solution to neutralize free protons ions in nafion to obtain the final pH as ~7) was added to the mixture as binding agent. The dispersion was then sonicated for 30 minutes, and further 20 µL of this dispersion was drop casted on a polished glassy carbon electrode (diameter 5 mm, supplied by PINE Research Instruments, USA). The electrode was dried under an infrared lamp (IR lamp) to obtain copper powder coated glassy carbon electrode for electrochemical analysis. The electrode thus made was used as working electrode for electrochemical measurements. Platinum mesh having significantly higher surface area than working electrode was used as a counter electrode. A Hg/HgO (in 0.3 M KOH solution and a

Hg/Hg_2SO_4 (in saturated K_2SO_4 solution) were used as reference electrodes in 0.5 M KOH and 0.01 M $HClO_4$ + 1 mM $PbCl_2$ solutions, respectively.

6.2.3 Equipments and Methods

All electrochemical measurements were carried out using Biologic potentiostat (model: VSP 300) with EC Lab 10.34 software for data measurement and analysis. The cyclic voltammetry (CV) of copper powder electrode was recorded in Ar saturated 0.5 M KOH solution at a scan rate of 50 mV/s from -1.2 V to 0.5 V vs. Hg/HgO electrode. Similarly, CV of copper powder electrode was recorded in Ar saturated 0.01 M $HClO_4$ + 1 mM $PbCl_2$ solution at a scan rate of 10 mV/s from -0.9 V to -0.58 V vs. Hg/Hg_2SO_4 electrode.

The SEM (scanning electron microscopy) images were captured at different magnification in a JEOL JSM 7600 (FEG-SEM) scanning electron microscope. For SEM analysis minute quantity of copper powder was dispersed in 1 mL of water by sonication for 10 minutes to break any agglomeration and obtain a uniform dispersion of copper particle. The suspension was then drop casted on a small piece of the aluminium foil and dried under IR lamp, and used for the SEM imaging. Moreover, as the particle size of the copper powder is in range of 10 microns, the particle size was also measured using optical microscopy. The optical microscope used for this measurement was Nikon made Eclipse Ti-s model. The copper powder was spread uniformly on a clean glass slide and then used for analysis. The optical images were captured at different magnification like 60X, 40X and 20X. At higher magnification, the particles images were not clear, and hence images obtained at 40X magnification has been used for the particle size estimation.

A Horiba scientific laser diffraction particle size distribution analyzer (“partica” model: LA 960) was used to estimate the particle size of the copper powder. A dispersion of few milligrams copper of powder in water was circulated through the instrument channel under continuous stirring and ultrasonication. The particle size data were collected five times, and the average value of the diameter has been used for the calculation of the surface area.

In addition to electrochemical measurements, microscopy and particle size analysis, BET surface area measurements were also performed using N_2 as the adsorbent in a Micromeritics (model ASAP 2020) physisorption system. The weight of the sample used for the analysis was measured before the analysis and degassing was done at 150 ^{0}C for four hours to remove any moisture adsorbed on the surface. After degassing, the weight of the sample was measured again. A net loss of 0.38 gm was observed.

6.3 Results and Discussion

6.3.1 Electrochemical Methods

A) Monolayer Oxidation of Copper in 0.5 M KOH

The first electrochemical method used for the measurement of the surface area was CV of copper powder electrode in Ar saturated 0.5 M KOH solution (Figure 6.1). The oxidation of copper in alkaline solution under applied potential results in the formation of different oxides and hydroxides of the copper as discussed in details in our earlier work (Giri and Sarkar 2016). As the potential is moved in a positive direction starting from -1.2 V, successive oxidation of the copper takes places resulting in the formation of Cu_2O, CuO and $Cu(OH)_2$, and other water soluble copper hydroxides. These processes manifest as two major oxidation peaks during the oxidation scan. In the reverse scan the oxides thus produced reduces back to copper in two or more stages and this manifests as two different current peaks (reduction scan). During oxidation scan, the first current peak (park A) corresponds to the formation of Cu_2O ($2Cu + 2OH^- \rightarrow Cu_2O + H_2O + 2e^-$), and for a small range of molarity of KOH (0.1 to 1 M) and scan rate (50 to 100 mV/s), it can be assumed that the oxidation of copper surface leads to the formation of a monolayer film. This corroborated well with existing experimental evidence (Fletcher, Barradas, and Porter 1978). Moreover, as mentioned by Fletcher et al. (Fletcher, Barradas, and Porter 1978), the charge density factor (charge per unit surface area) for the formation of the Cu_2O monolayer is 352 $\mu C/cm^2$. For the drop casted copper electrode, the Faradaic charge under peak A centered around -0.35 V was found to be 43 μC, after subtraction of the capacitive contribution (the baseline was assumed to be linear from -0.5 to -0.25 V). From the charge density factor and the total faradaic charge, the total surface area of the deposited copper was found to be 0.1222 cm^2. Further, taking into account, the mass of copper powder deposited, the resultant specific surface area of the copper equals to 611 cm^2/gm.

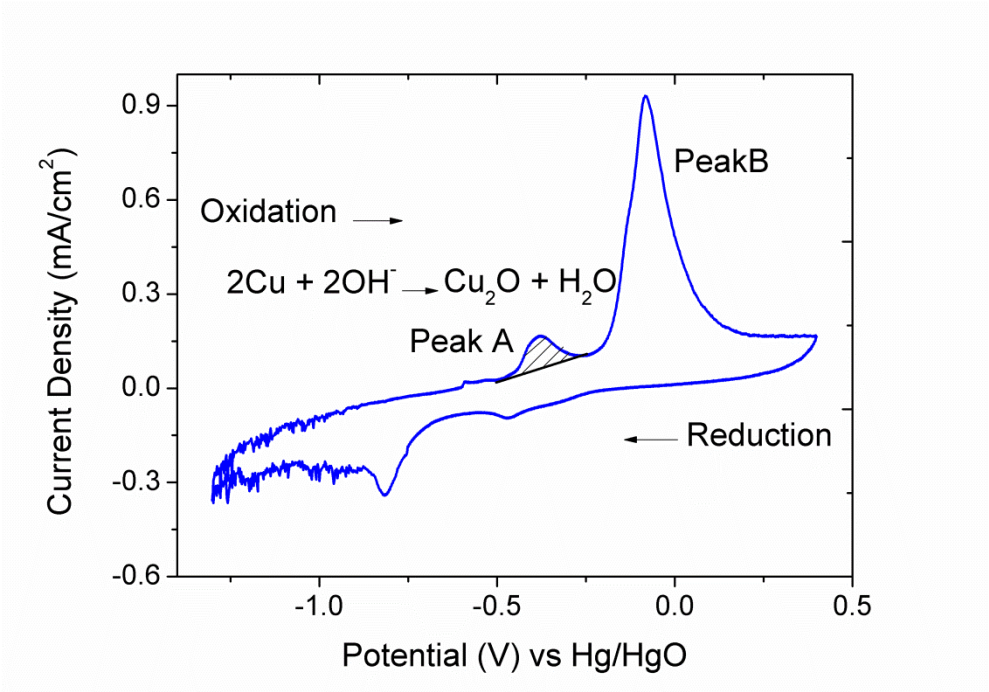

Figure 6.1: Cyclic voltammetry of copper powder in Ar saturated 0.5 M KOH solution at a scan rate of 50 mV/s.

B) Under Potential Deposition of Pb on Copper

The cyclic voltammogram of the copper powder electrode in Ar saturated 0.01 M $HClO_4$ + 1 mM $PbCl_2$ solution at a scan rate of 10 mV/s is shown in Figure 6.2. The first peak observed during the anodic scan (at around -0.85 V) is for the stripping of the bulk Pb that was deposited on the copper particles at a potential below the equilibrium (-0.85 V vs. Hg/Hg_2SO_4) of Pb in $PbCl_2$ solution. This peak is then followed by the peak (at around -0.7 V) for stripping of monolayer Pb deposited on the copper. The charge under this peak was selected for the measurement of the surface area of copper (hatched area in Figure 6.2). The charge under the Pb monolayer stripping peak was found to be 43.5 µC at a scan rate of 10 mV/s, indicating the surface area of the drop casted copper electrode is 0.174 cm^2. This result in a surface area of copper powder equal to 675 cm^2/gm.

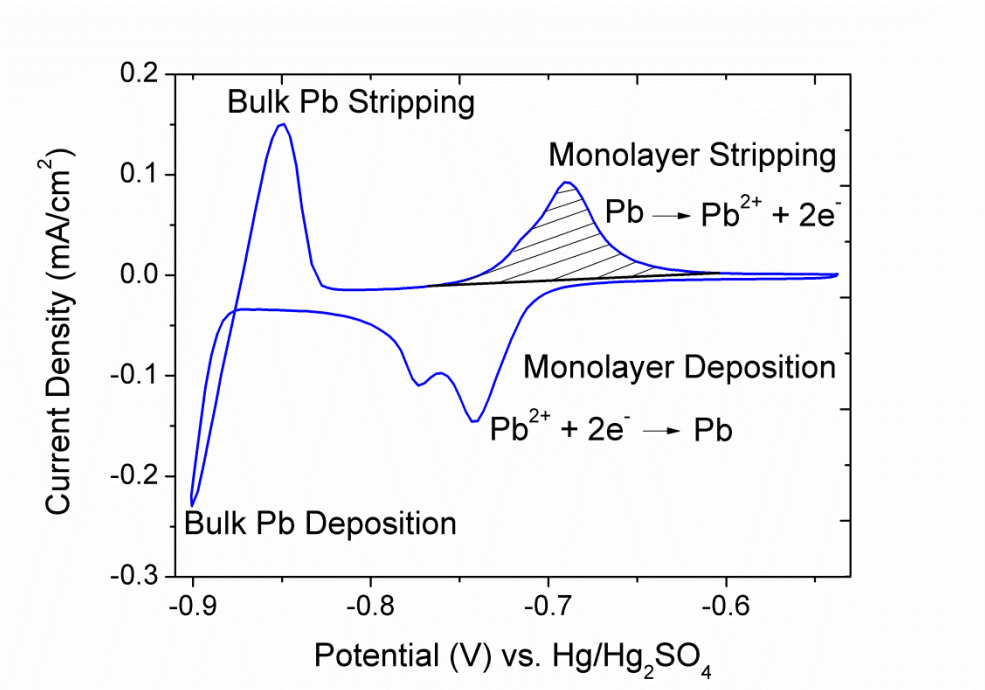

Figure 6.2: Cyclic voltammetry of copper powder in Ar saturated 0.01 M $HClO_4$ + 1 mM $PbCl_2$ solution at a scan rate of 10 mV/s.

6.3.2 Microscopy Methods

A) Scanning Electron Microscopy (SEM)

The SEM images of copper powder were captured at a different location on the sample (Figure 3 (A) shows one of the images). It can be seen from the SEM images, the particles are mostly spherical, and the approximate size was calculated as the surface mean diameter (d_{32}) the ratio of a cube of diameter to the square of the diameter and found to be equal to 10.53 µm (Figure 6.3 (A)).

$$d_{32} = \frac{\sum_{1}^{N} n_i \times d_i^3}{\sum_{1}^{N} n_i \times d_i^2}$$

Where, N – total number of particles.

More than 150 particle diameter was considered for estimating the average particle size. Using the average particle diameter d_{32}, the surface area ($S_{32} = \pi \times d_{32}^2$) and the volume

($V_{32} = \frac{\pi \times d_{32}^3}{6}$) was estimated. After that, the ratio of surface to volume was then divided by the density of copper powder ($\frac{S_{32}}{V_{32} \times \rho_{Cu}}$ Where ρ_{Cu} is copper powder density $\rho_{Cu} = 8.94$ gm/cm^3) to get the surface area per unit mass. It was found that the surface area of the copper equal to 637 cm^2/gm.

B) Optical Microscopy

The particle size was also measured using an optical microscope. Here also, the average particle size was estimated by considering more than 150 particles. As mentioned earlier, the particles are spherical, and it can be seen that the particles are mostly round in shape in the 2D representation (Figure 6.3 (B)). The particle size from the microscope image was measured using ImageJ software ((Rasband 1997)). In this case, the average diameter of the particles was taken as the average diameter of the sphere. The surface mean diameter (d_{32}) of the particle was estimated from the optical microscopy measurements and it was found to be equal to 11.09 µm. Again, similar to that for the SEM data, the ratio of the surface area and volume was determined, and by using the density of the copper powder, the surface area was estimated. The surface area of the copper was found to be equal to 606 cm^2/gm.

6.3.3 Particle Size Analyzer

A third method that was used for the estimating the average particle diameter followed by surface area estimation was particle size analyzer. This method estimates the particle size by laser diffraction, the angle of the diffraction (scattering angle) is measured to estimate the size of the particle. The scattering angle is a function of the particle size, and it is large particles and vice versa. The particle size analyzer estimated the average particles size to be 12.81 µm. As the particles are mostly spherical (see Figure 6.3 (A)), the particle size here corresponds to the diameter of the sphere and surface and volume of the single particle were estimated by the procedure mentioned earlier. Again, as in earlier cases, the specific surface area was estimated to be 524 cm^2/gm.

6.3.4 N_2 Adsorption Methods

Finally, the surface area of copper powder was estimated using BET analysis. Liquid nitrogen was used as adsorbent on copper. The surface area measurements were repeated

twice, and the average specific surface area was found to be 1173 cm^2/gm. The BET estimated specific surface area value is significantly higher than other methods and erroneous; possibly due to very low surface area of the copper powder (~ 0.07 m^2/gm or 0.875 m^2 for 12.5 mg of sample) which is almost 2 orders of magnitude less than the recommended range of 40 to 120 m^2 by the manufacturer (Micromeritics, n.d.).

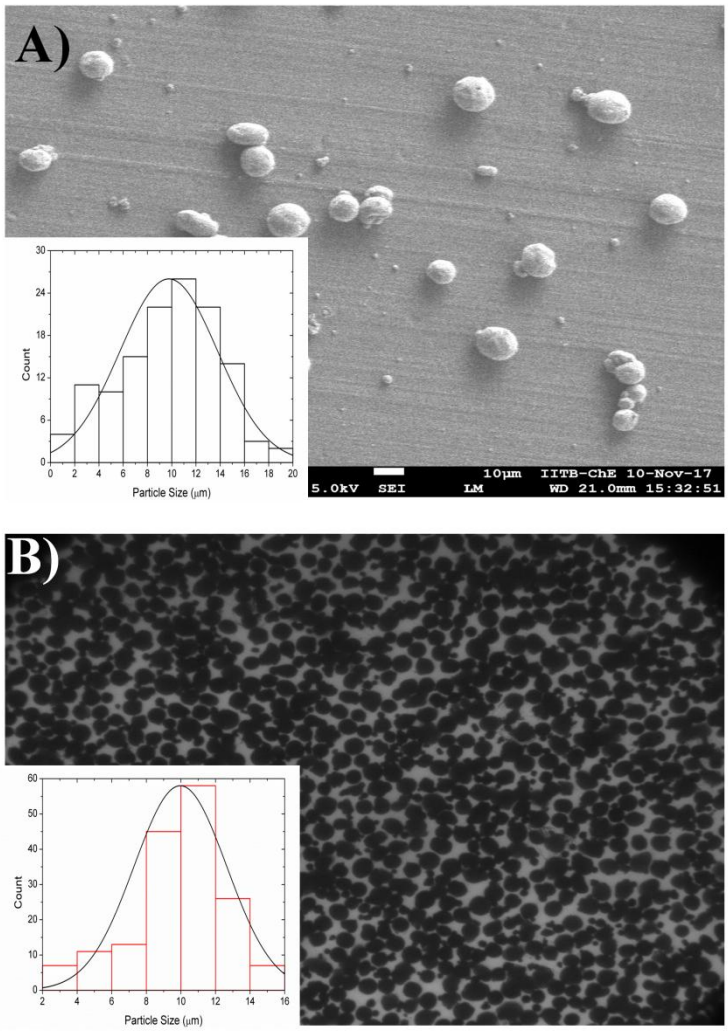

Figure 6.3: (A) SEM image of the copper powder and particle size distribution obtained from SEM images, (B) Optical microscopy image and particle size distribution obtained from optical microscopy images.

The surface area estimated by all the methods has been summarized in table 6.1. It can be seen from the table, the results obtained from both electrochemical methods (Cu_2O and UPD of Pb) are in good agreement with the result obtained from SEM, optical microscopy, and particle size analyzer. It needs to be pointed out that, the surface area estimated by the CV

in 0.5 M KOH solution is dependent strongly on the history of the sample and repeated oxidation-reduction cycles may lead to higher values because of needle like growth on the surface. However, we found that the method involving UPD of Pb is robust with good reproducibility.

Table 6.1: Surface area of the copper powder (cm^2/gm) estimated by different methods. **(*** Based on three experiments performed on freshly coated electrodes.**)**

Sr. No.	**Method**	**Diameter (μm)**	**Estimated Surface Area (cm^2/gm)**
1	Cyclic Voltammetry (Cu_2O monolayer)	-	$611 \pm 20^*$
2	Cyclic Voltammetry (UPD of Pb)	-	$675 \pm 30^*$
3	Scanning Electron Microscope (SEM)	10.53	637
4	Optical Microscopy	11.09	606
5	Particle Size Analyser	12.81	524

The use of the electrochemical methods elucidated here for the estimation of the surface area of copper has unique advantages over other conventional methods used for the estimation of surface area. First of all, the time of analysis is comparatively very small (few minutes) compared to few hours required for the chemisorption/physisorption analysis procedures and the electrochemical procedure does not require any specialized instruments. Second, for monolithic/bulk copper samples, other than electrochemical methods, most of the other methods would give inaccurate results. Moreover, in case of supported copper particles, the electrochemical methods can reliably estimate the surface area of copper particles alone, provided the support is electronically conductive.

6.4 Conclusion

The surface area estimated by both electrochemical methods (a monolayer of Cu_2O and UPD of Pb) is in fair agreement with the surface area estimated by the SEM, particle size analyzer and optical microscopy. We believe that the electrochemical methods and protocols outlined here can be used for quick and reliable estimation of the surface area of the copper catalyst.

Chapter 7

Electrochemical Reduction of CO_2 to C_1 and C_2 Carboxylic Acids on Mixed Oxides of Lanthanum, Calcium, and Copper

7.1 Introduction

As discussed earlier in chapters 4 and 5, copper produced from the reduction of copper oxides have shown a remarkable increase in the current density due to increase in the surface area. Further, the selectivity of oxide derived metallic copper towards the formation of formate ions has changed significantly after oxidation and it is higher in case of oxidized copper foils compared to un-oxidized copper foils. Although the results conclusively demonstrate that copper oxides are not stable at the potentials typically used for reducing CO_2, it might be instructive to investigate how copper oxides in conjugation with other oxides behave. The association might be just a mixture of other metal oxides along with copper oxides or solid solution of metal oxides or a compound of copper oxides and other metal oxides such as perovskites or spinels. The electrochemical reduction of CO_2 on mixed metal oxides and perovskites has been reported in the literature. The electrochemical reduction of CO_2 on metal oxides such as RuO_2, TiO_2, MoO_2 CoO_2 Rh_2O_3 studied by Bandi in 0.2 M Na_2SO_4 solution (pH = 4) results in the formation of methanol and formic acid as reduction products (Bandi 1990). In the same pursuit, Jianping et al. carried out CO_2 reduction on RuO_2 deposited on TiO_2 nanoparticles and nanotubes and then modified it with platinum (Qu et al. 2005). The most active electrode was RuO_2 deposited on TiO_2 nanotubes modified with platinum, which produces methanol with a current efficiency of 60.50%. Further, Andrews et al. deposited the nanoclusters of copper on single crystal zinc oxide and used for the reduction of CO_2 in bicarbonate solution (Andrews et al. 2013). The major products in liquid phase detected were methanol, ethanol, formate, methyl formate and a small amount of propanol. On the other hand, gas phase product consists of methane, ethylene along with CO and H_2. In more recent work, Tacconi et al. have reported the major products of CO_2 reduction on copper oxide - Copper Bromide electrode is hydrocarbons such as methane, ethane, ethylene, and propylene (de Tacconi et al. 2017). The catalyst (copper oxide-copper bromide) used for this reduction reaction was deposited on a gas diffusion layer in a film fashion by electrochemical method. Furthermore, Schwartz et al. (Schwartz et al. 1993) synthesized a series of perovskites type catalyst of copper with a stoichiometry of $A_{1.8}B_{0.2}CuO_4$ (A: La, Pr, and Gd,

B: Sr, Th). These catalysts then deposited on gas diffusion electrode, and CO_2 was reduced in KOH solution. The major products were methanol, ethanol, and n-propanol.

In this context, we have studied the effect in activity and selectivity of mixed metal oxides produced by solution combustion method. The effect of changing the fraction of lanthanum (La) in calcium and copper oxide ($La_xCa_{1-x}Cu$ (x = 0, 0.2, 0.4, 0.6, 0.8, 1.0)) on activity and selectivity for the CO_2 reduction in KOH solution has been reported here. All the catalysts were characterized by X-ray diffraction (XRD), scanning electron microscopy (SEM), and energy dispersive X-ray spectroscopy (EDS). The electrochemical reduction was carried out on gas diffusion electrode in a three-electrode flow cell arrangement. The major products of CO_2 reduction in liquid phase were acetate ions, formate ions, propanol and traces of butanol. Further, the possible mechanism for the formation of different reduction products has been discussed.

7.2 Experimentation

7.2.1 Synthesis of Catalyst

Metal oxide catalysts were synthesized by solution combustion method. Metal Nitrate salts of all the metals were dissolved in de-ionized water in required stoichiometry in a 500 ml conical flask, and citric acid was added as a fuel for the combustion. This mixture was then heated with continuous stirring on a magnetic stirrer with a hot plate. After evaporation of the water, a viscous paste forms which then undergoes self-ignition to leave behind the metal oxide flakes. The flakes were then crushed in agate mortar and pestle to get fine uniform powder. The fine powder was calcined at 800 ^{0}C for 10 hours in the air. After calcination in the air, the powder was crushed once again in agate mortar and pestle to get a fine powder, which was then characterized by different techniques and also used to make gas diffusion electrode.

7.2.2 Electrodes

A three electrode flow cell arrangement was used to carry out CO_2 reduction is shown in Figure 7.1. Working electrode used was a gas diffusion layer (GDL) type electrode made by airbrushing the catalyst ink on the carbon coated side of carbon paper (size 2.5 cm × 2.5 cm) whereas the other side of the carbon paper was pre-coated with polytetrafluoroethylene (PTFE) (supplied by Sainergy Fuel Cell India). Catalyst ink was prepared by dispersing 50 mg of catalyst in 5 ml of isopropyl alcohol (IPA) and 50 µl nafion (5 % nafion suspension

supplied by Sigma-Aldrich). To disperse the catalyst in IPA satisfactorily, the ink was sonicated for 15 minutes in an ultrasonicator bath. A 4 mg/cm^2 loading was generally achieved after airbrushing the ink on the carbon paper. On the other hand, the counter electrode was a platinum mesh, and reference electrode used was Hg/HgO containing 0.3 M KOH solution. The platinum mesh was folded in a square form (size 2.5 cm × 2.5 cm) to fix it in the flow cell.

7.2.3 Electrolytes

Electrochemical reduction of CO_2 was carried out in 0.5 M KOH solution. The 0.5 M KOH solution was prepared was dissolving the required quantity of KOH pellets in deionized water. The 0.5 M KOH solution was passed separately on working and counter electrode side. Counter electrode side electrolyte/anode side electrolyte/anolyte was re-circulated using the peristaltic pump (5 ml/min). However, working electrode side electrolyte/cathode side electrolyte/catholyte was passed only once, and the reduction product laden electrolyte was collected after every half an hour (approximately 10 ml/hour, flow rate was adjusted manually). The samples collected during CO_2 reduction was analyzed on a high performance liquid chromatography (HPLC) for identification and quantification of products. All the sample collected was acidified to pH 2.0 before injection into the HPLC by adding required quantity of 1 M H_2SO_4 (prepared by adding required quantity of concentrated H_2SO_4 (18 M) in deionized water and then sonicating it for 1 minute to remove the gases formed due to acidifying bicarbonates). The mobile phase used for the HPLC was 0.013 M H_2SO_4 solution prepared by adding required quantity of concentrated H_2SO_4 (18 M) in de-ionized water. The mobile phase was sonicated for 10 minutes after adding acid to water to remove any dissolved gases.

It need be noted here that the electrochemical reduction of CO_2 on the copper foils (both oxidized and un-oxidized) has been carried out in 0.5 M $NaHCO_3$ electrolyte under continuous purging of CO_2 in a five neck cell. However, the electrochemical reduction of the CO_2 in flow cell arrangement using powder catalyst has been carried out using 0.5 M KOH electrolyte. This change in electrolyte has been done after carrying out preliminary experiments using both 0.5 M $NaHCO_3$ and 0.5 M KOH solutions. The use of 0.5 M $NaHCO_3$ as an electrolyte in flow cell arrangements and LaCu as electrocatalyst resulted in the formation of formate ions only. On the other hand, with the same catalyst (LaCu) resulted in the formation of acetate ions, propanol and traces of butanol along with the formate ions when

0.5 M KOH was used as electrolyte. Due to a wide range of the products observed in 0.5 M KOH electrolyte with the same electrocatalyst we carried out all the experiments in 0.5 M KOH. It needs to point out here that the use of 0.5 M KOH for the reduction of CO_2 under constant purging in a five neck cell will ultimately result in the formation of bicarbonate ions and a drop in pH. It was observed that the pH of the solution dropped from 13.7 to 7.4 within 15 minutes after CO_2 purging when a 3 electrode system in a 5 neck electrochemical cell was used. However, under the present flow cell type arrangement, a small pH drop (0.1 unit) was observed after the catholyte flows through the cell indicating the very small formation of bicarbonate ions. It is equally likely that concomitant reduction of water to a large extent compensated for the hydroxyl ions lost due to reaction with carbon dioxide.

7.2.4 Equipments

Electrochemical reduction of CO_2 was carried out in the flow cell like the arrangement of the electrode as shown in Figure 7.1. The working electrode (GDL) was supported by a square piece of stainless steel (SS 316) of size 5 cm × 5 cm which also acted as the current collector. Through this SS support, a provision was made by serpentine channels to pass CO_2 gas on the back side of the GDL (PTFE Coated side). Working electrode side solution or the catholyte (0.5 M KOH) solution was passed through the catalyst side of the GDL (carbon coated side), by way of a PTFE frame filled with PPS (polyphenylene sulfide) fiber (TORCON^{TM} by TORAY). This arrangement allowed the GDL to remain in contact with the electrolyte soaked PPS matrix/felt throughout the experiment and the reduction products to diffuse out from the catalyst surface to the middle chamber. Additionally, a layer of celgard has been used to cover and wet the GDL surface uniformly. The working electrode (cathode) and counter electrode (anode) of the cell were separated by a cation ion exchange membrane (fumasep FKB-PK-130) of size 5 cm × 5 cm supplied by Fumatech Germany. The counter electrode was also supported on an SS support and through which 0.5 M KOH solution was re-circulated. The reference electrode was connected to the cell through a tube packed with PPS fibers. The CO_2 coming out from the cell was passed through a water column of 30 cm height to maintain small back pressure in the flow cell.

All experiments of electrochemical reduction of CO_2 reduction was carried out on a Biologic potentiostat (Model VSP 300), and the data was collected and analyzed using EC-Lab 10.40 software. The CO_2 reduction products were analyzed on Agilent 1260 infinity series model with Aminex HPX-87H column (supplied by BIO-RAD, USA) and with

refractive index detector (RID). The major products of CO_2 reduction were acetate ions, formate ions, and propanol. To further confirm the products (acetate ions and propanol) (as formate ions was confirmed for our earlier work) samples were analyzed by mass spectroscopy also. Acetate ions was also detected in an electrospray ionization-mass spectroscopy (ESI-MS) (mass spectrometer supplied by Bruker (Model: maXis Impact)) by coupling potassium as well as sodium atom to acetate ions. Further, propanol was detected on gas chromatography-mass spectroscopy (GC-MS). An Agilent (Model No. 7890) GC was used along JEOL (Model No. AccuTOF GCV) MS.

The X-ray diffraction (XRD) patterns of the catalysts were obtained by PANalytical diffractometer (Model: Empyrean). The XRD data was analyzed using X'pert HighScore Plus software. The morphology of the catalyst was studied by scanning electron microscopy (SEM) and transmission electron microscopy (TEM) for all catalysts sample. The SEM images at different magnification were obtained by JEOL FEG-SEM machine (Model: JSM 7600), and TEM images were obtained on JEOL machine (Model: JEM 2100 ultra HRTEM).

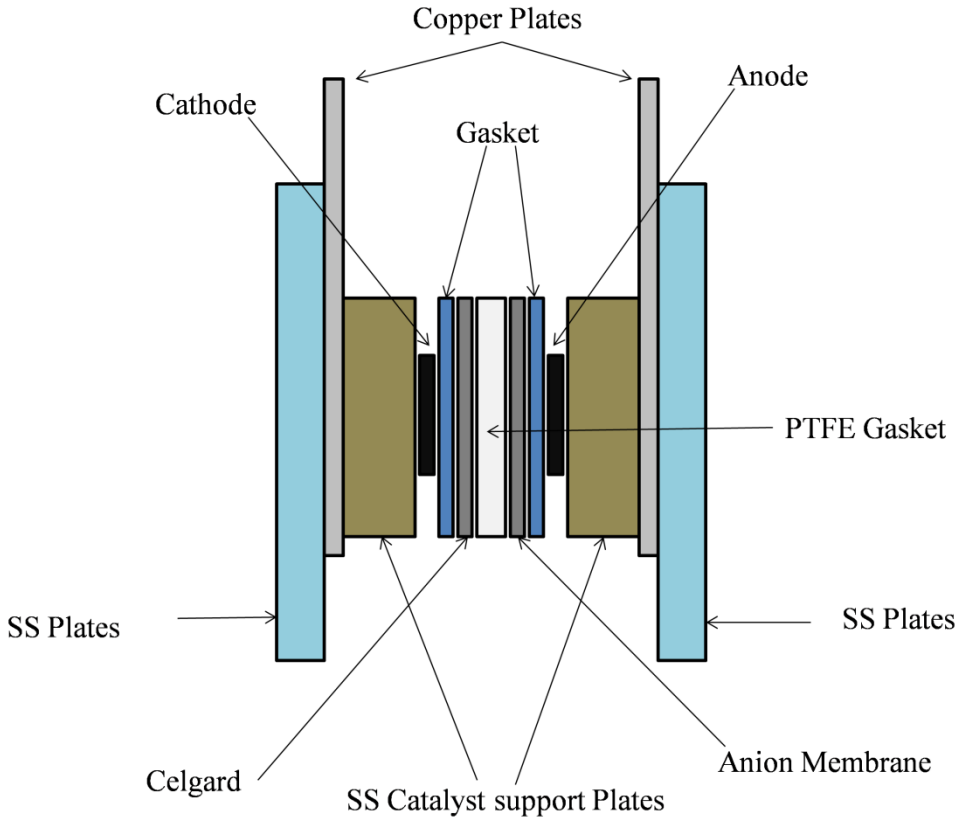

Figure 7.1: Schematic of flow cell used for the electrochemical reduction of the CO_2.

7.3 Results and Discussion

7.3.1 Catalyst Characterization

The elemental analysis of the as-synthesized and the calcined samples (calcined at 800 ^{0}C for 10 h in air) was performed using EDS analysis (energy dispersive X-ray spectroscopy), and the results are shown in Table 7.1. It can be seen from the values obtained by EDS analysis, the atomic ratios in the catalyst are matches fairly with the compositions aimed at (except for $La_{0.2}Ca_{0.8}Cu$) (Table 7.1). Scanning electron microscopy (SEM) observations confirmed that the calcined metal oxide particles are sub-micron in size (varying between 150 to 200 nm), except for CuO (of ~1.2 µm) (Figure 7.2).

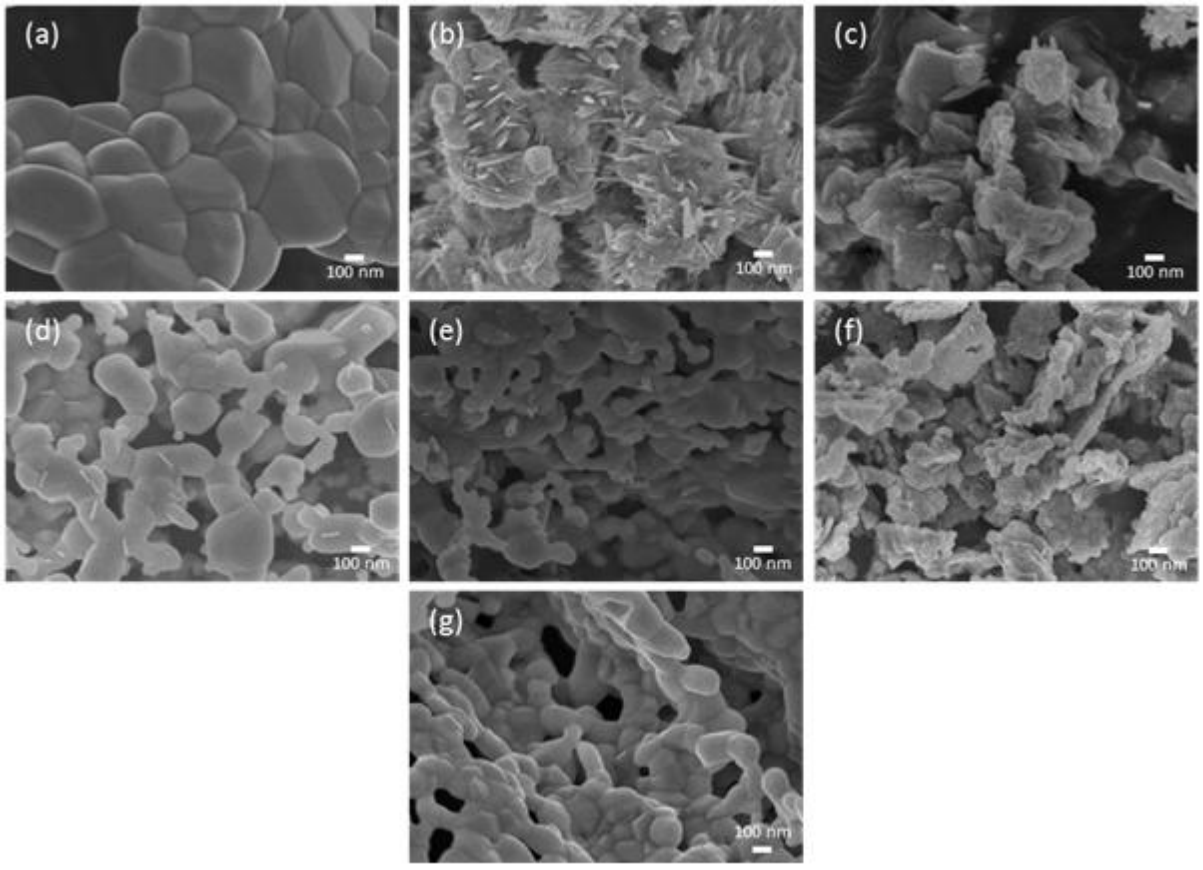

Figure 7.2: The SEM images obtained from the as-synthesized (a) Cu, (b) CaCu (c) $La_{0.2}Ca_{0.8}Cu$ (d) $La_{0.4}Ca_{0.6}Cu$ (e) $La_{0.6}Ca_{0.4}Cu$ (f) $La_{0.8}Ca_{0.2}Cu$ (g) LaCu.

The X-ray diffraction (XRD) patterns recorded for the calcined samples have been presented in Figure 7.3 (for the as-synthesized samples well formed crystalline phase was not observed). Overall, all the calcined metal oxides, except CuO, possess a layered perovskite crystal structure ($AO(ABO_3)n$); B = Cu, A = La or Ca) along with oxides of Ca and Cu. In these structures, Cu atoms are placed at the B-site, whereas either only La or Ca, or La, along

with Ca atoms, is doped at the A-site. Hence, the A-site composition varies with La doping (x), as in $La_xCa_{1-x}Cu$, where x varies from 0 to 1. Phase pure CuO was obtained for the sample without any doping (Figure 7.3 a). Upon doping with Ca, as in CaCu, two distinct phases have been obtained, which are dicalcium cuprate (orthorhombic; ICSD file no.: 68885) and copper oxide (monoclinic; ICSD file no.:16025) (Figure 7.3 b). Further doping with La has been done at the A-site of the atoms along with Ca. The compounds are $La_xCa_{1-x}Cu$, where x = 0.2 to 0.8. For these samples, three different phases have been detected in these oxides, which are di-lanthanum cuprate (orthorhombic; ICSD file no.:50265), di-calcium cuprate (orthorhombic; ICSD file no.: 68885) and copper oxide (monoclinic; ICSD file no.: 16025) (Figure 7.3 c to f). It was confirmed from Rietveld analysis that the volume fraction of di-lanthanum cuprate increased to eventually become greater than the di-calcium cuprate upon incorporation of a greater fraction of La, as compared to Ca at the A-site of the metal oxides (Table 7.2). However, when only La gets doped at the A-site, as in the case of LaCu, only di-lanthanum cuprate (orthorhombic; ICSD file no.: 50265) and copper oxide (monoclinic; ICSD file no.: 16025) phases could be detected. Overall, these doped compounds, consisting of more than one phase have been referred to as 'mixed metal oxide' electrocatalysts.

XRD analyses of the oxides post electrochemical reduction of CO_2 using 0.5 M KOH as the electrolyte at the potential of -1.6 V for 3 hours indicates the presence of more phases than the calcined counterparts (Figure 7.4). After the electrochemical CO_2 reduction, primarily two new phases Cu_2O (ICSD file no.: 52043) and $CuCO_3$ (ICSD file no.: 6179) were detected in the $LaCuO_3$ electro-catalyst (Figure 7.4 e). It is believed that CuO (as originally present) got reduced to metallic Cu, which reacted with ambient CO_2 and O_2 to form the oxides and carbonates after the electrochemical CO_2 reduction process. Other than these some higher oxides *viz.*, CuO_2 (ICSD file no.: 54126) was also detected. The intensities of the peaks corresponding to di-lanthanum cuprate (La_2CuO_4) and CuO (as originally present in the calcined samples) also got reduced significantly during the electrochemical CO_2 reduction experiments. For the other electro-catalyst, *viz.*, CaCu, X-ray diffraction analysis after electrochemical CO_2 reduction indicated the presence of small amounts of CuO and $CuCO_3$, whereas the originally present di-calcium cuprate (Ca_2CuO_3) could not be found; thus indicating that CaCu is also not electrochemically inert. In the case of $La_{0.2}Ca_{0.8}Cu$, $La_{0.6}Ca_{0.4}Cu$ and $La_{0.8}Ca_{0.2}Cu$, the originally present three phases, *i.e.*, lanthanum cuprate (orthorhombic; ICSD file no.:50265), di-calcium cuprate (orthorhombic; ICSD file no.:

68885) and copper oxide (monoclinic; ICSD file no.: 16025), have been found intact, albeit with reduced intensities, after electrochemical CO_2 reduction (see Figure 7.4 b to d).

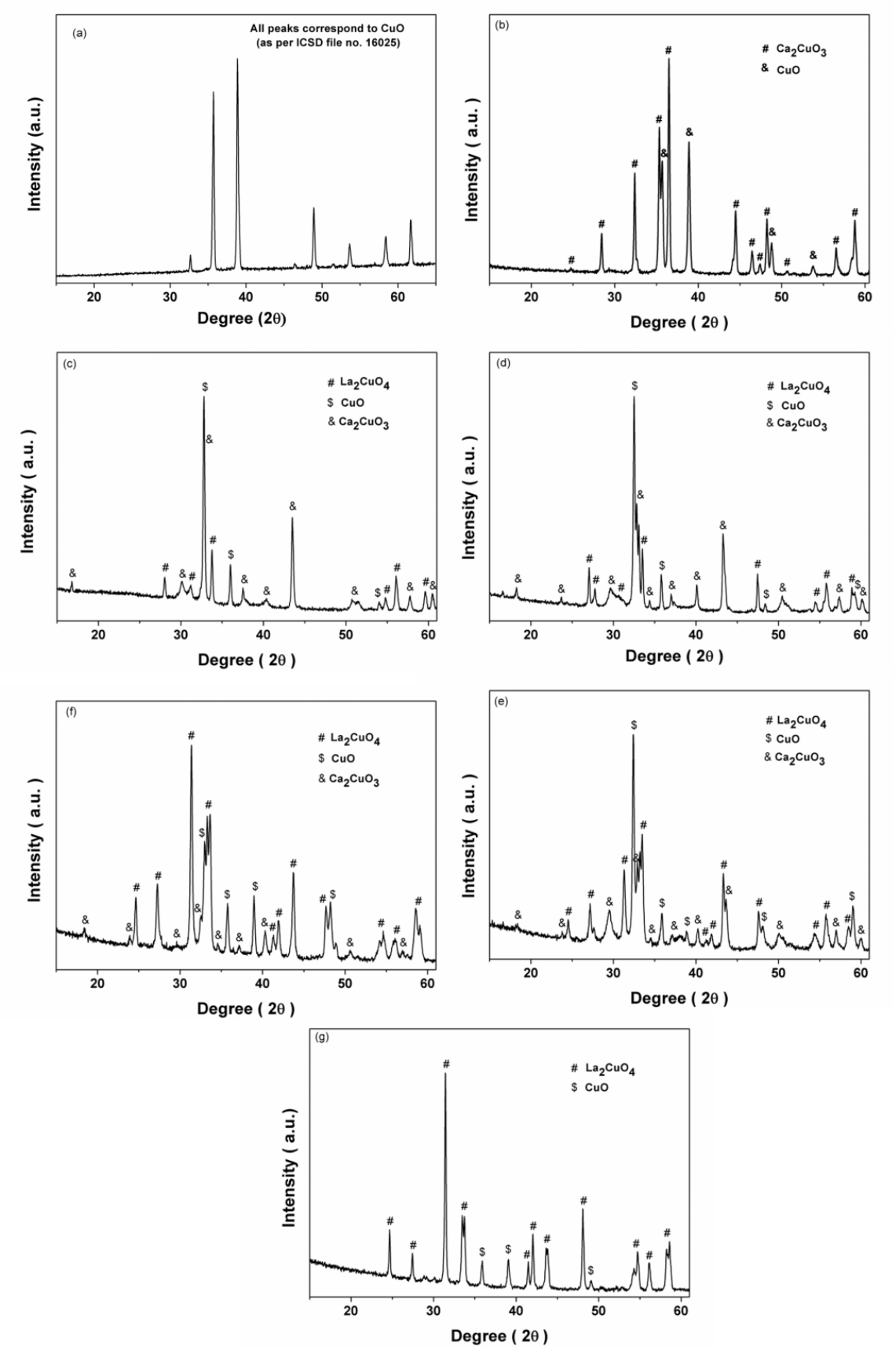

Figure 7.3: X-ray diffraction patterns recorded with the calcined (a) Cu (b) CaCu (c) $La_{0.2}Ca_{0.8}Cu$ (d) $La_{0.4}Ca_{0.6}Cu$ (e) $La_{0.6}Ca_{0.4}Cu$ (f) $La_{0.8}Ca_{0.2}Cu$ (g) LaCu.

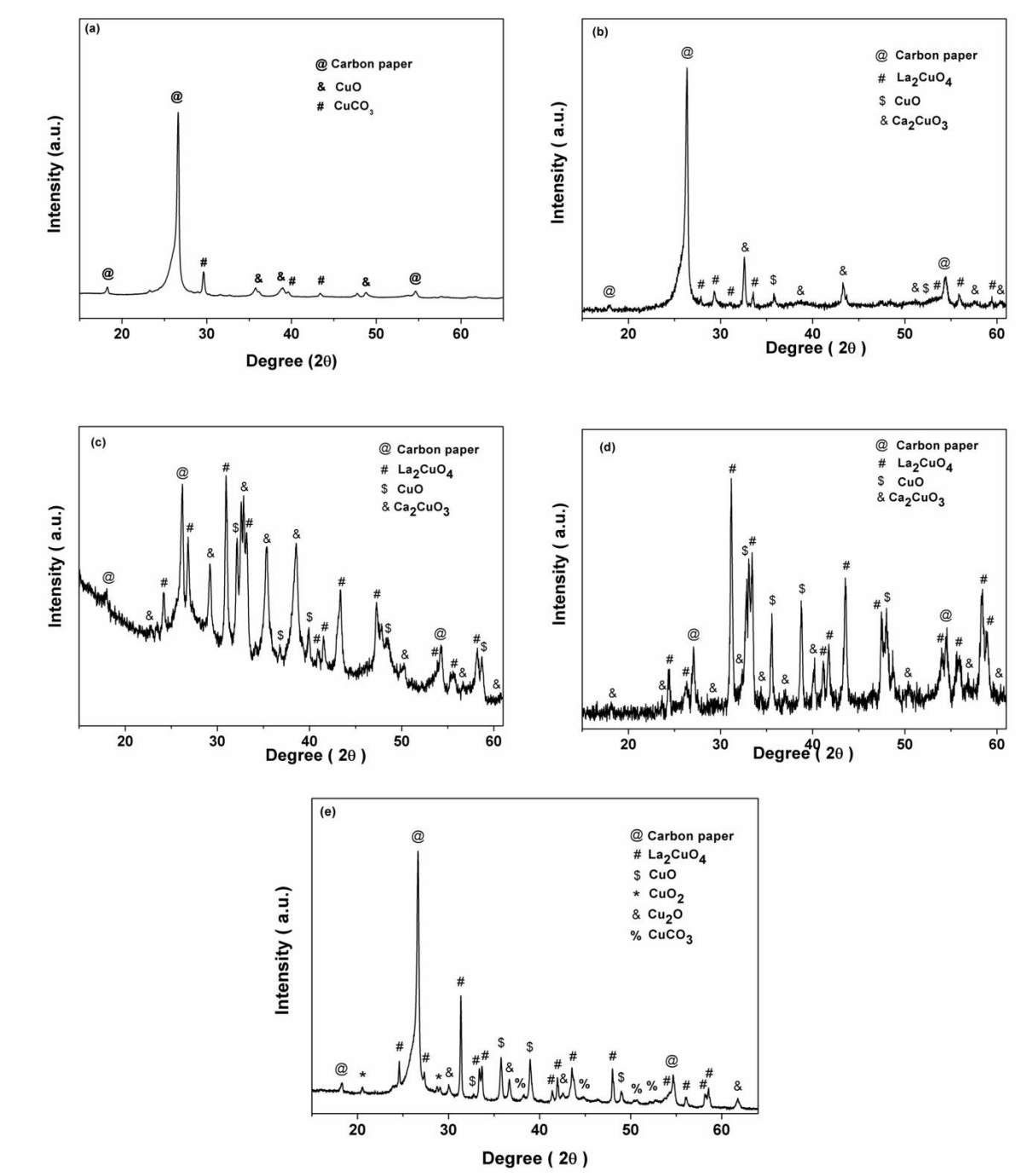

Figure 7.4: X-ray diffraction patterns recorded after electrochemical CO_2 reduction at -1.6 V (against Hg/HgO) with (a) CaCu (b) $La_{0.2}Ca_{0.8}Cu$ (c) $La_{0.6}Ca_{0.4}Cu$ (d) $La_{0.8}Ca_{0.2}Cu$ (e) LaCu.

Table 7.1: Series of the catalyst prepared by adding a different atomic fraction of lanthanum and calcium by keeping the atomic fraction of copper constant.

Sr No.	Catalyst Name	Copper atom fraction (Actual)	Calcium atom fraction (Actual)	Lanthanum atom fraction (Actual)
1	Cu	1 (1)	0	0
2	CaCu	0.5 (0.4412)	0.5 (0.5588)	0
3	$La_{0.2}Ca_{0.8}Cu$	0.5 (42.15)	0.4 (0.4649)	0.1 (0.1281)
4	$La_{0.4}Ca_{0.6}Cu$	0.5 (0.5107)	0.3 (0.2872)	0.2 (0.2020)
5	$La_{0.6}Ca_{0.4}Cu$	0.5 (0.5147)	0.2 (0.1907)	0.3 (0.2944)
6	$La_{0.8}Ca_{0.2}Cu$	0.5 (0.4975)	0.1	0.4 (0.3903)
7	LaCu	0.5 (0.5092)	0	0.5 (0.4908)

Table 7.2: Volume fraction of different metal oxides in the catalyst prepared by solution combustion method.

Sr. No.	**Catalyst Name**	**CuO**	**Ca_2CuO_4**	**La_2CuO_4**
1	Cu	1	-	-
2	CaCu	0.26	0.74	-
3	$La_{0.2}Ca_{0.8}Cu$	0.26	0.34	0.4
4	$L_{0.4}Ca_{0.6}Cu$	0.26	0.26	0.48
5	$La_{0.6}Ca_{0.4}Cu$	0.26	0.2	0.54
6	$La_{0.8}Ca_{0.2}Cu$	0.26	0.14	0.6
7	LaCu	0.26	-	0.74

7.3.2 Electrochemical Reduction of CO_2

The electrochemical reduction of CO_2 on the series of catalyst mentioned above was carried out in the flow cell. Figure 7.1, shows the schematic of the flow cell used. The electrochemical reduction of CO_2 on all the catalysts was studied as different potentials viz -1.4 V, -1.6 V, -1.8 V and -2.0 V vs. a Hg/HgO electrode in 0.5 M KOH solution. The amount of charge transferred during CO_2 reduction at different potential is shown in Figure 7.5. It may be noted that in this chapter instead of reduction current density vs. time data, reduction

charge vs. time data has been reported due to the fluctuating current profiles obtained for few catalysts which make the comparison among the current densities difficult. We suspect that the fluctuation in the current profiles may be due to the complex flow pattern of electrolyte in the flow cell. The major observations have been summarized below;

- Over a period of 3 hours, the amount of charge transferred increases linearly with the time indicating no major change in activity of the catalyst has been observed.
- The amount of charge transferred increases with increase in the reduction potential.
- The lowest charge transferred in case of LaCu and then $La_{0.8}Ca_{0.2}Cu$ or in other words when calcium atomic fraction was lowest.
- The highest charge at lower potentials (-1.4 V and -1.6 V) was observed for the catalyst CaCu and the higher potentials (-1.8 V and -2.0 V) for the catalyst $La_{0.6}Ca_{0.4}Cu$.

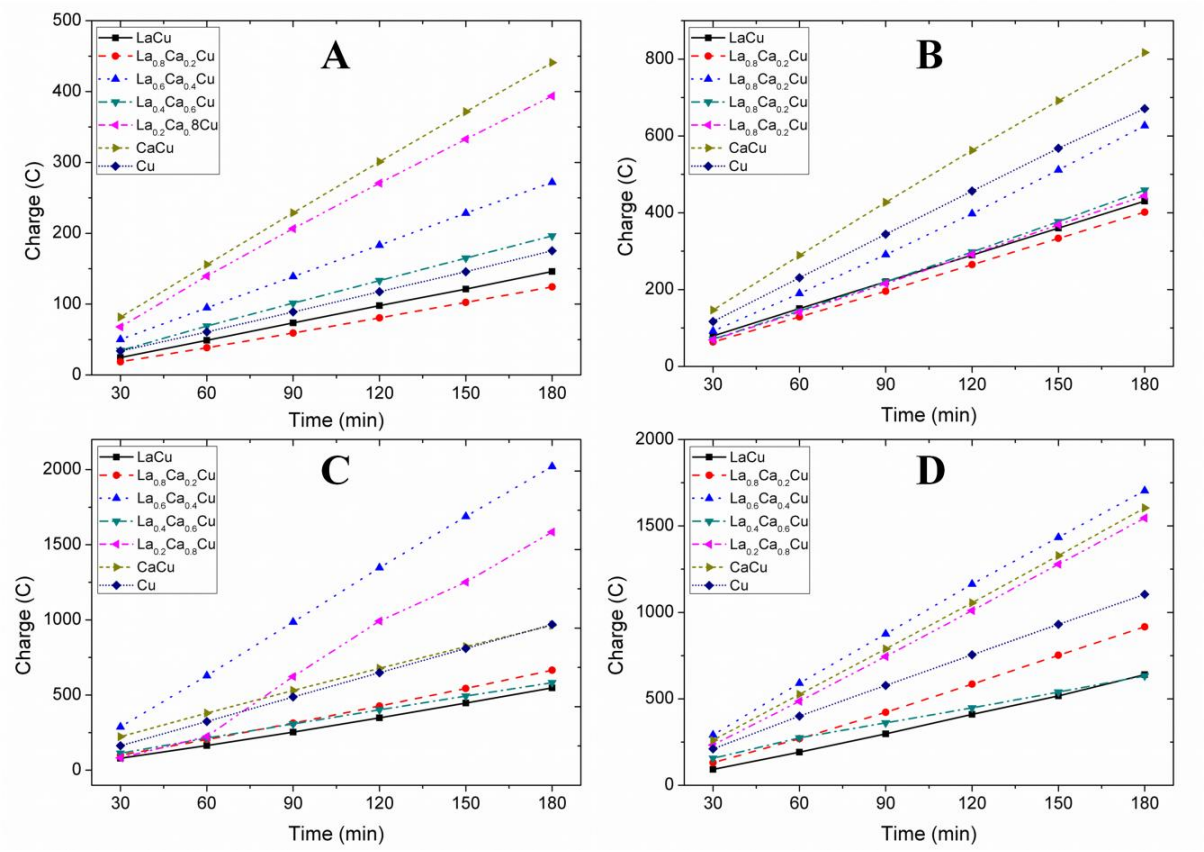

Figure 7.5: Amount of the charge transferred in each half hour during the CO_2 reaction at -1.4 V, -1.6 V, -1.8 V and -2.0 V vs. Hg/HgO on all the catalysts in the flow cell. The electrolyte used in the flow 0.5 M KOH solution.

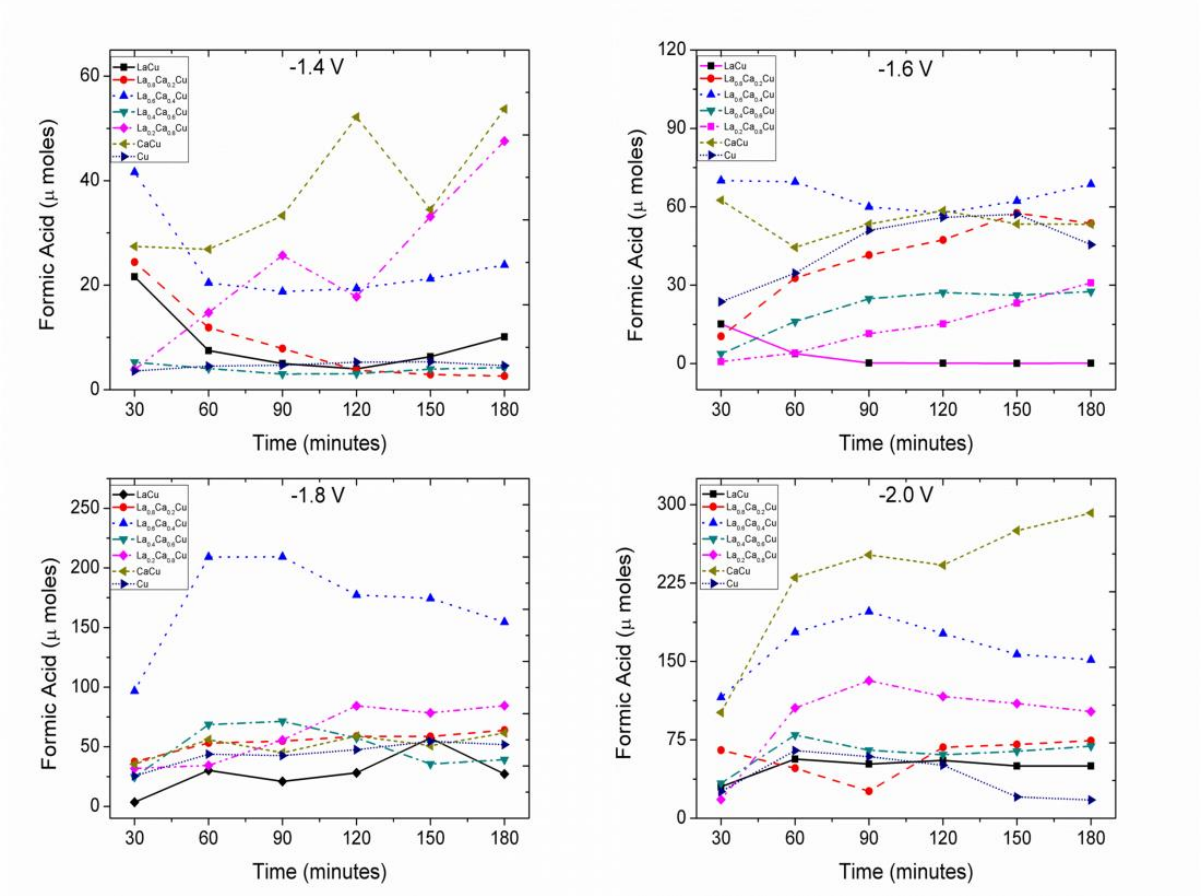

Figure 7.6: Amount of formate ions produced in μmoles at -1.4 V, -1.6 V, -1.8 V and -2.0 V vs. Hg/HgO in 0.5 M KOH solution.

Formate ions have been observed to be produced on all the catalysts at all the potentials. The amount of formate ions produced on the different catalyst at four potentials is shown in Figure 7.6, and the faradaic efficiency for formate ions has been shown in Figure 7.7. The major observation has been summarized below;

- The highest amount of formate ions was produced on CaCu catalyst for all potentials except at -1.8 V, where $La_{0.8}Ca_{0.2}Cu$ produced more amount of the formate ions than any other catalyst.
- The faradaic efficiency for formation of formate ions at -1.6 V, -2.0 V remains fairly constant or increases after first half an hour of operation for almost all the catalysts except in few cases (LaCu, $La_{0.6}Ca_{0.4}Cu$ at -1.6 V, Cu, LaCu, $La_{0.8}Ca_{0.2}Cu$ at -2.0 V) where it decreases with time.
- No particular trend was observed at -1.4 V and -1.8 V as far as the faradaic efficiency for formate ions is concerned.

- The highest faradaic efficiency for formate ions formation was observed at -1.4 V for $La_{0.8}Ca_{0.2}Cu$. At higher potential (-2.0 V) CaCu gives highest faradaic efficiency for formate ions.

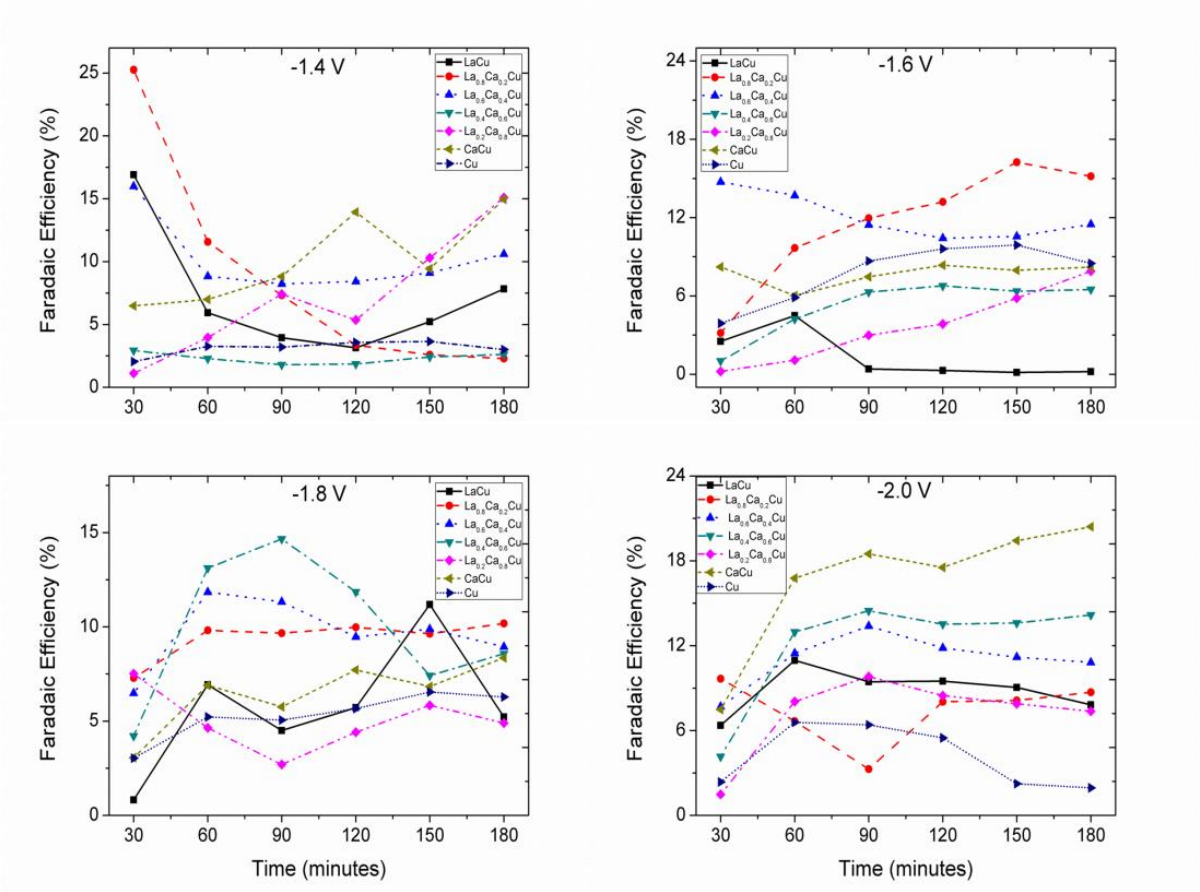

Figure 7.7: Faradaic efficiency for the formation of formate ions in 0.5 M KOH at -1.4 V, -1.6 V, -1.8 V and -2.0 V vs. Hg/HgO.

The amount of acetate ions produce as a function of potential on the different catalyst is shown in Figure 7.8. The highest quantity of acetate ions has been produced on LaCu electrode at all potentials followed by $La_{0.8}Ca_{0.2}Cu$. When the doping of calcium is increased, more than 0.2 very small amount of acetate ions was produced. However, there is a significant difference between the quantities of acetate ions produced by these two catalysts. The results obtained here also corroborate with the reported literature(Genovese et al. 2017; Grace et al. 2014; Lu et al. 2013). Further, the faradaic efficiency of acetate ions formation at the different potential on all the catalyst is shown in Figure 7.9. As the significant amount of acetate ions is produced only on LaCu and $La_{0.8}Ca_{0.2}Cu$, the faradaic efficiency values on all other catalyst are very low. Among these two catalysts, the amount of acetate ions produced on LaCu is

quite large hence the highest faradaic efficiency of 90.74% at -1.6 V was observed for LaCu. Due to this high faradaic efficiency for acetate ions formation, LaCu can be seen as a very promising catalyst for the reduction of CO_2. Curiously enough, the faradaic efficiency for acetate ions formation at lower potential (-1.4 V) is higher than 100%. Similar observations have been also made earlier by many researchers. However, we believe that in this case, the measurement of the charge transferred during the reduction may be erroneous. Further, we suspect the acetate ions produced at higher potentials has been soaked in PPS fibers, which comes out as a product at lower potential and hence more amount of the acetate ions has been observed at a lower potential.

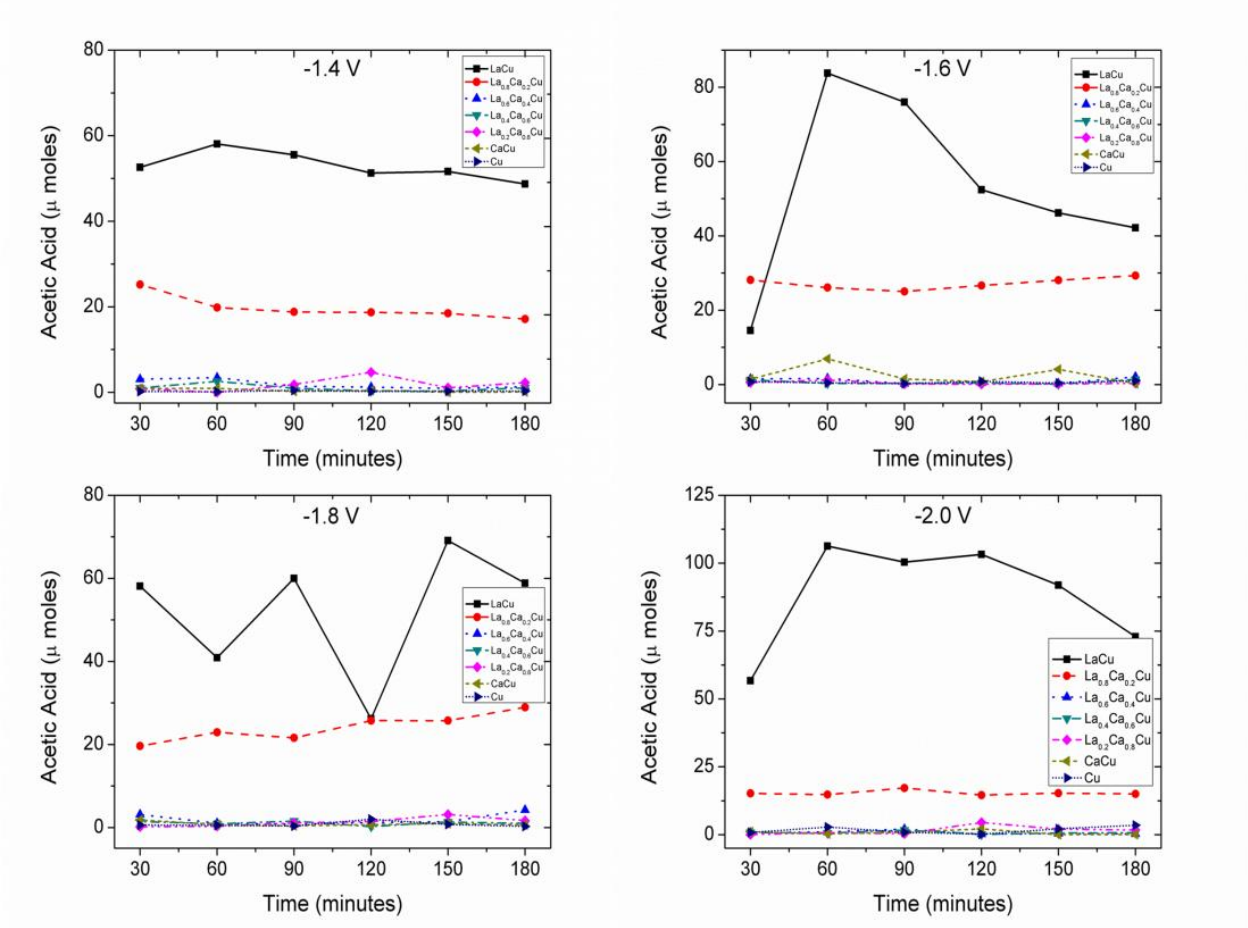

Figure 7.8: Amount of acetate ions produced in μmoles at -1.4 V, -1.6 V, -.8 V and -2.0 V vs. Hg/HgO in 0.5 M KOH solution.

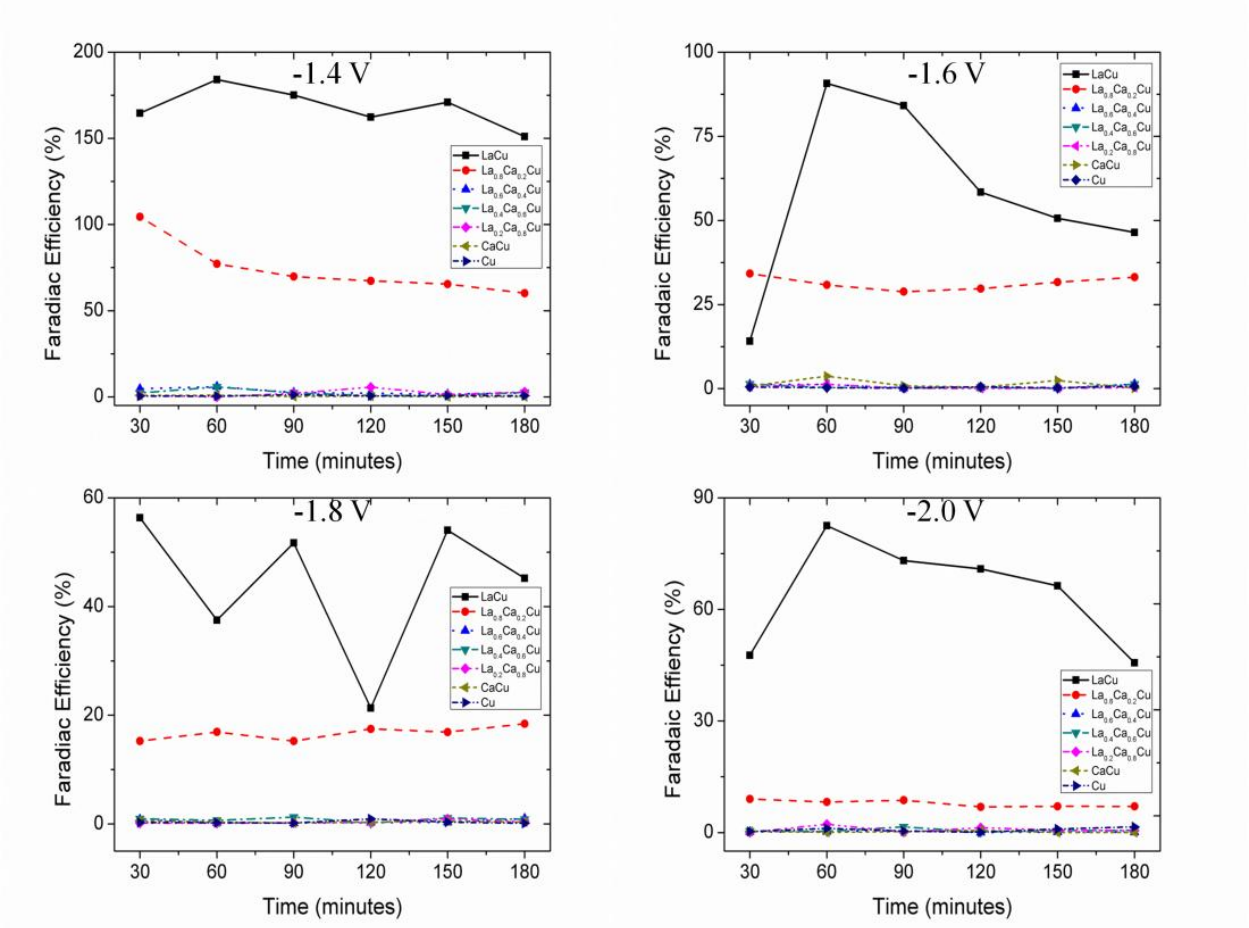

Figure 7.9: Faradaic efficiency for the formation of acetate ions in 0.5 M KOH at -1.4 V, -1.6 V, -1.8 V and -2.0 V vs. Hg/HgO (Faradaic efficiency values at -1.4 V are erroneous).

The production of acetic acid (acetate ions) as CO_2 reduction product has several advantages. Due to the use of acetic acid as a raw material in different processes, the commercial value of acetic acid is quite good. When acetic acid is produced from CO_2, the zero value of CO_2 (waste material) makes the overall economics of the process very promising. Further, calculations have shown that the energy efficiency for the production of acetic acid by formal chemical route is only 27% even after assuming 100% yield (Energy 2004). This shows that the significant amount of energy is lost by chemical route due to the losses in the different stages of formation. If the actual yield achieved is less than 100%, it will further decrease the energy efficiency of the chemical route for the production of acetic acid. Hence electrochemical reduction of CO_2 using LaCu as a catalyst is promising.

Further, propanol has been detected in HPLC analysis along with acetate and formate ions on the LaCu and $La_{0.8}Ca_{0.2}Cu$ catalysis. However, the amount of the propanol was very small hence it could not be measured with good accuracy which resulted in significant variation in the measured amount with time and applied potential. For further confirmation of

the presence of the propanol, GCMS analysis has been performed. The GCMS confirmed the presence of the propanol and additionally detected traces amount of the butanol in the product stream.

7.4 Conclusion

Over a period of 3 hours, the amount of charge transferred increases linearly with the time indicating no major change in activity of the catalyst during the experiments. Further, the amount of charge transferred increases with increase in the reduction potential. The lowest charge was transferred in the case of LaCu and then $La_{0.8}Ca_{0.2}Cu$ or in other words when calcium atomic fraction was lowest. On the other hand, the highest charge at lower potentials (-1.4 V and -1.6 V) was observed for the catalyst CaCu, and at higher potentials (-1.8 V and -2.0 V) for the catalyst $La_{0.6}Ca_{0.4}Cu$. The major products identified were formate ions and acetate ions. Formate ions have been produced on all the catalyst at all the potential used for the electrochemical reduction. Amount of formate ions produced is more when the fraction of La was small or zero. The faradaic efficiency for formate ions at -1.6 V to -2.0 V fairly remains constant after first an half hour for almost all catalyst except in few cases. At higher potential CaCu gives highest faradaic efficiency for formate ions at -2.0 V.

Very small amount of acetate ions was produced on catalyst when the atomic fraction of calcium is increased more than 0.1. The highest quantity of acetate ions has been produced on the $LaCuO_3$ electrode at all potentials followed by $La_{0.8}Ca_{0.2}Cu$. However, there is a significant difference between the quantities of acetate ions produced by these two catalysts. Among these two catalysts, the amount of acetate ions produced on LaCu is quite large hence the highest faradaic efficiency of 90.74% at -1.6 V was observed for LaCu. Due to this high faradaic efficiency for acetate ions formation, LaCu can be seen as a very promising catalyst for the reduction of CO_2.

Chapter 8

Conclusion and Future Scope

8.1 Conclusion

To control the increasing CO_2 concentration in the atmosphere and to avoid its effects in the form of climate change, we have to plant billions of trees to convert atmospheric CO_2 to back to carbohydrates. This method of planting and growing plants to trees can be a long term solution as it will take a lot of time and care as well as the resources in the form of land and water. Due to continuously growing population, both these resources (land and water) are now becoming increasingly rare. Therefore, we have to search for the new alternatives which are short term and has potential to benefit us economically too. Hence, it is important to find a solution where CO_2 can be captured and converted to useful products that can processed further.

Different methods for CO_2 reduction to useful chemicals and fuels has been studied and reported in the literature. Electrochemical method for the CO_2 reduction seems to be more promising due to the direct use of the electricity generated by nonconventional sources of the energy. Further, electrochemical reduction of CO_2 has been studied in aqueous and non aqueous solution by using different metal electrodes. Literature for many metals used for the electrochemical reduction of the CO_2 as electrocatalyst and the product of the reduction are available. The major disadvantage of the electrochemical method is a requirement of high overpotential for CO_2 reduction and the parallel HER. To make commercial use of the electrochemical reduction of the CO_2 to produce important chemicals and fuel, the overpotential need to be lowered in addition to increase the selectivity of the catalyst toward commercially important chemical compared to the hydrogen evolution.

Copper has been selected as an electrocatalyst in this study and the results we obtained has been concluded below.

Electrochemical Characterization of the Bulk and Monolayer Copper in Alkaline

The electrochemical characterization of the bulk and monolayer copper in alkaline solution has revealed many aspects of the copper oxide formation and their subsequent reduction. The main observations and conclusions summarized below:

- The Cu_2O produced by initial oxidation of copper results in the formation of a monolayer film for certain range of scan rate and pH. The formation of this monolayer appears as peak A.
- Upon increasing the potential, copper atoms oxidizes to form $Cu(OH)_2$ along with water soluble ($Cu(OH)_4^{2-}$) oxide. As the potential is increased further the formation of CuO takes place. The formation of these oxides of copper (Cu^{2+}) appears as peak B.
- The shape of the peak A is independent of the scan rate. However, in case of peak B, the shape changes significantly. Charge under both peaks (A and B) increases as the scan rate of CV decreases below 30 mV/s.
- The SEM images of the electrochemically oxidized copper foils by LSV below 30 mV/s scan rate indicates the formation of needle-like structures which might explain the atypical relation between the peak currents and scan.
- Voltammetry data suggest that the final product of oxidation is a mix of Cu_2O, CuO, and $Cu(OH)_2$. This has been verified further by XPS analysis of the oxidized copper foils.
- Subsequent reduction of the final products of oxidation proceeds in two stages (i) initially only a fraction of CuO gets reduced to metallic Cu (under peak C) and (ii) the rest of oxidized species gets reduced at a still lower potential (under peak D).
- The CV of monolayer copper deposited on platinum confirms the formation of Cu(I) oxides (Cu_2O) as potential moved towards positive potential. It was further confirmed form the oxidation charge calculations for Cu_2O.
- The dissolution of monolayer copper indeed takes place, but at significantly higher potential and only a fraction of Cu_2O reacts further to $Cu(OH)_2$. This suggests that the underlying platinum layer imparts a degree of nobility to copper monolayer with respect to oxidation. The initial stages of oxidation of copper seem to mimic that for bulk copper; the onset potential is significantly higher.
- Cyclic voltammogram of copper in 0.5 M Na_2CO_3 solution shows a different signature than that of in 0.5 M KOH solution. The shape, as well as the charge under peaks, is less than that observed in the CV of 0.5 M KOH. The reason for the less oxidation charge may be the formation of a passive oxide layer produced due to the interaction with carbonate ions present in the solution.
- Cyclic voltammogram of copper in 0.5 M $NaHCO_3$ solution shows slightly different signature than that of either 0.5 M KOH or 0.5 M Na_2CO_3. In case of 0.5 M $NaHCO_3$

solution also, the peak current increase with scan rate in studied potential scan rate unlike 0.5 M KOH.

Electrochemical Reduction of the CO_2 on Electrochemically Oxidized Copper Foil

The electrochemical reduction of the CO_2 was carried out on copper foil oxidized by CA, LSV and CV in CO_2 purged 0.5 M $NaHCO_3$ solution. The electrochemical oxidations of the copper foils were carried out in 0.5 M KOH solution. The important observations and conclusions have been summarized below:

- The electrochemical oxidation by these methods results in the formation of oxide film consisting of Cu_2O, CuO, and $Cu(OH)_2$.
- The XPS analysis shows that the oxides produced on the copper surface by electrochemical methods get reduced back to copper in first few minutes when oxidized copper foil subjected to the CO_2 reduction (at -1.6 V). Further, the spectrophotometric analysis of the reduced copper foils has also been used to corroborate the reduction of the copper oxides back to copper. The SEM images also show that the oxides needles go to extinction within five minutes of the CO_2 reduction.
- It has been conclusively demonstrated that the electrochemical reduction takes place on copper and not on the oxides of copper.
- The CO_2 reduction current density of the oxidized copper foils was significantly higher than un-oxidized copper foil. The copper oxidized by CV shows highest current density followed by LSV and then by CA oxidized copper foils.
- The reason of the increase in the current density was increase in the surface roughness/real surface area/EASA (measured by UPD of Pb) due to oxidation and subsequent reduction.
- The oxidation of copper by CV is more intense compared to LSV and CA, hence higher EASA and higher activity for CO_2 reduction. This manifests as higher current density by CV as compared to LSV and CA.
- The selectivity of the formate ions produced due to electrochemical reduction of CO_2 increases after oxidation of copper. The highest amount of formate ions was produced on the copper foil oxidized by CV.

Electrochemical Reduction of the CO_2 on Anodized and Annealed Copper Foil

The electrochemical reduction of the CO_2 on anodized (25 cycles of CV at a scan rate of 5 mV/s in Ar saturated 0.5 M KOH solution), annealed (heated at 400 ^{0}C for 10 hours in air) and un-oxidized copper in 0.5 M $NaHCO_3$ solution were compared. The important observations and conclusions have been summarized below:

- The electrochemical oxidation by these method results in the formation of oxide film consisting of Cu_2O, CuO, and $Cu(OH)_2$. The thermochemical oxidation results in the formation of Cu_2O, CuO, and Cu_3O_4.
- The annealing has produced a thicker layer of oxides on copper foil compared to the anodized copper foil. The thick layer of oxides upon reduction results in higher EASA compared to the anodized copper foil.
- The EASA was measured by UPD of Pb. Due to higher EASA for annealed copper foil, the current density for CO_2 reduction is more for the annealed copper.
- With the increase in reduction potential, the difference between the reduction current density of anodized and annealed copper foils decreases drastically.
- The selectivity of the formate ion formation due to electrochemical reduction of CO_2 increases on the oxidized copper foils compared to un-oxidized copper foils. The amount of formate ions produced was highest for copper oxidized by annealing.
- In contrast, the faradaic efficiency for formate ion formation is higher for copper foil oxidized by anodization. The faradaic efficiency of anodized copper foil was lower than annealed copper foil at -2.0 V may be due to dominating HER at this potential than at lower potentials.

Estimation of Copper Powder Surface Area by Electrochemical, Microscopy and Laser Diffraction Methods

For determination of the EASA of copper foil after oxidation, UPD of Pb has been used extensively. Here, we have cross checked the accuracy and reliability of the electrochemical method viz UPD of Pb and Cu_2O monolayer by comparing the surface area estimated these methods with surface area estimated other methods. Along with electrochemical method, microscopy (optical and scanning electron) and laser diffraction methods have been used. The major observations and conclusion have been summarized below.

- Commercial copper powder with spherical particles and 10 micron size was used for this study.
- SEM images were captured and used to find the average particle size and using the density of the copper powder, the surface area of the copper powder was estimated.
- Optical microscopy images were used to estimate the particle size of the copper particle and surface area of the copper powder was determined.
- Laser diffraction technique has been used to estimate the particle size and then the surface area of the copper powder.
- The surface area estimated by the electrochemical methods and other methods are in good agreement.
- The electrochemical method has few more advantages over the conventional surface estimating methods. The electrochemical method can be used for the monolithic as well as supported catalysts where BET or other methods fail. Electrochemical methods can estimate the surface area rapidly compared to the other methods. Further, the requirement of the chemical and equipment is minimum.

Electrochemical Reduction of CO_2 to C_1 and C_2 Carboxylic Acids on Mixed Oxides of Lanthanum, Calcium, and Copper

Copper derived from the copper oxides was found to be more active for the electrochemical reduction of CO_2. Additionally, the selectivity for the formation of formate ions has been changed significantly after the oxidation. Here, the effect of the presence of the other metal oxides has been investigated. The major observations and conclusions have been summarized below.

- The CO_2 reduction charges remain fairly constant throughout the experiment suggesting no major surface modification occurred.
- As the atomic fraction of Ca decreases (La atomic fraction increased), lower reduction charges have been observed.
- The highest charge at lower potentials (-1.4 V and -1.6 V) was observed for the catalyst CaCu while at higher potentials (-1.8 V and -2.0 V) it was observed for the catalyst $La_{0.6}Ca_{0.4}Cu$.

- The major products produced were formate ions and acetate ions, along with propanol and traces of the butanol.
- Formate ions have been produced on all the catalyst and at all the potential used for the electrochemical reduction. Amount of formate ions produced is more when the fraction of La was small or zero.
- The faradaic efficiency for formate ions at -1.6 V to -2.0 V remains fairly constant after first half hour for almost all the catalyst except in few cases. At higher potential CaCu gives highest faradaic efficiency for formate ions at -2.0 V.
- Very small amount of acetic acid was produced on catalyst when the atomic fraction of calcium is increased from 0.1.
- The highest quantity of acetic acid has been produced on LaCu electrode at all potentials followed by $La_{0.8}Ca_{0.2}Cu$. There is a significant difference between the quantities of acetic acid produced by these two catalysts.
- Among these two catalysts (LaCu and $La_{0.8}Ca_{0.2}Cu$) the amount of acetic acid produced on LaCu is quite large hence the highest faradaic efficiency of 90.74 % at -1.6 V was observed for LaCu. Due to this high faradaic efficiency for acetic acid formation, LaCu can be seen as a very promising catalyst for the reduction of CO_2.

8.2 Future Scope

As observed from our experiments, the oxidation of copper increases the surface area of copper which results in an increase in the formation of formate ions. The increase in the surface area depends on the extent of the oxidation. The extent of the oxidation copper foil can be carried out more systematically to observe up to what extent the increase in the surface area helps in increasing the activity and the selectivity of CO_2 reduction. Further, thermochemical oxidation has been done at only at one temperature for 10 hours, and it will be interesting to study the effect of the oxidation temperature and the duration of the oxidation on selectivity and the activity of CO_2 reduction. Moreover, the electrochemical reduction on oxidized copper foils in other aqueous electrolytes can be studied to see the effect of the electrolyte on the selectivity of CO_2 reduction. It will also be worthwhile to identify and quantify the gaseous products formed while electrochemical reduction of CO_2.

Mixed metal oxides of Cu, Ca and La has been studied here, another set of the catalyst can be prepared by the replacement of Ca with other metals with two or more oxidation state such as Fe, Mn, Co, etc. and the effect of this replacement on the selectivity of the product will be interesting. Further, other methods for the synthesis of mixed metal oxides can also be used so the effect of the synthesis method is elucidated. Moreover, the effect of the particle size and shape on the selectivity of the product can be studied. Additionally, the flow cell arrangements can be further improved for the collection of the gaseous samples as well as current fluctuation observed during the experiments can be minimized.

It will be interesting to check if the feasibility of the UPD of Pb used for the measurement of the EASA of the copper can be extended for the estimation of the EASA of other metal electrode or metal powder. Studies can be carried out in finding suitable metal for which under potentially deposition on another metal surface can be carried out successfully.

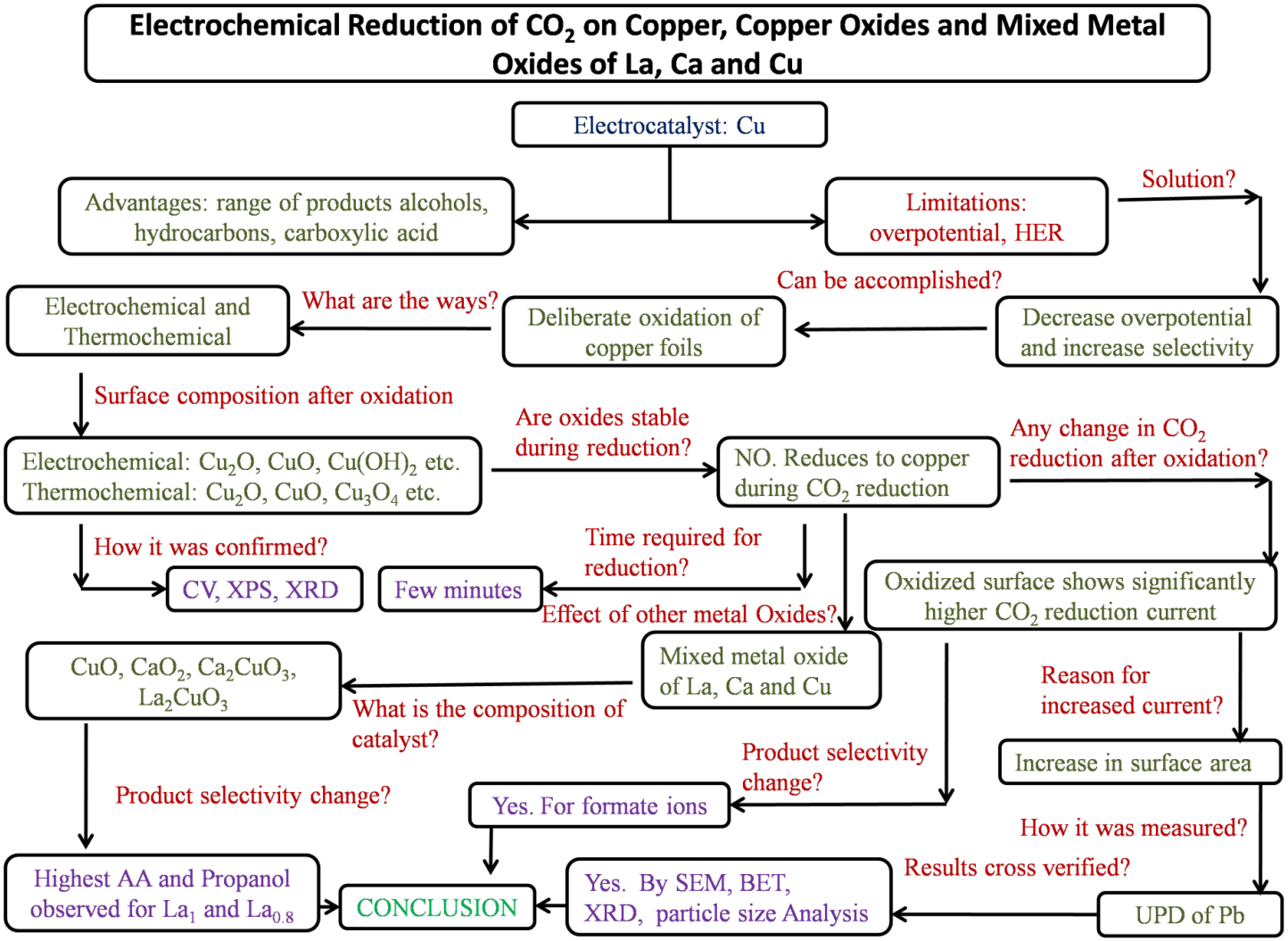

Overview of Research Work

References

Amatore, Christian, and Jean Michel Saveant. 1981. "Mechanism and Kinetic Characteristics of the Electrochemical Reduction of Carbon Dioxide in Media of Low Proton Availability." *Journal of the American Chemical Society*, 103 (17), 5021–23.

Ambrose, J, R G Barradas, and D W Shoesmith. 1973a. "Investigations of Copper in Aqueous Alkaline Solutions by Cyclic Voltammetry." *Journal of Electroanalytical Chemistry and Interfacial Electrochemistry*, 47 (1), 47–64.

Ambrose, J, R G Barradas, and D W Shoesmith. 1973b. "Rotating Copper Disk Electrode Studies of the Mechanism of the Dissolution-Passivation Step on Copper in Alkaline Solutions." *Journal of Electroanalytical Chemistry and Interfacial Electrochemistry*, 47 (1), 65–80.

Andrews, Evan, Maoming Ren, Fei Wang, Ziyu Zhang, Phillip Sprunger, Richard Kurtz, and John Flake. 2013. "Electrochemical Reduction of CO_2 at Cu nanocluster/(1010) ZnO Electrodes." *Journal of The Electrochemical Society*, 160 (11), H841–46.

Ayers, W. M. 1994. "An Overview of Electrochemical Carbon Dioxide Reduction: Special Publication Royal Society of Chemistry." *Carbon Dioxide Chemistry*, 153 (1), 365.

Aylmer-Kelly, A W B, A Bewick, P R Cantrill, and A M Tuxford. 1973. "Studies of Electrochemically Generated Reaction Intermediates Using Modulated Specular Reflectance Spectroscopy." *Faraday Discussions of the Chemical Society*, 56, 96–107.

Azuma, Masashi, Kazuhito Hashimoto, Masahiro Watanabe, and Tadayoshi Sakata. 1990. "Electrochemical Reduction of Carbon Dioxide to Higher Hydrocarbons in a $KHCO_3$ Aqueous Solution." *Journal of Electroanalytical Chemistry and Interfacial Electrochemistry*, 294 (1–2), 299–303.

Bamberger, C E, and Paul R Robinson. 1980. "Thermochemical Splitting of Water and Carbon Dioxide with Cerium Compounds." *Inorganica Chimica Acta*, 42, 133–37.

Bandi, A. 1990. "Electrochemical Reduction of Carbon Dioxide on Conductive Metallic Oxides." *Journal of the Electrochemical Society*, 137 (7), 2157–60.

Bard, A. J. 1976. *Encyclopedia of Electrochemistry of the Elements*. Dekker New York.

Beverskog, B, and I Puigdomenech. 1997. "Revised Pourbaix Diagrams for Copper at 25 to 300 ^{0}C." *Journal of The Electrochemical Society*, 144 (10), 3476–83.

Brisard, G M, J D Rudnicki, F McLarnon, and E J Cairns. 1995. "Application of Probe Beam Deflection to Study the Electrooxidation of Copper in Alkaline Media." *Electrochimica Acta*, 40 (7), 859–65.

Brisard, Gessie M, Entissar Zenati, Hubert A Gasteiger, Nenad M Marković, and Philip N Ross. 1997. “Underpotential Deposition of Lead on Cu (100) in the Presence of Chloride: Ex-Situ Low-Energy Electron Diffraction, Auger Electron Spectroscopy, and Electrochemical Studies.” *Langmuir*, 13 (8), 2390–97.

Choi, Sunho, Jeffrey H Drese, and Christopher W Jones. 2009. “Adsorbent Materials for Carbon Dioxide Capture from Large Anthropogenic Point Sources.” *ChemSusChem* 2, (9), 796–854.

Coehn, Alfred, and Stefan Jahn. 1904. “Ueber Elektrolytische Reduction Der Kohlensäure.” *European Journal of Inorganic Chemistry*, 37 (3), 2836–42.

Cook, Ronald L, Robert C MacDuff, and Anthony F Sammells. 1989. “Evidence for Formaldehyde, Formic Acid, and Acetaldehyde as Possible Intermediates during Electrochemical Carbon Dioxide Reduction at Copper.” *Journal of the Electrochemical Society*, 136 (7), 1982–84.

Crundwell, F K. 1992. “The Anodic Dissolution of Copper in Hydrochloric Acid Solutions.” *Electrochimica Acta*, 37 (15), 2707–14.

Deroubaix, G, and P Marcus. 1992. “X-ray Photoelectron Spectroscopy Analysis of Copper and Zinc Oxides and Sulphides.” *Surface and Interface Analysis*, 18 (1), 39–46.

Dignam, M J, and D B Gibbs. 1970. “Anodic Oxidation of Copper in Alkaline Solution.” *Canadian Journal of Chemistry*, 48 (8), 1242–50.

Din, A M Shams El, and F M Abd El Wahab. 1964. “The Behaviour of the Copper Electrode in Alkaline Solutions upon Alternate Anodic and Cathodic Polarization.” *Electrochimica Acta*, 9 (1), 113–21.

Energy, U.S. Department of. 2004. “U.S. Department of Energy, Exergy Analysis: A Powerful Tool for Identiying Process Inefficiencies in the U.S. Chemical Industry.” In .

Essalik, A, K Amouzegar, and O Savadogo. 1995. “Quantitative Determination of Dispersed Platinum in Carbon by Cyclic Voltammetry.” *Journal of Applied Electrochemistry*, 25 (4), 404–7.

Fletcher, S, R G Barradas, and J D Porter. 1978. “The Anodic Oxidation of Copper Amalgam and Polycrystalline Copper Electrodes in LiOH Solution.” *Journal of The Electrochemical Society*, 125 (12), 1960–68.

Francke, Robert, Victor Climent, Helmut Baltruschat, and Juan M Feliu. 2008. “Electrochemical Deposition of Copper on Stepped Platinum Surfaces in the [01] Zone Vicinal to the (100) Plane.” *Journal of Electroanalytical Chemistry*, 624 (1), 228–40.

Frese, Karl W. 1991. “Electrochemical Reduction of CO_2 at Intentionally Oxidized Copper Electrodes.” *Journal of the Electrochemical Society*, 138 (11), 3338–44.

Frese, Ko W, and S Leach. 1985. “Electrochemical Reduction of Carbon Dioxide to Methane, Methanol, and CO on Ru Electrodes.” *Journal of the Electrochemical Society*, 132 (1), 259–60.

Furuya, Nagakazu, Tsuyoshi Yamazaki, and Masami Shibata. 1997. “High Performance Ru-Pd Catalysts for CO_2 Reduction at Gas-Diffusion Electrodes.” *Journal of Electroanalytical Chemistry*, 431 (1), 39–41.

Gattrell, M, N Gupta, and A Co. 2006. “A Review of the Aqueous Electrochemical Reduction of CO_2 to Hydrocarbons at Copper.” *Journal of Electroanalytical Chemistry*, 594 (1), 1–19.

Genovese, Chiara, Claudio Ampelli, Siglinda Perathoner, and Gabriele Centi. 2017. “Mechanism of C–C Bond Formation in the Electrocatalytic Reduction of CO_2 to Acetic Acid. A Challenging Reaction to Use Renewable Energy with Chemistry.” *Green Chemistry*, 19 (10), 2406–2415.

Gerischer, H. 1956. “P. Delahay, New Instrumental Methods in Electrochemistry. XVII, 437 S. Interscience Publishers Inc., New York 1954. Preis: Geb. $11.50.” *Berichte Der Bunsengesellschaft Für Physikalische Chemie*, 60 (5), 521–22.

Getoff, N, G Scholes, and J Weiss. 1960. “Reduction of Carbon Dioxide in Aqueous Solutions under the Influence of Radiation.” *Tetrahedron Letters*, 1 (39), 17–23.

Giri, Sachin D., and A. Sarkar. 2016. “Electrochemical Study of Bulk and Monolayer Copper in Alkaline Solution.” *Journal of The Electrochemical Society*, 163 (3), H252–59.

Gliński, Marek, Urszula Ulkowska, and Ewa Iwanek. 2016. “Application of Heterogeneous Copper Catalyst in a Continuous Flow Process: Dehydrogenation of Cyclohexanol.” *Journal of Chemical Education*, 93 (9), 1623–25.

Gonzalez, S, M Perez, M Barrera, A R Gonzalez Elipe, and R M Souto. 1998. “Mechanism of Copper Passivation in Aqueous Sodium Carbonate− Bicarbonate Solution Derived from Combined X-Ray Photoelectron Spectroscopic and Electrochemical Data.” *The Journal of Physical Chemistry B*, 102 (28), 5483–89.

Grace, Andrews Nirmala, Song Yi Choi, Mari Vinoba, Margandan Bhagiyalakshmi, Dae Hyun Chu, Yeoil Yoon, Sung Chan Nam, and Soon Kwan Jeong. 2014. “Electrochemical Reduction of Carbon Dioxide at Low Overpotential on a polyaniline/Cu_2O Nanocomposite Based Electrode.” *Applied Energy*, 120, 85–94.

Green, Clare L, and Anthony Kucernak. 2002. “Determination of the Platinum and Ruthenium Surface Areas in Platinum− Ruthenium Alloy Electrocatalysts by Underpotential Deposition of Copper. I. Unsupported Catalysts.” *The Journal of Physical Chemistry B*, 106 (5), 1036–47.

Haber, J, T Machej, L Ungier, and J Ziółkowski. 1978. “ESCA Studies of Copper Oxides and Copper Molybdates.” *Journal of Solid State Chemistry*, 25 (3), 207–18.

Haleem, S M Abd El, and Badr G Ateya. 1981. “Cyclic Voltammetry of Copper in Sodium Hydroxide Solutions.” *Journal of Electroanalytical Chemistry and Interfacial Electrochemistry*, 117 (2), 309–19.

Hampson, N A, J B Lee, and K I MacDonald. 1971. “Oxidations at Copper Electrodes: Part 2. A Study of Polycrystalline Copper in Alkali by Linear Sweep Voltammetry.” *Journal of Electroanalytical Chemistry and Interfacial Electrochemistr,y* 32 (2), 165–73.

Hara, Kohjiro, Akihiko Kudo, and Tadayoshi Sakata. 1995. “Electrochemical Reduction of Carbon Dioxide under High Pressure on Various Electrodes in an Aqueous Electrolyte.” *Journal of Electroanalytical Chemistry*, 391 (1–2), 141–47.

Haynes, Louis V, and Donald T Sawyer. 1967. “Electrochemistry of Carbon Dioxide in Dimethyl Sulfoxide at Gold and Mercury Electrodes.” *Analytical Chemistry*, 39 (3), 332–38.

Hori, Y. 2008. “Electrochemical CO_2 Reduction on Metal Electrodes.” In *Modern Aspects of Electrochemistry*, 89–189.

Hori, Y, H Konishi, T Futamura, A Murata, O Koga, H Sakurai, and K Oguma. 2005. “‘Deactivation of Copper Electrode’ in Electrochemical Reduction of CO_2.” *Electrochimica Acta*, 50 (27), 5354–69.

Hori, Yoshio, Katsuhei Kikuchi, and Shin Suzuki. 1985. “Production of CO and CH_4 in Electrochemical Reduction of CO_2 at Metal Electrodes in Aqueous Hydrogencarbonate Solution.” *Chemistry Letters*, 14 (11), 1695–98.

Hori, Yoshio, Akira Murata, and Ryutaro Takahashi. 1989. “Formation of Hydrocarbons in the Electrochemical Reduction of Carbon Dioxide at a Copper Electrode in Aqueous Solution.” *Journal of the Chemical Society, Faraday Transactions 1: Physical Chemistry in Condensed Phases*, 85 (8), 2309–26.

Hori, Yoshio, Akira Murata, Ryutaro Takahashi, and Shin Suzuki. 1987. “Electroreduction of Carbon Monoxide to Methane and Ethylene at a Copper Electrode in Aqueous Solutions at Ambient Temperature and Pressure.” *Journal of the American Chemical Society*, 109

(16), 5022–23.

Ikeda, Shoichiro, Takehiko Takagi, and Kaname Ito. 1987. “Selective Formation of Formic Acid, Oxalic Acid, and Carbon Monoxide by Electrochemical Reduction of Carbon Dioxide.” *Bulletin of the Chemical Society of Japan,* 60 (7), 2517–22.

Ishimaru, S, R Shiratsuchi, and G Nogami. 2000. “Pulsed Electroreduction of CO_2 on Cu-Ag Alloy Electrodes.” *Journal of The Electrochemical Society*, 147 (5), 1864–67.

Ito, Kaname, Shoichiro Ikeda, Nobuhiro Yamauchi, Takaya Iida, and Takehiko Takagi. 1985. “Electrochemical Reduction Products of Carbon Dioxide at Some Metallic Electrodes in Nonaqueous Electrolytes.” *Bulletin of the Chemical Society of Japan*, 58 (10), 3027–28.

Jee, Hae Sung, Naomichi Nishio, and Shiro Nagai. 1988. “Continuous CH_4 Production from H_2 and CO_2 by Methanobacterium Thermoautotrophicum in a Fixed-Bed Reactor.” *Journal of Fermentation Technology*, 66 (2), 235–38.

Jitaru, M, D A Lowy, M Toma, B C Toma, and L Oniciu. 1997. “Electrochemical Reduction of Carbon Dioxide on Flat Metallic Cathodes.” *Journal of Applied Electrochemistry*, 27 (8), 875–89.

Jordan, J, and P T Smith. 1960. “Free-Radical Intermediate in the Electroreduction of Carbon Dioxide.” *Proceedings of The Chemical Society of London*, 7, 246–247.

Jouzel, Jean, Valérie Masson-Delmotte, Olivier Cattani, Gabrielle Dreyfus, Sonia Falourd, Georg Hoffmann, Bénédicte Minster, J Nouet, Jean-Marc Barnola, and Jérôme Chappellaz. 2007. “Orbital and Millennial Antarctic Climate Variability over the Past 800,000 Years.” *Science*, 317 (5839), 793–96.

Kapusta, S, and N Hackerman. 1983. “The Electroreduction of Carbon Dioxide and Formic Acid on Tin and Indium Electrodes.” *Journal of The Electrochemical Society*, 130 (3), 607–13.

Kas, Recep, Ruud Kortlever, Alexander Milbrat, Marc T M Koper, Guido Mul, and Jonas Baltrusaitis. 2014. “Electrochemical CO_2 Reduction on Cu_2O-Derived Copper Nanoparticles: Controlling the Catalytic Selectivity of Hydrocarbons.” *Physical Chemistry Chemical Physics*, 16 (24), 12194–201.

Katoh, Akihiro, Hiroyuki Uchida, Masami Shibata, and Masahiro Watanabe. 1994. “Design of Electrocatalyst for CO_2 Reduction V. Effect of the Microcrystalline Structures of Cu-Sn and Cu-Zn Alloys on the Electrocatalysis of Reduction.” *Journal of the Electrochemical Society*, 141 (8), 2054–58.

Keeling, R F, S C Piper, A F Bollenbacher, and J S Walker. 2009. “Atmospheric Carbon

Dioxide Record from Mauna Loa." ESS-DIVE (Environmental System Science Data Infrastructure for a Virtual Ecosystem); Oak Ridge National Laboratory (ORNL), Oak Ridge, TN (United States).

Koga, Osamu, and Yoshio Hori. 1993. "Reduction of Adsorbed Co on a Ni Electrode in Connection with the Electrochemical Reduction of CO_2." *Electrochimica Acta*, 38 (10), 1391–94.

Lamy, E, L Nadjo, and J M Saveant. 1977. "Standard Potential and Kinetic Parameters of the Electrochemical Reduction of Carbon Dioxide in Dimethylformamide." *Journal of Electroanalytical Chemistry and Interfacial Electrochemistry*, 78 (2), 403–7.

Lehn, Jean-Marie, and Raymond Ziessel. 1982. "Photochemical Generation of Carbon Monoxide and Hydrogen by Reduction of Carbon Dioxide and Water under Visible Light Irradiation." *Proceedings of the National Academy of Sciences*, 79 (2),701–4.

Leitner, Walter. 1995. "Carbon Dioxide as a Raw Material: The Synthesis of Formic Acid and Its Derivatives from CO_2." *Angewandte Chemie International Edition*, 34 (20), 2207–21.

Li, Christina W, and Matthew W Kanan. 2012. "CO_2 Reduction at Low Overpotential on Cu Electrodes Resulting from the Reduction of Thick Cu_2O Films." *Journal of the American Chemical Society*, 134 (17), 7231–34.

Lide, David R. 1947. "CRC Handbook of Chemistry and Physics." *12J204*.

Lu, Guang, Hui Wang, Zhaoyong Bian, and Xin Liu. 2013. "Electrochemical Reduction of CO_2 to Organic Acids by a Pd-MWNTs Gas-Diffusion Electrode in Aqueous Medium." *The Scientific World Journal* 2013.

Lunsford, Jack H, and John P Jayne. 1965. "Formation of CO_2-Radical Ions When CO_2 Is Adsorbed on Irradiated Magnesium Oxide." *The Journal of Physical Chemistry*, 69 (7), 2182–84.

Lüthi, Dieter, Martine Le Floch, Bernhard Bereiter, Thomas Blunier, Jean-Marc Barnola, Urs Siegenthaler, Dominique Raynaud, Jean Jouzel, Hubertus Fischer, and Kenji Kawamura. 2008. "High-Resolution Carbon Dioxide Concentration Record 650,000–800,000 Years before Present." *Nature*, 453 (7193), 379–82.

Mandler, Daniel, and Itamar Willner. 1988. "Photochemical Fixation of Carbon Dioxide: Enzymic Photosynthesis of Malic, Aspartic, Isocitric, and Formic Acids in Artificial Media." *Journal of the Chemical Society, Perkin Transactions, 2*, 997–1003.

Manuel M Baizer and Henning Lund. 1991. *Organic Electrochemistry - Ab Introduction and a Guide,*. New York: Marcel Dekker.

Martins, M E, and A J Arvia. 1980. “The Activation of Polycrystalline Gold to the Hydrogen Electrode Reaction Promoted with Repetitive Potentiodynamic Perturbations.” *Journal of The Electrochemical Society*, 127, (12), 2628–2634.

Martins, M E, and A J Arvia. 1984. “Enhancement of Current Peak Multiplicity Related to Cuprous Oxide Electroreduction and Transient Copper Activation in Alkaline Solution.” *Journal of Electroanalytical Chemistry and Interfacial Electrochemistry*, 165 (1–2), 135–45.

Mayer, Steven T, and Rolf H Muller. 1992. “An in Situ Raman Spectroscopy Study of the Anodic Oxidation of Copper in Alkaline Media.” *Journal of The Electrochemical Society*, 139 (2), 426–34.

McIntyre, N S, and M G Cook. 1975. “X-Ray Photoelectron Studies on Some Oxides and Hydroxides of Cobalt, Nickel, and Copper.” *Analytical Chemistry*, 47 (13), 2208–13.

McIntyre, N S, S Sunder, D W Shoesmith, and F W Stanchell. 1981. “Chemical Information from XPS—applications to the Analysis of Electrode Surfaces.” *Journal of Vacuum Science and Technology*, 18 (3), 714–21.

Metz, Bert, Ogunlade Davidson, Heleen De Coninck, Manuela Loos, and Leo Meyer. 2005. “IPCC Special Report on Carbon Dioxide Capture and Storage.” Intergovernmental Panel on Climate Change, Geneva (Switzerland). Working Group III.

Micromeritics, ASAP. n.d. “2020 Accelerated Surface Area and Porosimetry System Operator’s Manual, V4. 01.”

Miller, B. 1969. “Split-ring Disk Study of the Anodic Processes at a Copper Electrode in Alkaline Solution.” *Journal of the Electrochemical Society*, 116 (12), 1675–80.

Miller, J D, S Veeramasuneni, J Drelich, M R Yalamanchili, and G Yamauchi. 1996. “Effect of Roughness as Determined by Atomic Force Microscopy on the Wetting Properties of PTFE Thin Films.” *Polymer Engineering & Science*, 36 (14), 1849–55.

Moffat, Thomas P. 1998. “Oxidative Chloride Adsorption and Lead Upd on Cu (100): Investigations into Surfactant-Assisted Epitaxial Growth.” *The Journal of Physical Chemistry B*, 102 (49),10020–26.

Mohite, Rajendra G, and Anurag Garg. 2017. “Performance of Heterogeneous Catalytic Wet Oxidation for the Removal of Phenolic Compounds: Catalyst Characterization and Effect of pH, Temperature, Metal Leaching and Non-Oxidative Hydrothermal Reaction.” *Journal of Environmental Chemical Engineering*, 5 (1), 468–78.

Naitoh, A, K Ohta, T Mizuno, H Yoshida, M Sakai, and H Noda. 1993. “Electrochemical

Reduction of Carbon Dioxide in Methanol at Low Temperature." *Electrochimica Acta*, 38 (15), 2177–79.

Newsome, David S. 1980. "The Water-Gas Shift Reaction." *Catalysis Reviews Science and Engineering*, 21 (2), 275–318.

Oniciu, L, I A Silberg, D A Lowy, M Jitaru, F Ciomos, O H Oprea, B C Toma, and M Toma. 1990. "Effect of Surfactants on the Electroreduction of Acrylonitrile." *Revue Roumaine De Chimie*, 35 (7–9), 859–66.

Pachauri, Rajendra K, Myles R Allen, Vicente R Barros, John Broome, Wolfgang Cramer, Renate Christ, John A Church, Leon Clarke, Qin Dahe, and Purnamita Dasgupta. 2014. *Climate Change 2014: Synthesis Report. Contribution of Working Groups I, II and III to the Fifth Assessment Report of the Intergovernmental Panel on Climate Change*. IPCC.

Paik, W, T N Andersen, and H Eyring. 1969. "Kinetic Studies of the Electrolytic Reduction of Carbon Dioxide on the Mercury Electrode." *Electrochimica Acta*, 14 (12), 1217–32.

Parkinson, Bruce A, and Paul F Weaver. 1984. "Photoelectrochemical Pumping of Enzymatic CO2 Reduction." *Nature*, 309 (5964), 148–49.

Peterson, Andrew A, Frank Abild-Pedersen, Felix Studt, Jan Rossmeisl, and Jens K Nørskov. 2010. "How Copper Catalyzes the Electroreduction of Carbon Dioxide into Hydrocarbon Fuels." *Energy & Environmental Science*, 3 (9),1311–15.

Qu, Jianping, Xiaogang Zhang, Yonggang Wang, and Chengxi Xie. 2005. "Electrochemical Reduction of CO_2 on RuO_2/TiO_2 Nanotubes Composite Modified Pt Electrode." *Electrochimica Acta*, 50 (16), 3576–80.

Quinn, Elton L, and Charles L Jones. 1936. *Carbon Dioxide*. Reinhold Publishing Corporation; New York.

Rasband, W S. 1997. "ImageJ Software." *National Institutes of Health: Bethesda, MD, USA* 2012.

Reyter, David, Marek Odziemkowski, Daniel Bélanger, and Lionel Roué. 2007. "Electrochemically Activated Copper Electrodes Surface Characterization, Electrochemical Behavior, and Properties for the Electroreduction of Nitrate." *Journal of the Electrochemical Society*, 154 (8), K36–44.

Rodríguez, José M Doña, José Alberto Herrera Melián, and Jesús Pérez Peña. 2000. "Determination of the Real Surface Area of Pt Electrodes by Hydrogen Adsorption Using Cyclic Voltammetry." *J. Chem. Educ*, 77 (9), 1195.

Santos, A, P Yustos, A Quintanilla, and F Garcia-Ochoa. 2005. "Influence of pH on the Wet

Oxidation of Phenol with Copper Catalyst." *Topics in Catalysis*, 33 (1–4), 181–92.

Schiffrin, D J. 1973. "Application of the Photo-Electrochemical Effect to the Study of the Electrochemical Properties of Radicals: CO_2 and CH_3." *Faraday Discussions of the Chemical Society*, 56, 75–95.

Schwartz, Michael, Ronald L Cook, Victoria M Kehoe, Robert C MacDuff, Jay Patel, and Anthony F Sammells. 1993. "Carbon Dioxide Reduction to Alcohols Using Perovskite-Type Electrocatalysts." *Journal of the Electrochemical Society*, 140 (3), 614–18.

Scibioh, M Aulice, and B Viswanathan. 2004. "Electrochemical Reduction of Carbon Dioxide: A Status Report." In *Proc Indian Natn Sci Acad*, 70:1–56.

Shoesmith, D W, S Sunder, M G Bailey, G J Wallace, and F W Stanchell. 1983. "Anodic Oxidation of Copper in Alkaline Solutions: Part IV. Nature of the Passivating Film." *Journal of Electroanalytical Chemistry and Interfacial Electrochemistry*, 143 (1–2), 153–65.

Siegenthaler, H, and K Jüttner. 1984. "Voltammetric Investigation of Lead Adsorption on Cu (111) Single Crystal Substrates." *Journal of Electroanalytical Chemistry and Interfacial Electrochemistry*, 163 (1–2), 327–43.

Somorjai, G A. 1978. "Catalysis on the Atomic Scale (Emmett Award Lecture of 1977)." *Catalysis Reviews Science and Engineering*, 18 (2), 173–97.

Spichiger-Ulmann, M, and J Augustynski. 1986. "Specific Cation Effect upon the Rate of Cathodic Reduction of Bicarbonate Anion at Palladium." *Nouveau Journal de Chimie*, 10 (8–9), 487–91.

Sugimura, Kenji, Susumu Kuwabata, and Hiroshi Yoneyama. 1989. "Electrochemical Fixation of Carbon Dioxide in Oxoglutaric Acid Using an Enzyme as an Electrocatalyst." *Journal of the American Chemical Society*, 111 (6), 2361–62.

Summers, David P, and Karl W Frese Jr. 1988. "Mechanistic Aspects of the Electrochemical Reduction of Carbon Monoxide and Methanol to Methane at Ruthenium and Copper Electrodes." ACS Publications, 518–527.

Tacconi, Norma R de, Wilaiwan Chanmanee, Brian H Dennis, and Krishnan Rajeshwar. 2017. "Composite Copper Oxide–copper Bromide Films for the Selective Electroreduction of Carbon Dioxide." *Journal of Materials Research*, 32 (9), 1727–34.

Taniguchi, I, B Aurian-Blajeni, and J Bockris. 1984. "The Reduction of Carbon Dioxide at Illuminated P-Type Semiconductor Electrodes in Nonaqueous Media." *Electrochimica*

Acta, 29 (7), 923–32.

Trasatti, S, and O A Petrii. 1992. "Real Surface Area Measurements in Electrochemistry." *Journal of Electroanalytical Chemistry,* 327 (1–2), 353–76.

Vassiliev, Yu B, V S Bagotsky, N V Osetrova, O A Khazova, and N A Mayorova. 1985. "Electroreduction of Carbon Dioxide: Part I. The Mechanism and Kinetics of Electroreduction of CO_2 in Aqueous Solutions on Metals with High and Moderate Hydrogen Overvoltages." *Journal of Electroanalytical Chemistry and Interfacial Electrochemistry,* 189 (2), 271–94.

Vilche, J R, and K Jüttner. 1987. "Anion Effects on the Underpotential Deposition of Lead on Cu (111)." *Electrochimica Acta,* 32 (11), 1567–72.

Vuković, M, H Angerstein-Kozlowska, and B E Conway. 1982. "Electrocatalytic Activation of Ruthenium Electrodes for the Cl_2 and O_2 Evolution Reactions by Anodic/cathodic Cycling." *Journal of Applied Electrochemistry,* 12 (2), 193–204.

Wagman, Donald D, William H Evans, Vivian B Parker, Richard H Schumm, and Iva Halow. 1982. "The NBS Tables of Chemical Thermodynamic Properties. Selected Values for Inorganic and C1 and C2 Organic Substances in SI Units." National Standard Reference Data System.

Wan, Ye, Yundian Zhang, Xianle Wang, and Qing Wang. 2013. "Electrochemical Formation and Reduction of Copper Oxide Nanostructures in Alkaline Media." *Electrochemistry Communications,* 36, 99–102.

Whipple, Devin T, and Paul J A Kenis. 2010. "Prospects of CO_2 Utilization via Direct Heterogeneous Electrochemical Reduction." *The Journal of Physical Chemistry Letters,* 1 (24), 3451–58.

Wu, Her-Chiang, and Shueh-Lin Yau. 2001. "In Situ Scanning Tunneling Microscopy of Underpotential Deposition of Lead on Cu (100) in Sulfuric Acid Solutions." *The Journal of Physical Chemistry B,* 105 (29), 6965–71.

Yadav, V S K, and M K Purkait. 2016. "Effect of Copper Oxide Electrocatalyst on CO_2 Reduction Using Co3O4 as Anode." *Journal of Science: Advanced Materials and Devices,* 1 (3), 330–36.

Yamamoto, K, D M Kolb, R Kötz, and G Lehmpfuhl. 1979. "Hydrogen Adsorption and Oxide Formation on Platinum Single Crystal Electrodes." *Journal of Electroanalytical Chemistry and Interfacial Electrochemistry,* 96 (2), 233–39.

Appendix I

The equilibrium constant calculations for the formation and dissolution of copper oxide/hydroxide species in a reversible reaction at standard conditions is given in detail in this appendix.

1. **The procedure and the calculations of the equilibrium constant for reaction 3.3 are explained in detail below. The Reaction is**

$$Cu_2O + 2OH^- + H_2O \Leftrightarrow 2Cu(OH)_2^- \qquad (K_{eq} = 1.4316 \times 10^{-6}) \ldots\ldots\ldots\ldots\ldots\ldots\ldots (3.3)$$

The Gibbs energy of formation of these species in J/mol

$$\begin{aligned} Cu_2O &= -147900 \\ OH^- &= -157200 \\ H_2O &= -237140 \\ 2Cu(OH)_2^- &= -333050 \end{aligned}$$

The Gibbs free energy change for the reaction can be calculated as,

$$\Delta G^\circ = \text{Gibbs Energy for Formationon of Product} - \text{Gibbs Energy for Formationon of Reactant}$$

$$\Delta G^\circ = 2 \times -333050 - \left(-147900 + 2 \times -157200 - 237140\right)$$

$$\Delta G^\circ = 33340 \text{J/mol}$$

$$K_{eq} = e^{\frac{-\Delta G^\circ}{RT}} = e^{\frac{-33340}{8.314 \times 298}} = e^{-13.4567}$$

$$K_{eq} = 1.4316 \times 10^{-6}$$

2. **The procedure and the calculations of the equilibrium constant for reaction 3.5 are explained in detail below. The Reaction is**

$$2Cu(OH) \Leftrightarrow Cu_2O + H_2O \qquad (K_{eq} = 4.0811 \times 10^{24}) \ldots\ldots\ldots\ldots\ldots\ldots\ldots\ldots (3.5)$$

The Gibbs energy of formation of these species in J/mol

$Cu(OH) \quad = \quad -122320$

$Cu_2O \quad = \quad -147900$

$H_2O \quad = \quad -237140$

$\Delta G^\circ = \text{Gibbs Energy for Formationon of Product} - \text{Gibbs Energy for Formationon of Reactant}$

$\Delta G^\circ = (-147900 - 237140) - (2 \times -122320)$

$\Delta G^\circ = -140400 \text{ J/mol}$

$K_{eq} = e^{\frac{-\Delta G^\circ}{RT}} = e^{\frac{140400}{8.314 \times 298}} = e^{56.6684}$

$K_{eq} = 4.0811 \times 10^{24}$

3. The procedure and the calculation of equilibrium constant for reaction 3.8 are explained in detail below. The Reaction is

$Cu(OH)_2 \rightarrow CuO + H_2O \qquad (K_{eq} = 20.1447).....(3.8)$

The Gibbs energy of formation of these species in J/mol

$Cu(OH)_2 \quad = \quad -359400$

$CuO \quad = \quad -129700$

$H_2O \quad = \quad -237140$

$\Delta G^\circ = \text{Gibbs Energy for Formationon of Product} - \text{Gibbs Energy for Formationon of Reactant}$

$\Delta G^\circ = (-129700 - 237140) - (-359400)$

$\Delta G^\circ = -7440 \text{ J/mol}$

$K_{eq} = e^{\frac{-\Delta G^\circ}{RT}} = e^{\frac{7440}{8.314 \times 298}} = e^{3.0029}$

$K_{eq} = 20.1447$

4. The procedure and the calculations of the equilibrium constant for reaction 3.12 are explained in detail below. The Reaction is

$$Cu(OH)_4^{2-} \Leftrightarrow Cu(OH)_2 + 2OH^- \qquad (K_{eq} = 725.6734).....(3.12)$$

The Gibbs energy of formation of these species in J/mol

$$\begin{aligned} Cu(OH)_4^{2-} &= -657480 \\ Cu(OH)_2 &= -359400 \\ OH^- &= -157200 \end{aligned}$$

$$\Delta G^\circ = \text{Gibbs Energy for Formationon of Product} - \text{Gibbs Energy for Formationon of Reactant}$$

$$\Delta G^\circ = \left(-359400 + 2 \times -157200\right) - \left(-657480\right)$$

$$\Delta G^\circ = -16320 \text{ J/mol}$$

$$K_{eq} = e^{\frac{-\Delta G^\circ}{RT}} = e^{\frac{16320}{8.314 \times 298}} = e^{6.5871}$$

$$K_{eq} = 725.6734$$

Appendix II

A) Calculation of charge density (μC/cm^2) factor for the under potential deposition (UPD) of lead (Pb) on copper.

1. **Number of atoms per cm^2 of copper (Cu)**

Bulk copper electrode used was made up of polycrystalline copper. For the simplicity of the calculation, it is assumed that the polycrystalline copper is made up of equal percentage of three basic planes (100), (110) and (111) plane. The planar density of these three basic planes for a face centred cubic (FCC) crystal structure (copper is a FCC crystal structure) is

$$\text{(100) plane} = \frac{0.25}{R^2},$$

$$\text{(110) plane} = \frac{0.177}{R^2} \text{ and}$$

$$\text{(111) plane} = \frac{0.29}{R^2}$$

Where R is atomic radius. The planar density gives the number of atoms per unit area.

From the crystal atrucure of the copper we have taken the value of lattice parameter "a" for copper equal to 3.6149 A^o i.e. 0.36149 nm.

The atomic radius is calculated from the FCC crystal structure as

$$\text{R} = \frac{\sqrt{2} \times a}{4} =$$

$$\text{R} = \frac{\sqrt{2} \times 0.36149}{4}$$

$$\text{R} = 0.1278 \text{ nm}$$

$$\text{Planar density of Cu (100) plane} = \frac{0.25}{0.1278^2} = 15.3065 \frac{\text{atoms}}{\text{nm}^2} = 15.3065 \times 10^{14} \frac{\text{atoms}}{\text{cm}^2}$$

$$\text{Planar density of Cu (110) plane} = \frac{0.177}{0.1278^2} = 10.8371 \frac{\text{atoms}}{\text{nm}^2} = 10.8371 \times 10^{14} \frac{\text{atoms}}{\text{cm}^2}$$

Planar density of Cu (111) plane = $\frac{0.29}{0.1278^2} = 17.7556 \frac{\text{atoms}}{\text{nm}^2} = 17.7556 \times 10^{14} \frac{\text{atoms}}{\text{cm}^2}$

Average density for poly-crystalline lead sample = 14.6331×10^{14} atoms/cm^2

2. Number of atoms per cm^2 of lead (Pb)

As lead has been deposited on the poly-crystalline copper, it will have same planes but different number of atoms per cm2 due to the difference between the atomic radiuses. The lattice parameter "a"of the lead is equal to 4.9508 Ao i.e. 0.49508 nm.

The atomic radius is calculated from the FCC crystal structure as

$$R = \frac{\sqrt{2} \times a}{4} =$$

$$R = \frac{\sqrt{2} \times 0.49508}{4}$$

$$R = 0.175 \text{ nm}$$

Planar density of Pb (100) plane = $\frac{0.25}{0.175^2} = 8.1633 \frac{\text{atoms}}{\text{nm}^2} = 8.1633 \times 10^{14} \frac{\text{atoms}}{\text{cm}^2}$

Planar density of Pb (110) plane = $\frac{0.177}{0.175^2} = 5.7796 \frac{\text{atoms}}{\text{nm}^2} = 5.7796 \times 10^{14} \frac{\text{atoms}}{\text{cm}^2}$

Planar density of Pb (111) plane = $\frac{0.29}{0.175^2} = 9.4694 \frac{\text{atoms}}{\text{nm}^2} = 9.4694 \times 10^{14} \frac{\text{atoms}}{\text{cm}^2}$

Average density for poly-crystalline lead sample = 7.8041×10^{14} atoms/cm^2

The coverage of monolayer of Pb on Cu = $\frac{7.8041}{14.6331} = 0.5333$

The coverage of monolayer of Pb on Cu = 53.33 %

The Pb deposition on Cu is as per the following reaction

$$Cu + Pb^{2+} + 2e^{-} \rightarrow CuPb$$

The amount of charge transfer for the formation of Pb monolayer on Cu as per the reaction above,

Charge transferred = Total atoms of Pb required per cm^2 × No. electrons transferred × Charge on one electron in coulombs

Charge transferred = $(7.8041\times10^{14}) \times (2) \times (1.6022\times10^{-19})$

Charge transferred = 25.0097×10^{-5} C/cm2

Charge transferred ≈ 250 µC/cm^2.

B) Calculation of charge density (µC/cm^2) factor for the under potential deposition (UPD) of copper (Cu) on platinum.

Number of atoms per cm^2 of Platinum (Pt)

Platinum (20 wt% on carbon) electrode used was made up of polycrystalline platinum. For the simplicity of the calculation, it is assumed that the polycrystalline platinum is made up of equal percentage of three basic planes (100), (110) and (111) plane. The planar density of these three basic planes for a face centred cubic (FCC) crystal structure (platinum is a FCC crystal structure) is

$$(100)\text{ plane} = \frac{0.25}{R^2},$$

$$(110)\text{ plane} = \frac{0.177}{R^2}\text{ and}$$

$$(111)\text{ plane} = \frac{0.29}{R^2}$$

Where R is atomic radius. The planar density gives the number of atoms per unit area.

From the crystal atrucure of the copper we have taken the value of lattice parameter "a" for copper equal to 3.9242 A^o i.e. 0.39242 nm.

The atomic radius is calculated from the FCC crystal structure as

$$R = \frac{\sqrt{2}\times a}{4} =$$

$$R = \frac{\sqrt{2} \times 0.39242}{4}$$

$$R = 0.1387 \text{ nm}$$

Planar density of Cu (100) plane = $\frac{0.25}{0.1387^2} = 15.3065 \frac{\text{atoms}}{\text{nm}^2} = 12.9953 \times 10^{14} \frac{\text{atoms}}{\text{cm}^2}$

Planar density of Cu (110) plane = $\frac{0.177}{0.1387^2} = 10.8371 \frac{\text{atoms}}{\text{nm}^2} = 9.2007 \times 10^{14} \frac{\text{atoms}}{\text{cm}^2}$

Planar density of Cu (111) plane = $\frac{0.29}{0.1387^2} = 17.7556 \frac{\text{atoms}}{\text{nm}^2} = 15.0746 \times 10^{14} \frac{\text{atoms}}{\text{cm}^2}$

Average density for poly-crystalline lead sample = 12.4235×10^{14} atoms/cm^2

The coverage of monolayer of Pb on Cu = $\frac{14.6331}{12.4235} = 1.1537$

The coverage of monolayer of Pb on Cu = 115.37 %

However, the maximum possible atoms for monolayer should equal to number platinum atoms per cm^2. Hence the monolayer coverage is <u>100%</u>. In this case, monolayer percentage is exceeding 100% due to smaller atom of copper than platinum.

The Cu deposition on Pt is as per the following reaction

$$Pt \quad + \quad Cu^{2+} \quad + 2e^{-} \quad \rightarrow PtCu$$

The amount of charge transfer for the formation of Pb monolayer on Cu as per the reaction above,

Charge transferred = Total atoms of Pb required per cm^2 × No. electrons transferred × Charge on one electron in coulombs

Charge transferred = $(12.4235 \times 10^{14}) \times (2) \times (1.6022 \times 10^{-19})$

Charge transferred = 39.8098×10^{-5} C/cm^2

Charge transferred ≈ 400 µC/cm^2.

But, conventionally the monolayer charge is taken equal to 420 µC/cm^{2}of platinum.

Appendix III

Calibration Curve

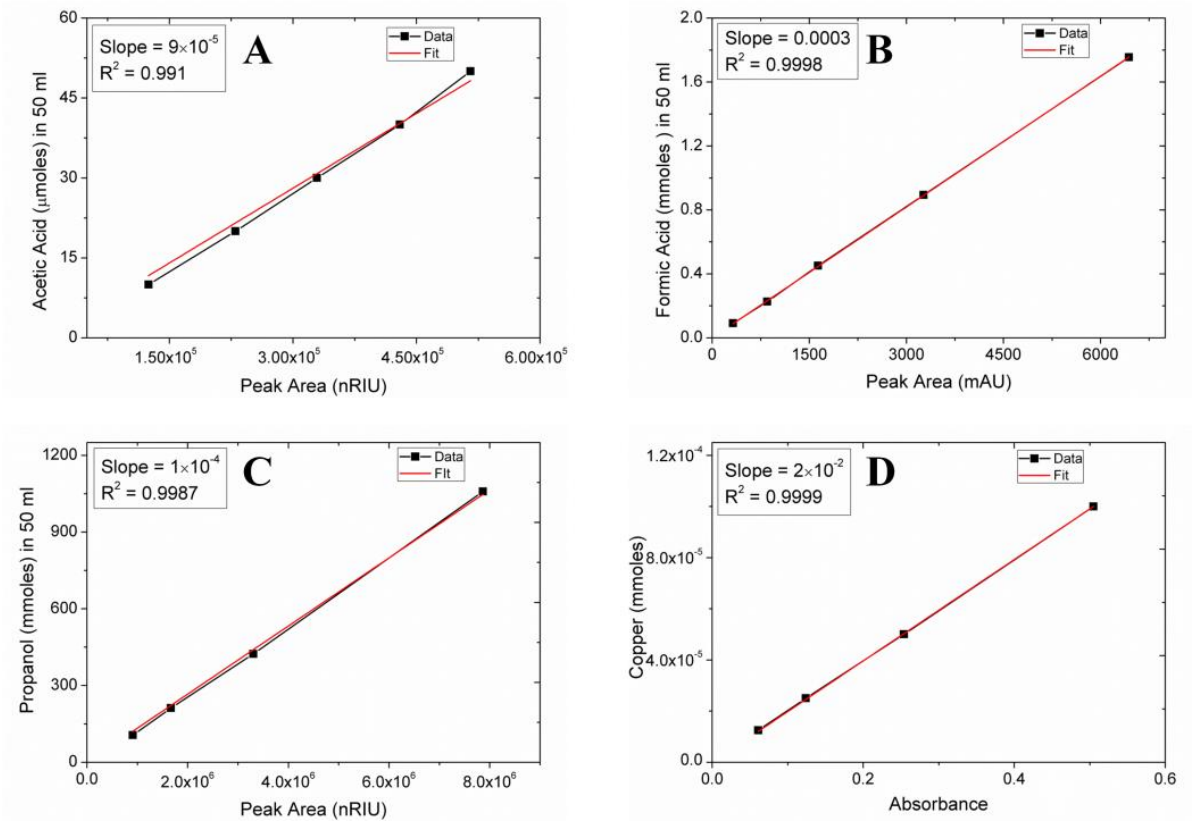

Figure 1: Calibration curve for A) Acetic acid, B) Formic Acid C) Propanol on HPLC. Calibration curve for D) Copper ions on spectrophotometer.

Appendix IV

Table 1: CO_2 reduction potential of oxidized copper foils

Sr. No.	Potential (V)	CO_2 Reduction Pontetial (μmoles/(cm^2*s)		CO_2 Reduction Pontetial (moles/(m^2*hr)	
		Anodized Copper Foil	Annealed Copper Foil	Anodized Copper Foil	Annealed Copper Foil
1	-1.4	0.0531	0.0692	1.9127	2.4900
2	-1.6	0.0941	0.1816	3.3879	6.5389
3	-1.8	0.1245	0.1457	4.4816	5.2480
4	-2	0.1889	0.0950	6.8015	3.4324

Table 2: CO_2 Reduction Potential of Mixed Metal Oxides of the La, Ca, and Cu

Sr. No	Potential (V)	CO_2 Reduction Potential (μmol/(cm^2*s))						
		LaCu	$La_{0.8}Ca_{0.2}Cu$	$La_{0.6}Ca_{0.4}Cu$	$La_{0.4}Ca_{0.6}Cu$	$La_{0.2}Ca_{0.8}Cu$	CaCu	Cu
1	-1.4	0.0110	0.0046	0.0024	0.0008	0.0013	0.0026	0.0004
2	-1.6	0.0152	0.0075	0.0065	0.0015	0.0006	0.0052	0.0032
3	-1.8	0.0100	0.0088	0.0188	0.0063	0.0031	0.0051	0.0040
4	-2.0	0.0239	0.0069	0.0160	0.0072	0.0095	0.0205	0.0063

Sr. No	Potential (V)	CO_2 Reduction Potential (mol/(m^2*hr))						
		LaCu	$La_{0.8}Ca_{0.2}Cu$	$La_{0.6}Ca_{0.4}Cu$	$La_{0.4}Ca_{0.6}Cu$	$La_{0.2}Ca_{0.8}Cu$	CaCu	Cu
1	-1.4	0.3958	0.1650	0.0876	0.0294	0.0474	0.0919	0.0153
2	-1.6	0.5485	0.2716	0.2329	0.0534	0.0208	0.1865	0.1137
3	-1.8	0.3584	0.3170	0.6759	0.2251	0.1116	0.1837	0.1434
4	-2.0	0.8614	0.2477	0.5761	0.2587	0.3423	0.7383	0.2253

Table 3: Energy Efficiency for Electrochemical Reduction of CO_2

Catalayst	voltage (V)	Current (A)	Power (W)	Energy Spent half hr (J)	HCOOH (µ mole/ half hr)	CH_3COOH (µ mole/ half hr)	Total CO_2 reacted (µ mole/ half hr)	Energy utilized for FA (J)	Energy utilized for AA (J)	Total Utilized (J)	Energy Efficiency (%)
LaCu	2	0.04	0.08	150.66	15.51	83.80	183.11	4.46	72.70	77.16	51.22
CaCu	1.8	0.04	0.07	129.60	62.51	6.90	76.31	17.97	5.99	23.96	18.49
Cu	1.9	0.04	0.08	136.80	44.62	0.60	45.82	12.83	0.52	13.35	9.76

Publications

Journal Publications

- **Giri Sachin D**., and A. Sarkar. "Electrochemical Study of Bulk and Monolayer Copper in Alkaline Solution." *Journal of The Electrochemical Society*, 163.3 (2016): H252-H259.
- **Giri, Sachin D.,** Sarkar, A., Mahajani, S., & Suresh, A. K.. Electrochemical Reduction of CO_2 on Copper Oxidized by Electrochemical Methods. *ECS Transactions*, *75*(48), (2017): 19-31.
- **Giri, Sachin D.,** Sarkar, A., Mahajani, S., & Suresh, A. K., Electrochemical Reduction of CO_2 on Oxidized Copper: Influence of Surface area (Under review: Electrocatalysis).
- **Giri, Sachin D.,** Sarkar, A., Surface Area of Copper Powder: A Comparison between Electrochemical, Microscopy and Laser Diffraction Methods (Under review: Journal of Applied Catalysis – A General).
- **Giri, Sachin D.,** Sarkar, A., Electrochemical Reduction of CO_2 on Mixed Metal Oxides of Lanthanum, Calcium, and Copper (Under preparation).

Presentations at International/National Conferences

- **Giri Sachin D.**, A. Sarkar, Sanjay M. Mahajani and A. K. Suresh, "Electrochemical reduction of CO_2 on Copper oxidized by different Electrochemical Methods" presented at PRiME 2016 held during 2nd to 7th October 2016 at Honolulu, Hawaii, USA.
- **Giri Sachin D**., and A. Sarkar. "Nano and Micro Structured Growth of Copper Oxides on Copper Surface by Electrochemical Oxidation in Alkaline solution" presented at RSS 2016 held on 13th February 2016 at IIT Bombay, India.